UNIVERSITY OF CALIFORNIA

Los Angeles

Search for Ultra High Energy Cosmic Ray Anisotropy with Auger

A dissertation submitted in partial satisfaction of the

Requirements for the degree Doctor of Philosophy

In Physics and Astronomy

by

Pedram Boghrat

2008

This page intentionally left blank.

COPYRIGHT PAGE

This dissertation of Pedram Boghrat is approved.

_____

Alexander Kusenko

_____

Jay Hauser

_____

Robert Brown

_____

Katsushi Arisaka, Committee Chair

University of California, Los Angeles

2008

DEDICATION

This document is dedicated to Lily and Lucy.

Table of Contents

Table of Figures

Index of Tables

ACKNOWLEDGMENTS

I would like to thank the many people in the Auger collaboration who worked so hard for science and whose work taught me so much. Also, I have much appreciation for the Auger group at UCLA, many thanks to Joong Lee, Matt Healy, Artin Teymourian, Stephen Hoover and Dave Barnhill. I would like to thank my advisor Dr. Katsushi Arisaka for his teachings and advice over the years and Drs. Alexander Kusenko, Jay Hauser, William Slater, Robert Cousins and Charles Whitten for the many salient physics discussions. The love and support of my family has been invaluable, thanks Mom and Baba.

VITA

September 6, 1977	Born: Tehran, Iran
2001 to present	Teaching Assistant Department of Physics and Astronomy University of California Los Angeles, California
2005	M.S. Physics and Astronomy University of California Los Angeles, California
2000	B.S. Mechanical Engineering University of Pittsburgh Pittsburgh, Pennsylvania

AWARDS

2000 Award for Excellence in Undergraduate Writing from University of Pittsburgh

PUBLICATIONS AND PRESENTATIONS

Presentation on AGN, Large Scale Structure and Great Attractor September 14, 2006 Auger South Analysis Meeting, Chicago Illinois.

ABSTRACT OF THE DISSERTATION

Search for Ultra High Energy Cosmic Ray Anisotropy with Auger

by

Pedram Boghrat
Doctor of Philosophy in Physics and Astronomy
University of California, Los Angeles, 2008

Professor Katsushi Arisaka, Chair

Although the existence of ultra high energy cosmic rays (UHECR) with energies on the order of 10^{20} eV, has been shown by past experiments, the source of these particles is not yet understood. Theoretical models motivate the consideration of nearby active galactic nuclei (AGN) as a source candidate. However, AGN have not been declared as the source unambiguously and alternative hypotheses have also been made claiming radio galaxies are a significant source of UHECR. A third source candidate named Centaurus A (Cen A) is also considered.

The focus of this thesis will be to test these hypotheses using the Pierre Auger detector, which observes the air showers generated by the UHECR primary after entering the Earth's atmosphere. The detector utilizes an array of 1600 ground detectors, each consisting of 12 metric tons of water spread over roughly 3000 km^2. Each tank of water is watched by three 9" photomultipliers that detect Cherenkov radiation emitted by air shower particles passing through the

water. The light emitted by atmospheric nitrogen that has been excited by passing air shower particles is also observed in order to obtain a calorimetric measurement of the energy of the UHECR.

The first hypothesis that will be tested concerns the possibility that UHECR with energies larger than 57EeV correlate within 3.2^0 of AGN within 0.018 redshift. Given that the region 3.2^0 around these AGN covers 23% of the sky, on average 2.3 events out of 10 are expected to correlate within 3.2^0 of an AGN under the assumption of isotropy. Given only one out of 10 events in an independent data set are found to correlate, this hypothesis is disfavored.

The second hypothesis that will be tested claims an excess of UHECR are found within 3.5^0 of radio galaxies within about 70 Mpc. Given that the region 3.5^0 around radio galaxies covers 10% of the sky, on average one out of 10 events are expected to correlate within 3.5^0 of a radio galaxy, under the assumption that the UHECR are isotropic. In fact, no events out of 10 events in an independent data set are found to correlate. Therefore, this hypothesis is also disfavored.

The region 17^0 around Cen A is shown to have an excess of UHECR with energies larger than 57EeV with a confidence of 2.3×10^{-3}. However, Cen A is not shown to be the source unambiguously. Despite this, Cen A is the closest radiogalaxy, at 3.4 Mpc, whose radio lobes extend over about 10^o of the sky and is the most likely source of this anisotropy.

CHAPTER 1

Scientific Motivation

The study of radiation begins at the turn of the 19th century with the discovery of radioactivity by Becquerel in 1896 [1]. It was found that radioactive particles emanating from naturally radioactive substances had the capacity to ionize the air molecules that they passed through. At this time, the device used to measure the amount of ionization was the gold leaf electroscope. This device would have a charge placed on it causing the gold leaves to separate due to the electrostatic repulsion of like charge on both leaves. As time would pass, the charge on the leaves would begin to leak off. It was found that this leakage was a result of the ions present in the area around the electroscope. The amount of ionization in the surrounding air could be measured by observing how quickly the charge on the gold leaves dissipated. This dissipation was indicated by the decrease in the amount of electrostatic deflection of the gold leaves from each other.

Such ionization tests were carried out in places that contained no known radioactive sources. It became apparent that ionization of the air around the electroscope could occur even when there was no known source of radioactivity in the vicinity of the scope. The question arose concerning the nature and source of these ionizing particles.

In 1910, Wulf showed that the amount of ionization actually decreased at the top of the Eiffel Tower, 330 meters above the Earth, relative to the amount of ionization he observed on the ground

[1]. This experiment suggested that the source of the ionizing particles was the Earth itself. These altitude experiments were continued by Hess in 1912-1913 using a hot air balloon. Hess was thus able to measure the amount of ionization at much higher altitudes. Up to about 1.5 kilometers, the ionization decreased in agreement with Wulf. However, above this altitude, the amount of ionization began to increase. He measured the amount of ionization up to a height of nine kilometers above the Earth's surface. His results showed that although the Earth appeared to be the source of some radioactivity, there appeared to be ionizing particles coming from the heavens.

In the late 1920's and early 1930's, with the advent of new technology such as Geiger counters and cloud chambers, it became possible to take photographs of the tracks of these particles in a cloud chamber in order to deduce more about their properties. The Geiger counters could be used to trigger the camera as the cosmic ray traveled through the cloud chamber leaving a track of ionized molecules behind. By including magnets in conjunction with the cloud chambers, one could measure the deflection of the particles. The small amount of deflection seen indicated that the particles were very energetic. In 1929, Skobelzyn determined that the particles had energies around 15 MeV [1].

In 1933, Bruno Rossi (while studying cosmic rays on an expedition to Africa) found that detectors spaced apart from each other occasionally triggered in coincidence [2]. He deduced that the coincidence was the result of an extended air shower of particles caused by the interaction of a single cosmic ray with particles in the atmosphere. Pierre Auger, along with collaborators, took up this work on extensive air showers and determined that “we should be able to recognize it [single primary particle] by the existence of a 'coherence' of these shower particles, the multiple effects of a single initial particle remaining bound in time and in space.”[3]. He was also able to get an estimate for the energy of the primary by assuming 10^6 shower particles with approximate energies of 10^8 eV

including for a 10% energy attenuation in the atmosphere of 10^6 x 10^8 eV x10~10^{15} eV. This was a very large energy as compared to even the largest energies produced by the contemporary particle accelerator Tevatron at Fermilab of about 10^{12} eV.

In February 1962, an UHECR was seen by the MIT Volcano Ranch detector, with an estimated energy of 10^{20} eV or 100 EeV [4]. Later in 1991, an even higher energy cosmic ray was seen by the HiRes detector, with an estimated energy of about 300 EeV [5]. This particle (dubbed the "Oh My God Particle") was shockingly energetic. It had an energy equivalent to the kinetic energy of a macroscopic object; such as, a baseball traveling at 60 miles per hour. This particle had an energy hundreds of millions times larger than that able to be produced at Fermilab. The Akeno Giant Air Shower Array (AGASA), which operated in Japan from 1991 until 2004, also reported the observation of these UHECR.

1.1 Spectrum

Over time as more events were recorded, it became clear that the cosmic ray spectrum extended up to and beyond 10^{20} eV. Figure 1 taken from [6] shows this spectrum along with some of its important features. The dashed line shows an E^{-3} spectrum. The fact that we see the spectrum extending to such high energies is very exciting because these particles will allow a glimpse into the past. These particles allow the study of the Universe at very high energies and will give us clues about the early energetic Universe, the Universe at its early stages of evolution.

The "knee" region of the spectrum showing a greater drop in flux around 10^{16} eV is believed to be due to the fact that these particles are no longer trapped inside our own galaxy. Particles with energies lower than this undergo more deflection inside the galaxy, and are thereby trapped inside

the Milky Way, and will not leak out [7]. Consequently, we observe more of the lower energy particles before the knee and less beyond the knee.

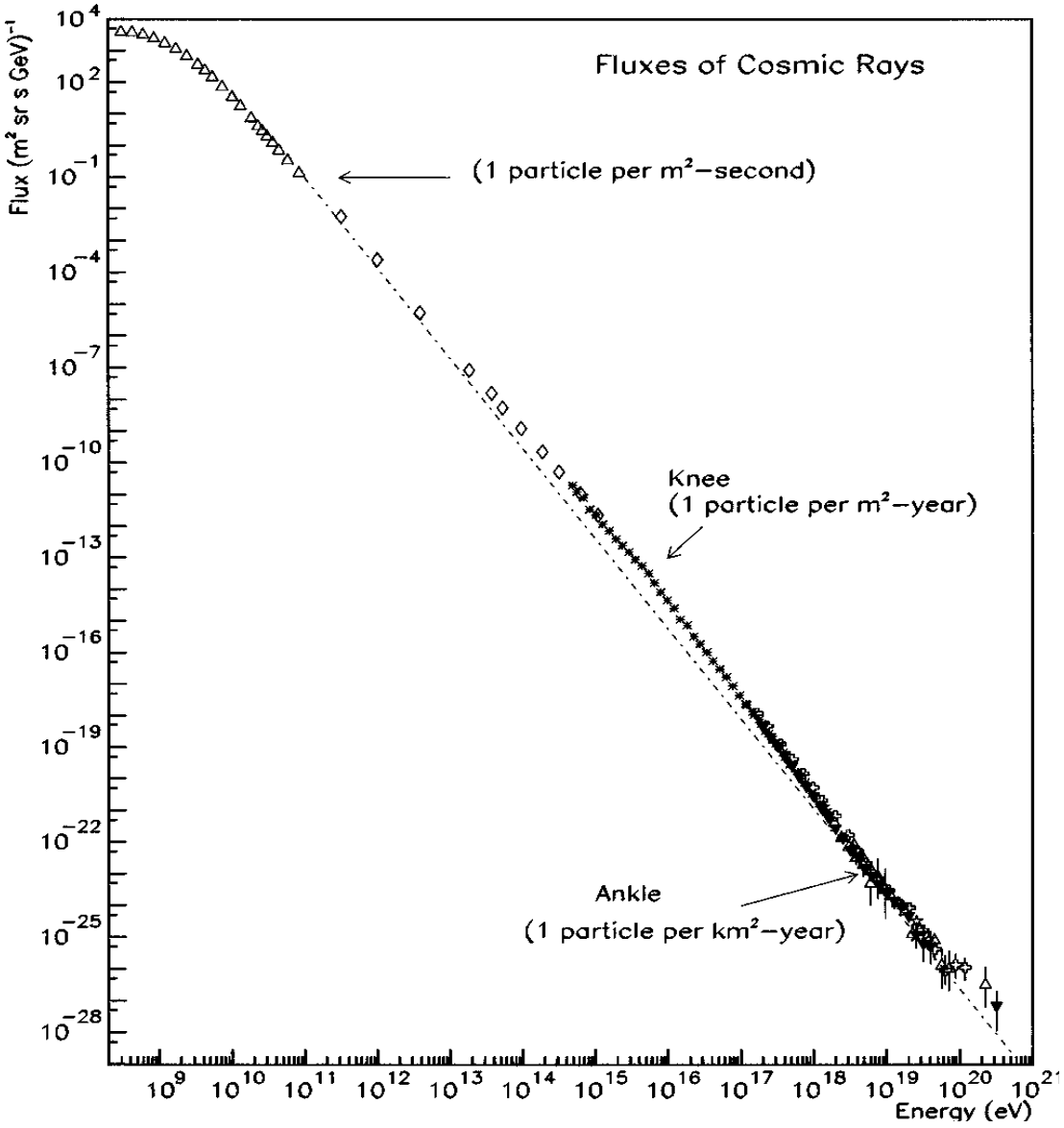

Figure 1: Cosmic ray spectrum taken from [6].

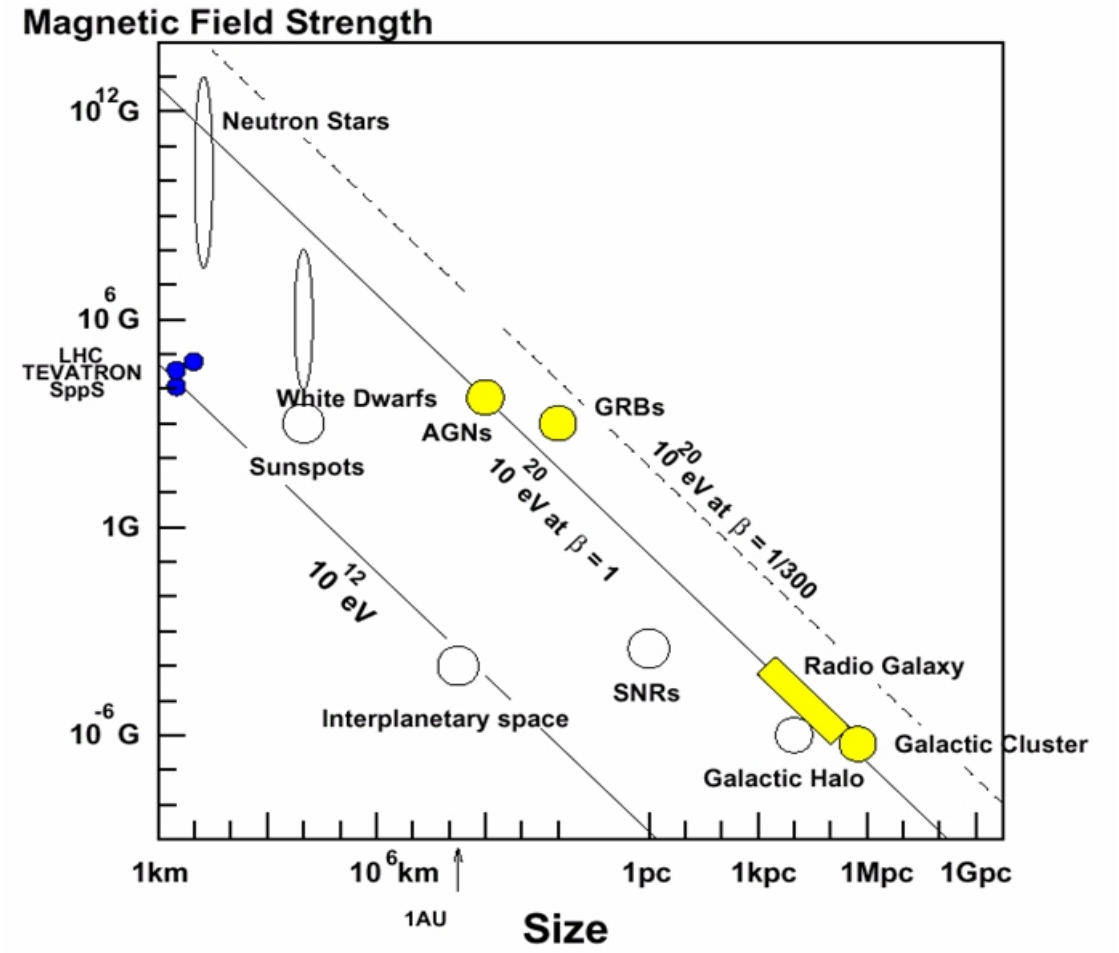

Figure 2: Hillas plot with magnetic field versus size of accelerator.

The region above about 10^{18} eV is termed the "ankle" on the cosmic ray spectrum. Above this energy, another deviation from the E^{-3} spectrum, illustrated by the dashed line in Figure 1, occurs. These particles' compositions and source have thus been unknown (mostly because they are rarely seen due to their incredibly low flux). For example: Events above 100 EeV are only observed about once per square kilometer per century.

1.2 Source Candidates

Although the source of UHECR has not yet been pinpointed, possible source candidates have been proposed. The candidates are proposed as possible sources based on criteria that must be met in order to accelerate particles up to these incredible energies. In order to trap a particle in an acceleration region, a minimum magnetic field is required.

Imagine a cyclotron accelerating charged particles that uses a magnetic field to keep the charged particles in the acceleration region of the machine. The magnetic field forces the charged particles to move in a circle repeatedly. An analogous situation must occur in the acceleration regions of astronomical objects for them to be considered as a possible source of UHECR. Very large magnetic fields like those of neutron stars (10^{12} G) are able to trap charged particles in smaller acceleration regions on the order of kilometers. Therefore, small astronomical objects with smaller acceleration regions require large magnetic fields to trap the particles in the acceleration region of the astronomical object.

On the other hand, if the magnetic fields of an astronomical object are small, say on the order of 10^{-6} G, and cannot trap high energy particles in small regions, a larger acceleration region on the order of Mpc is required. This is illustrated in the Hillas plot of Figure 2 taken from [8]. The diagonal lines illustrate the magnetic field with corresponding acceleration region size required for an astronomical object to accelerate particles up to the stated energy. The first solid diagonal line corresponds to 10^{12} eV accelerators like the Tevatron. The second solid diagonal line corresponds to 10^{20} eV iron nuclei. While, the third dashed diagonal line corresponds to 10^{20} eV protons. The region above 10^{20} eV is of particular interest as it is incredibly difficult to accelerate up to these

energies. Possible acceleration regions include neutron stars, active galactic nuclei, and radio galaxies.

1.3 UHECR Deflection Away from Source

While the source and composition of UHECR are still open to discussion, there has been some evidence from past experiments (such as AGASA in Japan and HiRes in Utah) that these cosmic ray particles may originate from point sources. If we can determine where these particles are coming from, it would help greatly in determining their composition.

The distinction between an UHECR with electromagnetic charge and those without electromagnetic charge is important to make because neutral particles will point back to their source unaffected by magnetic fields. A charged particle moving through the magnetic fields will be deflected away from the source by electromagnetic forces. If UHECR are photons from the decay of some super-heavy unknown particle, as some top-down models suggest; then, the neutral photon will point straight back to the source. However, photon flux measurements appear to disfavor these top-down models [9]. Bottom-up mechanisms that say the UHECR are accelerated from low energy to high energy require that the particle have a charge. As the top-down mechanism is disfavored by photon flux measurements, it is believed that these particles may be protons or other atomic nuclei which have charge. Being charged particles, they will undergo deflection while traveling through the galactic and extra-galactic magnetic fields.

The magnitude of these fields is not yet well-known. However, it is thought that the galactic magnetic field is on the order of 10^{-6} G, while that outside the galaxies is on the order of 10^{-9} G. Therefore, as these particles travel through these magnetic fields, they will undergo deflection causing the UHECR arrival direction to not coincide with the exact location of the source. Figure 3

taken from [10] shows the deflections undergone by a 40 EeV proton traveling 107 Mpc. The proton primary undergoes larger deflections as it moves through regions with large fields that coincide with locations of high mass density. Figure 3 is specific for a proton of 40 EeV from 107 Mpc away. In general, the amount of deflection δ any charged particle with charge Z and energy E traveling through a magnetic field B for a distance L is proportional to:

$$\delta \propto \frac{ZBL}{E} \tag{1}$$

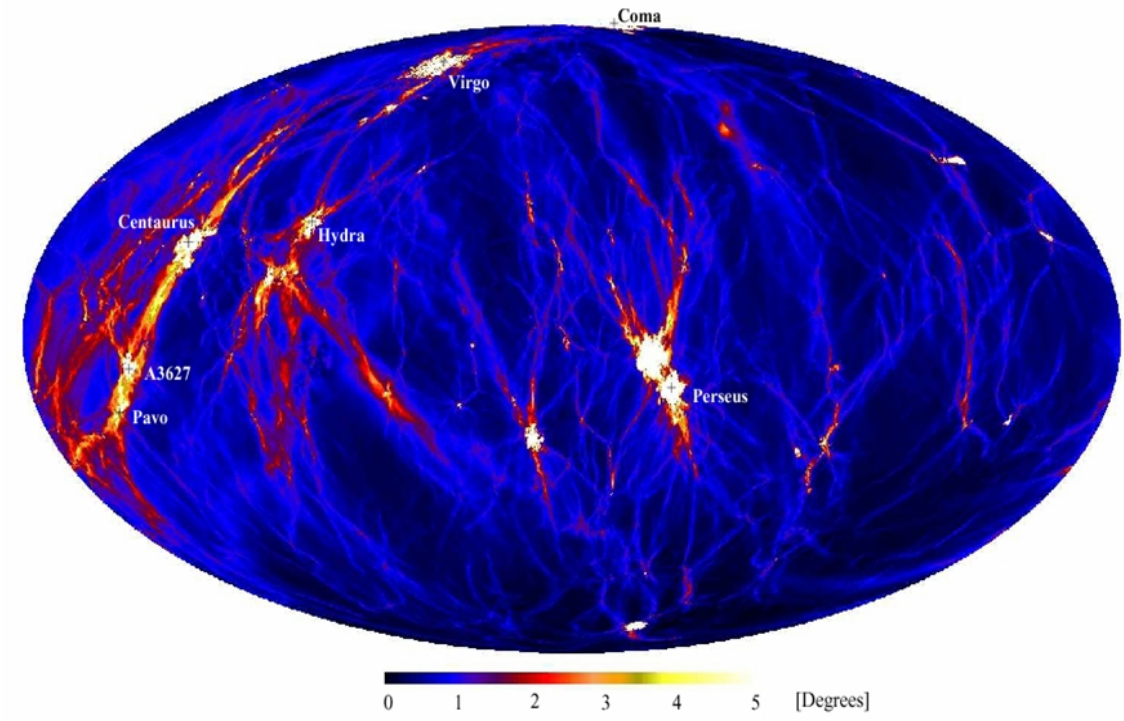

Figure 3: Full sky map in galactic coordinates with galactic anti-center at center showing deflections for 40 EeV protons from 107 Mpc away. Picture taken from [10].

The Larmor radius R_L in Mpc for a charged particle moving in a magnetic field is determined in [11] to be:

$$R_L(Mpc) \approx \frac{100}{Z} \times \frac{E(100\text{EeV})}{B(nG)} \tag{2}$$

where Z is the charge, *E(100EeV)* is the particle energy in units of 100EeV, *B (nG)* is the magnetic fields in units of 10^{-9} G. The coherent length for the magnetic fields is on the order of 0.5-1 Mpc [11]. If the Larmor radius of a particle is much larger than the coherent length of the fields, then the particle will undergo almost straight line trajectories with small deviations given by:

$$\delta \approx \frac{0.3^0 L(Mpc) Z B(nG)}{E(100\text{EeV})} \tag{3}$$

where *L(Mpc)* is the distance traveled by the charged particle in units of Mpc [11]. If the Larmor radius gets closer to the coherent length of the magnetic fields, the deflection undergone by the charged particle is more accurately determined by a random walk away from the source given by:

$$\delta \approx 0.54^0 \left(\frac{l}{1\,Mpc}\right)^{\frac{1}{2}} \frac{L(Mpc)^{\frac{1}{2}} Z B(nG)}{E(100\text{EeV})} \tag{4}$$

where *l* is the coherent length of the fields [11]. If the deflections of the UHECR are large, then it will be difficult to accurately determine the source location, as they will be scrambled all over the sky.

1.4 Greisen-Zatsepin-Kuzmin Cut-Off

The Greisen-Zatsepin-Kuzmin (GZK) affect, which describes the interaction of the UHECR with the Cosmic Microwave Background (CMB), predicts a sharp drop in the flux of UHECR. Figure 4

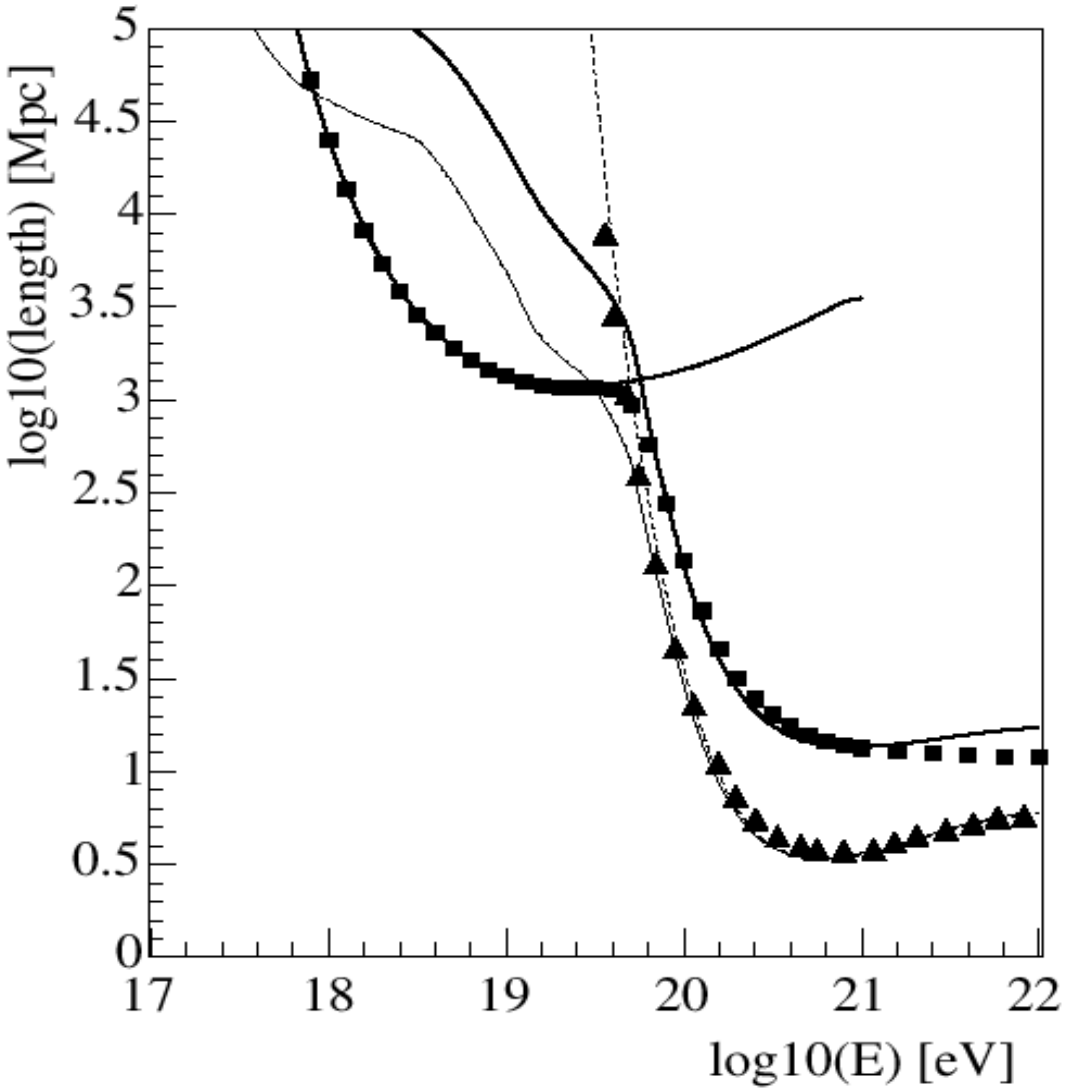

Figure 4: Taken from [12]. Dashed line, solid line and triangles show the interaction lengths. The thick solid lines and squares are the loss lengths for photopion production (on the right) and of pair production (on the left).

taken from [12] shows that the distance a UHECR can travel decreases dramatically due to photopion production. The plot shows that as the energy of the primary increases, the distance that it can travel is greatly reduced. Additionally, it shows two different mechanisms for energy loss: pair production and pion production. For the higher energy primaries, it can be seen that the primary source of energy loss is by pion production. This substantial reduction in the UHECR energy means that any cosmic ray that still has high energy has not traveled very far through the opaque Universe. For a 100 EeV proton, the photopion production decreases the distance of travel from about 1 Gpc down to about 10 Mpc. Interaction with the roughly 3^0 Kelvin CMB photons causes the primary cosmic ray particle to become excited giving a Δ^+, which quickly decays into a nucleon of lesser energy and a pion as shown below.

$$p + \gamma_{CMB} \rightarrow \Delta^+ \rightarrow p + \pi \tag{5}$$

A proton primary of energy 100 EeV has a cross section of about 200 μbarn to interact with the $7 \cdot 10^{-4}$ eV photons of the approximately 3^0 black-body CMB spectrum [13]. The mean free path of interaction for a 100 EeV proton primary with the 550 cm^{-3} CMB photons is a few Mpc, while the loss length is about 10 Mpc. Therefore, we expect any detected UHECR particles to have sources in our cosmic neighborhood, otherwise the primary would have lost a substantial amount of its energy.

1.5 Scientific Motivation Summary

The GZK effect tells us that any UHECR that are detected should have come from nearby. In addition, the very high energies of the particles indicate that their deflections will likely be small. This makes it possible to do UHECR astronomy.

The photon flux determined by the Pierre Auger Observatory shows that the UHECR are not photons, disfavoring a top-down mechanism for UHECR creation. Instead, a bottom-up mechanism for UHECR creation requires that the source have the correct combination of sufficiently large magnetic field strength to trap the charged particle in the acceleration region and acceleration region size. This allows us to narrow our search for a source to very specific types of objects; like, active galactic nuclei and radio galaxies.

CHAPTER 2

How to Detect UHECR

The UHECR that happen to cross Earth's path strongly interact with the molecules in our atmosphere. This strong interaction results in the creation of pions. The initial interaction, which starts the shower cascade, happens in the upper atmosphere at a depth of about 70 gm/cm^2 for protons and less for heavier nuclei. The charged pions decay into muons and its corresponding neutrino. The neutral pion decays very quickly electromagnetically into two photons, which continue to interact creating the electromagnetic component of the shower.

About a third of the initial primary's energy goes towards neutral pion production, which starts the electromagnetic component of the shower. This component of the shower consists of pair produced electrons and positrons, along with the emission of more photons. Figure 5 shows a cartoon illustration of this interaction. The electrons and positrons that constitute about 90% of the shower reach the ground with energies of approximately MeV. The electromagnetic component initiated by photons produced in the neutral pion decay will pair produce after a radiation length roughly splitting its energy equally between the electron and positron. These particles will emit photons themselves splitting their energy by about another half after a radiation length. These photons themselves pair produce and split their energy on average equally between an electron and

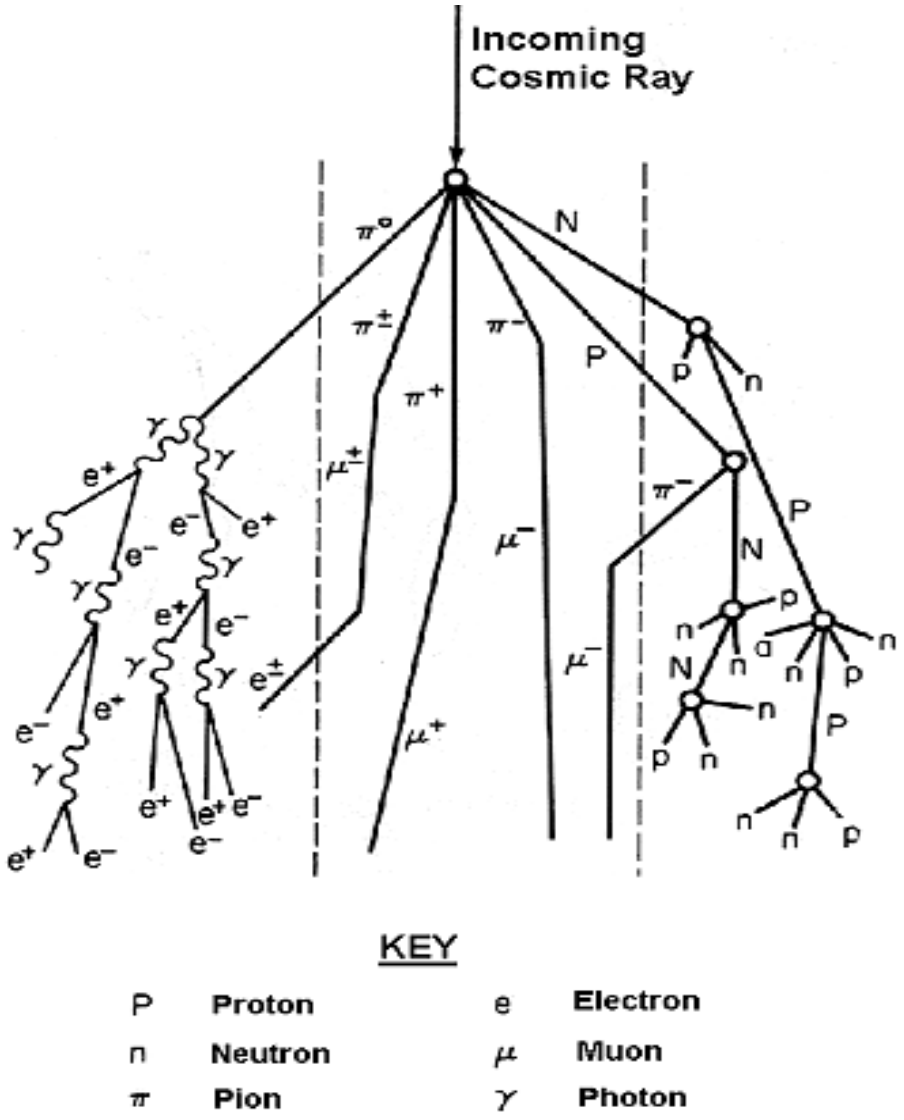

Figure 5: Shower of particles resulting after primary interacts with atmospheric molecules [14]. As the UHECR primary enters the atmosphere, it will undergo strong interactions resulting in the creation of pions. The neutral pions will decay into two photons which will start electromagnetic cascades, while the charged pions will decay into muons and its corresponding neutrino.

positron pair after another radiation length. This process continues until the electromagnetic shower particle's energy falls below some critical value.

This critical energy corresponds to the regime in which energy losses due to ionization outweigh that due to bremsstrahlung. In this regime, no new particles are produced and the size of the shower begins to decrease. The size of the shower at its maximum will then be proportional to the energy of the initial photons. The distance from the initiation of the shower in the upper atmosphere down to the ground where the surface array is located is about 27 radiation lengths.

The muonic component, which constitutes about 10% of the shower, reaches the ground with particle energies of about GeV. These particles are produced by the charged pions generated in the initial interaction of the primary in the atmosphere. The distance at the top of the atmosphere where the shower first begins down to the ground is about 11 interaction lengths.

The existence of the initial primary UHECR will be deduced by observing the particle shower in the atmosphere initiated by the UHECR. The particles in the shower can be observed if we exploit their high energies and speeds. Two different methods of detection can be used to see the shower of secondary particles initiated by the primary.

The first method of shower detection allows for the observation of the lateral distribution of the shower. In this method, a ground array is used to measure the signal deposited by the passing shower front. Using this method, one can determine the direction and the relative size of the shower. The Akeno Giant Air Shower Array utilized this method.

The second method of shower detection consists of observing the fluorescent light emitted by nitrogen in the atmosphere that has been excited by the passing shower fronts particles. This method allows for the determination of the shower energy calorimetrically. Additionally, the longitudinal

profile of the shower can be observed along with the direction from which the primary particle came from. This method was employed by the HiRes detector in Utah.

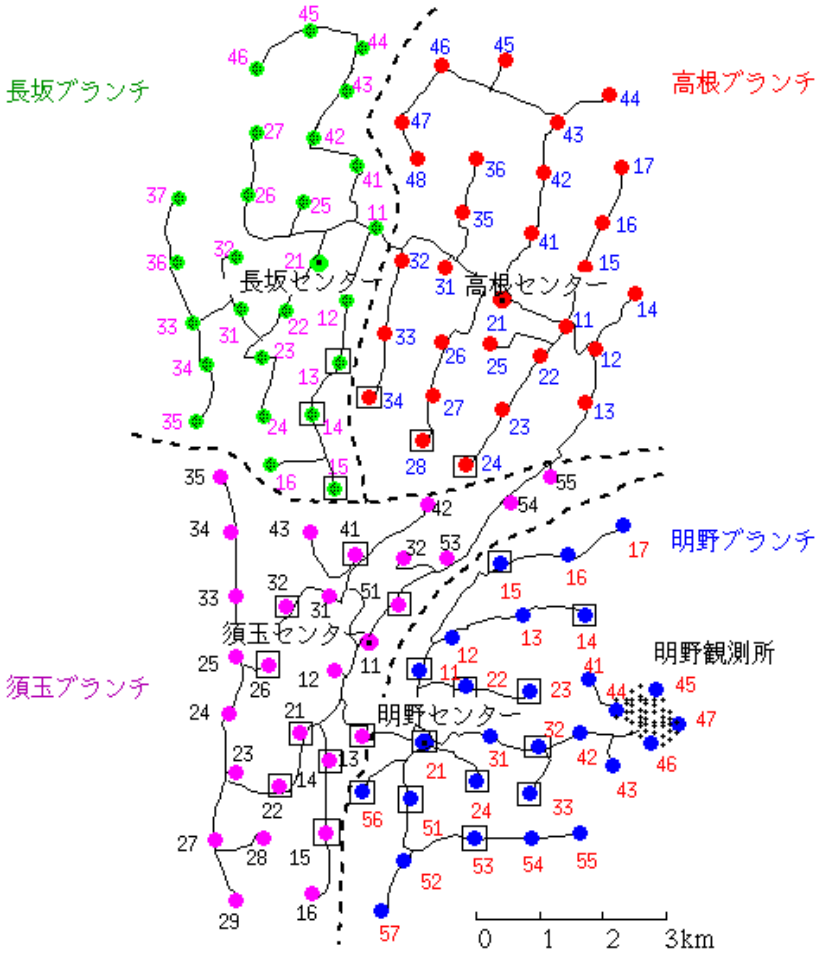

Figure 6: AGASA ground array taken from [15]. The array is about 100 km^2 and includes electron detectors and muon detectors.

2.1 Surface Detector

The first method of shower detection was employed by the Akeno Giant Air Shower Array (AGASA) in Japan shown in Figure 6 taken from [15]. The array is about 100 km^2 and includes 111

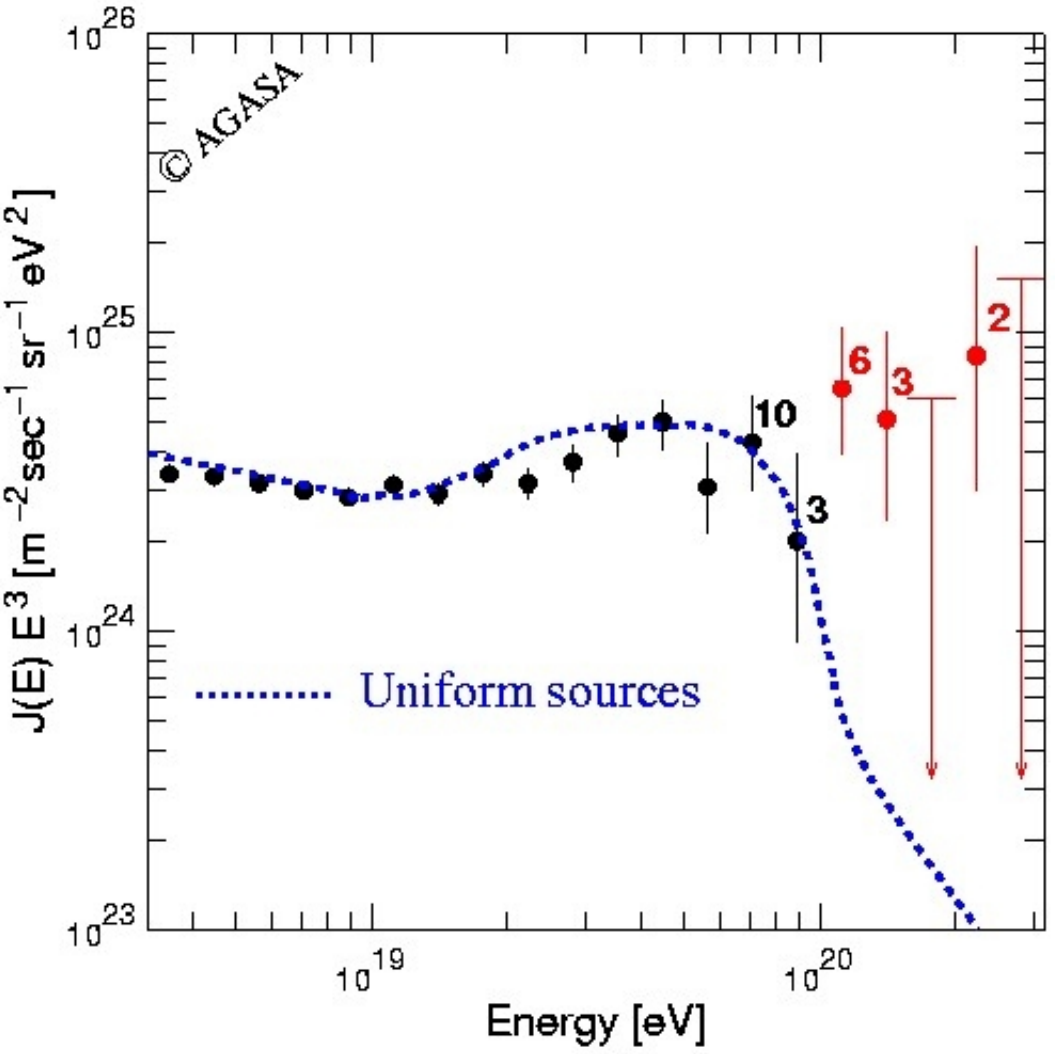

Figure 7: AGASA Spectrum taken from [16]. Blue dashed line expected for uniformally distributed extragalactic sources. The events beyond 10^{20} eV suggest a top-down mechanism for UHECR creation and unknown particle physics.

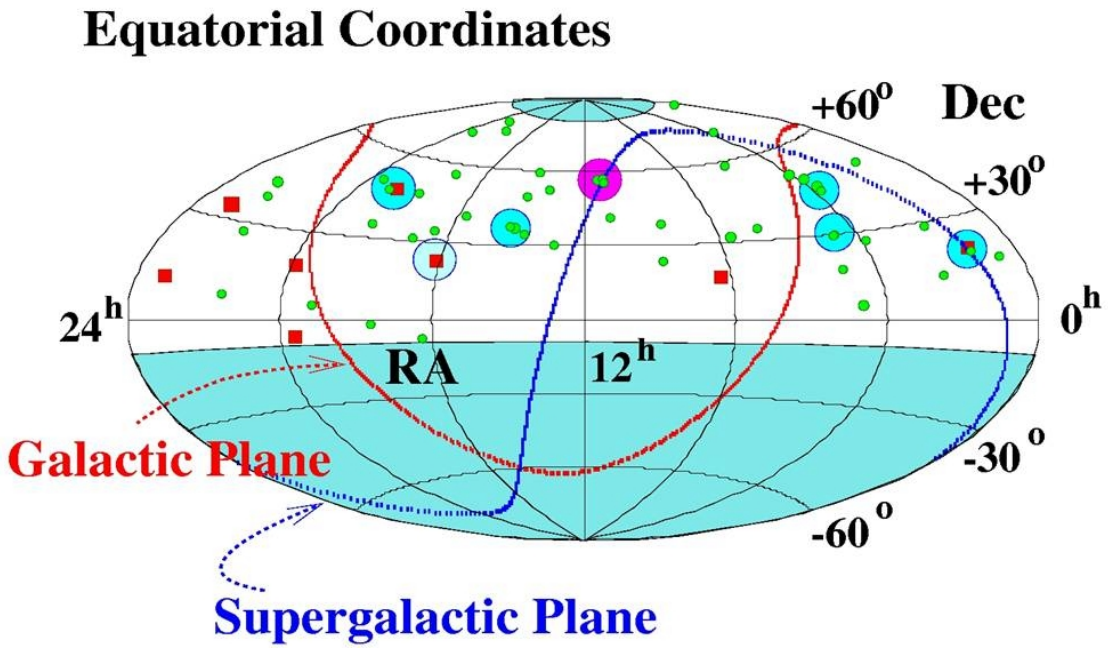

Figure 8: AGASA equatorial sky map taken from [17]. The UHECR events with energies between 40-100EeV are shown as green circles while events with energies larger than 100EeV are shown as red squares. The Galactic Plane is shown as the red line and the Supergalactic Plane is shown as the blue line. The six doublets are shown as blue circles and the triplet is shown as the purple circle. The shaded blue region is not seen by the AGASA Detector.

electron detectors and 27 muon detectors. It was operational from 1991 until 2004 with integrated exposure of 1.6×10^3 km^2.sr.year. AGASA was able to determine a spectrum that is shown in Figure 7 taken from [16]. This spectrum showed events beyond the GZK cutoff. This suggested that perhaps the UHECR were originating nearby as a result of the decay of some mysterious unknown

particle. This spectrum illustrates important differences with the spectrum found with HiRes.

In addition, AGASA concluded that, among the 56 events above 40 EeV, clustering occurs at 2.5 degrees at 10^{-4} significance. Figure 8 taken from [17] shows the equatorial sky map produced by AGASA showing events above 40 EeV, within 45 degrees zenith. The map is in equatorial coordinates with the Galactic Plane shown as the red line and the Supergalactic Plane shown as a blue line. The blue-shaded region is not visible to the AGASA Detector. There are six doublets shown (as blue circles) and a triplet shown (as a purple circle). The events above 100EeV are shown as red squares, while those between 40-100EeV are shown as green circles.

2.2 Fluorescence Detector

The second method of detecting the shower is by observing the fluorescence of the nitrogen when excited by the passing shower particles. The HiRes detector located in Utah used this method to observe the shower of secondary particles passing through the atmosphere. Figure 9 shows the HiRes2 detector, which includes 42 mirrors able to observe between 3 degrees and 31 degrees in elevation. HiRes was able to observe events beyond the ankle and determine the cosmic ray spectrum shown in Figure 10.

This spectrum is multiplied by E^3 in order to make subtle changes in the spectrum more obvious. This spectrum shows consistency with a bottom-up acceleration of the UHECR. This means that the particle initially has a low energy and is accelerated up to higher energies in acceleration regions. The spectrum is consistent with the GZK affect in that the flux of particles drops off abruptly at the very end of the spectrum as the Universe becomes opaque for these UHECR. The solid green line in Figure 10 from [18] shows the spectrum expected if the source of

Figure 9: HiRes2 from G. Thomson. The HiRes detector sees the fluorescence of the atmospheric nitrogen that have been excited by passing shower particles.

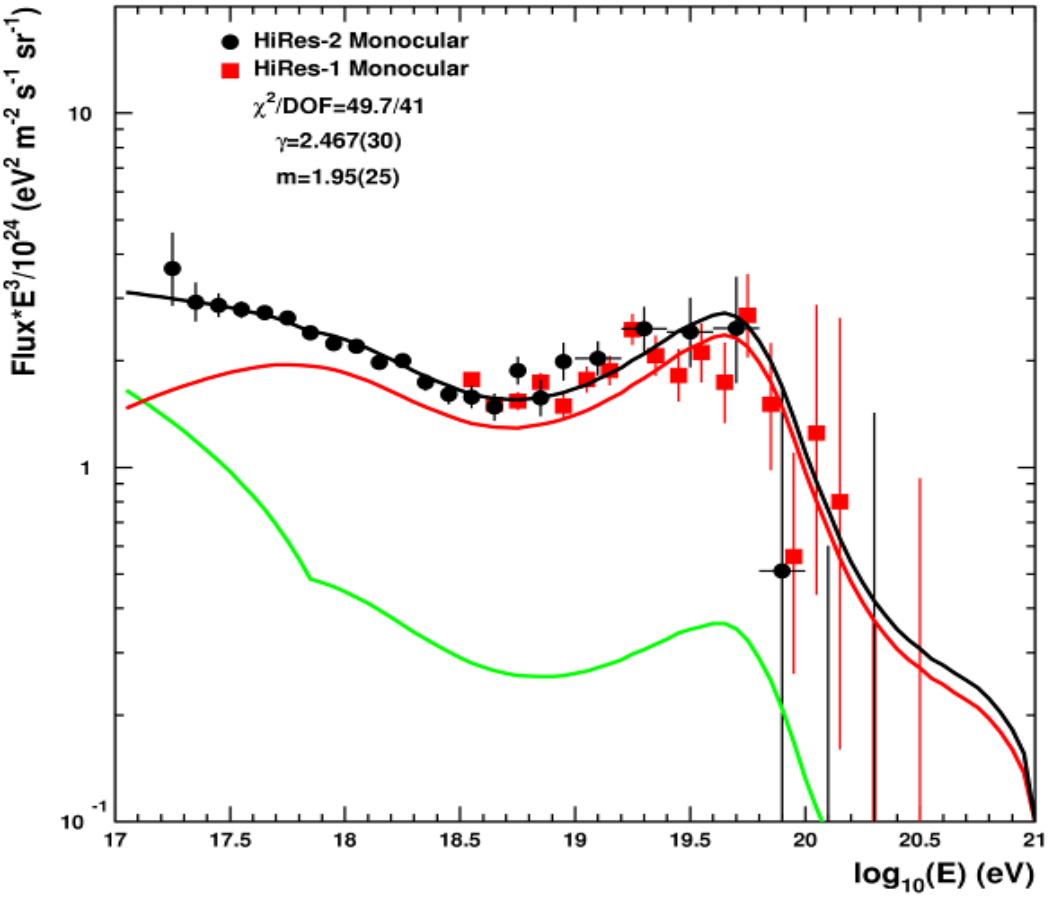

Figure 10: HiRes Spectrum. Green line theoretical spectrum for galactic sources. Red and black lines consistent with uniformly distributed extragalactic sources. The HiRes spectrum shows the GZK feature as the flux drops drastically after 10^{20}eV. The HiRes spectrum suggests that the UHECR are created via a bottom-up mechanism by extragalactic sources. Taken from [18].

the UHECR was galactic, while the red and black solid lines are expected for UHECR whose source is uniformally distributed and extragalactic in origin. Therefore, the HiRes spectrum indicates that the UHECR are extragalactic in origin.

In addition to the spectrum, HiRes was able to observe the longitudinal profile of the shower generated by the secondary particles initiated by the primary particle, and thereby deduce the direction from which the particle came. HiRes observed that the direction from which these UHECR came, coincided with the direction of extragalactic objects known as BL Lacertae. These BL Lacertae are a subclass of active galactic nuclei, which are thought to be super-massive black holes at the centers of galaxies.

In the end, these two detectors did not confirm each others' findings. The HiRes spectrum and the direction from which the UHECR come from indicate that the UHECR are likely accelerated in extragalactic objects known as BL Lacertae. On the other hand, AGASA shows evidence of events beyond the GZK and clustering of its events. This indicates that the observed UHECR may result from the decay of strange unknown massive particles, thereby achieving their incredible energies via a top down mechanism. Both of these observations need to be confirmed with an independent data set.

2.3 UHECR Detection Summary

In the end, AGASA showed super GZK events that suggested a top-down mechanism for UHECR creation, possibly the result of the decay of some unknown super-massive particle. The clustering of UHECR that AGASA saw added the chance of locating the source of these particles. HiRes, on the other hand, showed a spectrum that was consistent with the GZK effect and suggested that a bottom-up mechanism may be at play in the acceleration of these particles. The Pierre Auger Observatory was specifically made to provide the evidence to determine what the true origin of these particles is.

CHAPTER 3

Pierre Auger Observatory

The UHECR that will allow us to do our astronomy are very special. They have extremely high energies and are very rare. Above 100 EeV, only one particle per square kilometer per century is expected. In order to collect enough of them to do analysis in a reasonable amount of time, a very large detector is needed. The Auger Observatory in Malargue, Argentina was built very large specifically for this reason. The detector covers 3,000 km^2. Figure 11 shows the detector layout where each red dot represents a surface detector (SD) spaced 1.5 km apart from its neighbors. The Pierre Auger Observatory (PAO) utilizes both of these methods of detection. It includes 24 fluorescence telescopes housed at four locations on the periphery of a massive ground array.

More than 280 scientists, from 17 different countries and over 70 different institutions, belong to the collaboration that built and maintained the detector. The size and complexity of the detector required the work and input of many hands. With the help of all these people, I was able to do this analysis.

3.1 PAO Fluorescence Detector

There are four fluorescence detectors (FD) on the periphery of the ground array whose names are

shown in yellow boxes in Figure 11. The green lines emanating from each of the four FD detectors are 20 kilometers long. Each of the four fluorescence detectors on the periphery of the grid contain six telescopes. One of the four stations around the periphery of the ground array is shown in Figure 12. This station contains six individual 11 m^2 mirrors shown in Figure 13. This figure also shows the 22x20 array of PMTs that collect the light reflected off of the mirrors and feed it to a 12-bit ADC every 100ns [19]. In front of the mirror, there is a filter that only allows fluorescent light in the range of 300-400 nm to pass through corresponding to the light emitted by the excited atmospheric nitrogen.

The down side of the FD detector is that it can only work on dark moonless nights; whereas, the SD can operate all the time. The purpose of the FD is to measure the longitudinal profile of the shower as it moves through the atmosphere. Specifically, we want to measure the number of particles at the shower maximum N_{max}, which will allow a calorimetric measurement of the primary UHECR energy.

A complete calibration of the FD is done a couple times a year by illuminating the PMT with a known light source and monitoring the response of the detector. This complete calibration is labor intensive. So, an easier calibration of the PMT is done on a nightly basis by illuminating the PMT with a known LED light source, and comparing the PMT response against that of a calibrated PMT. The attenuation of the fluorescent light as it travels through the atmosphere must also be known in order to get an accurate N_{max}; and therefore, atmospheric conditions are monitored so that corrections can be made. In the end, FD measures the depth of shower maximum X_{max} with a resolution of 20 gm/cm^2 and a 10% error in energy [20].

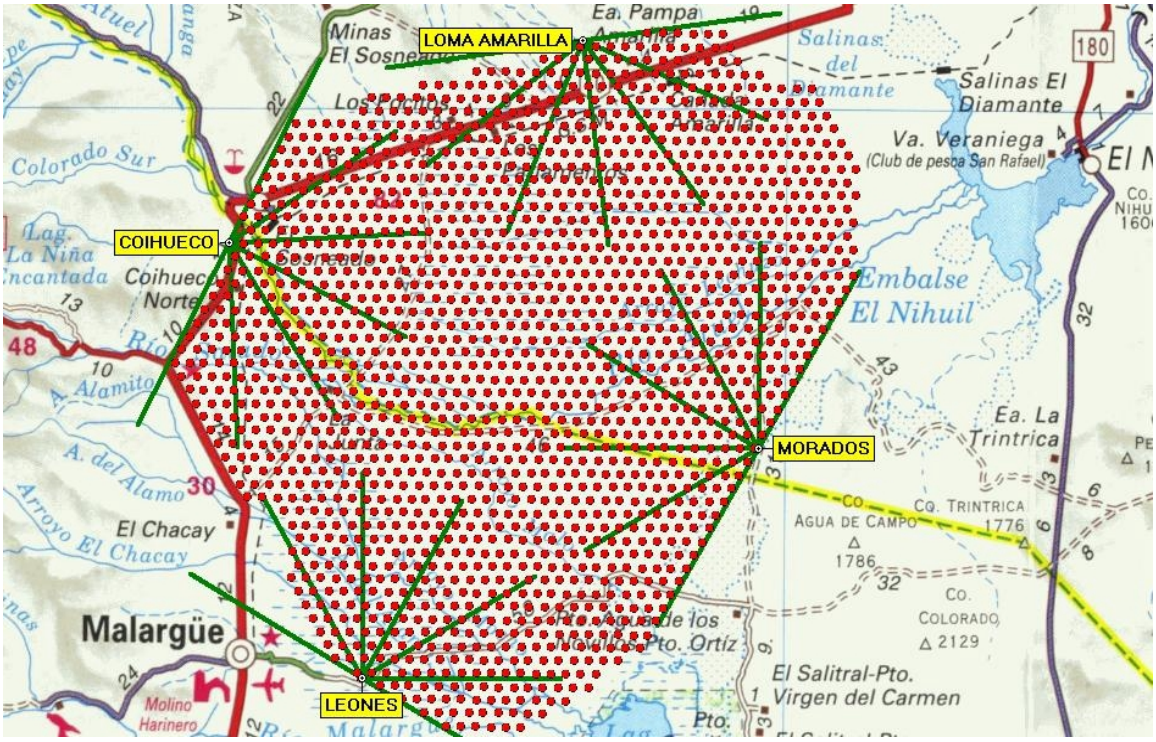

Figure 11: Pierre Auger Observatory when completed will have 1600 surface detectors spaced 1.5 km apart covering 3000 km^2. Each one of the red dots shown above is a single SD station. The four fluorescence detectors are on the periphery of the ground array with their names shown in the yellow boxes. The green lines emanating from each of the four FD detectors are 20 kilometers long.

Figure 12: One of four FD stations on the periphery of the SD array. The FD station contains six mirrors that reflect fluorescence from the excited atmospheric nitrogen on an array of 440 PMTs.

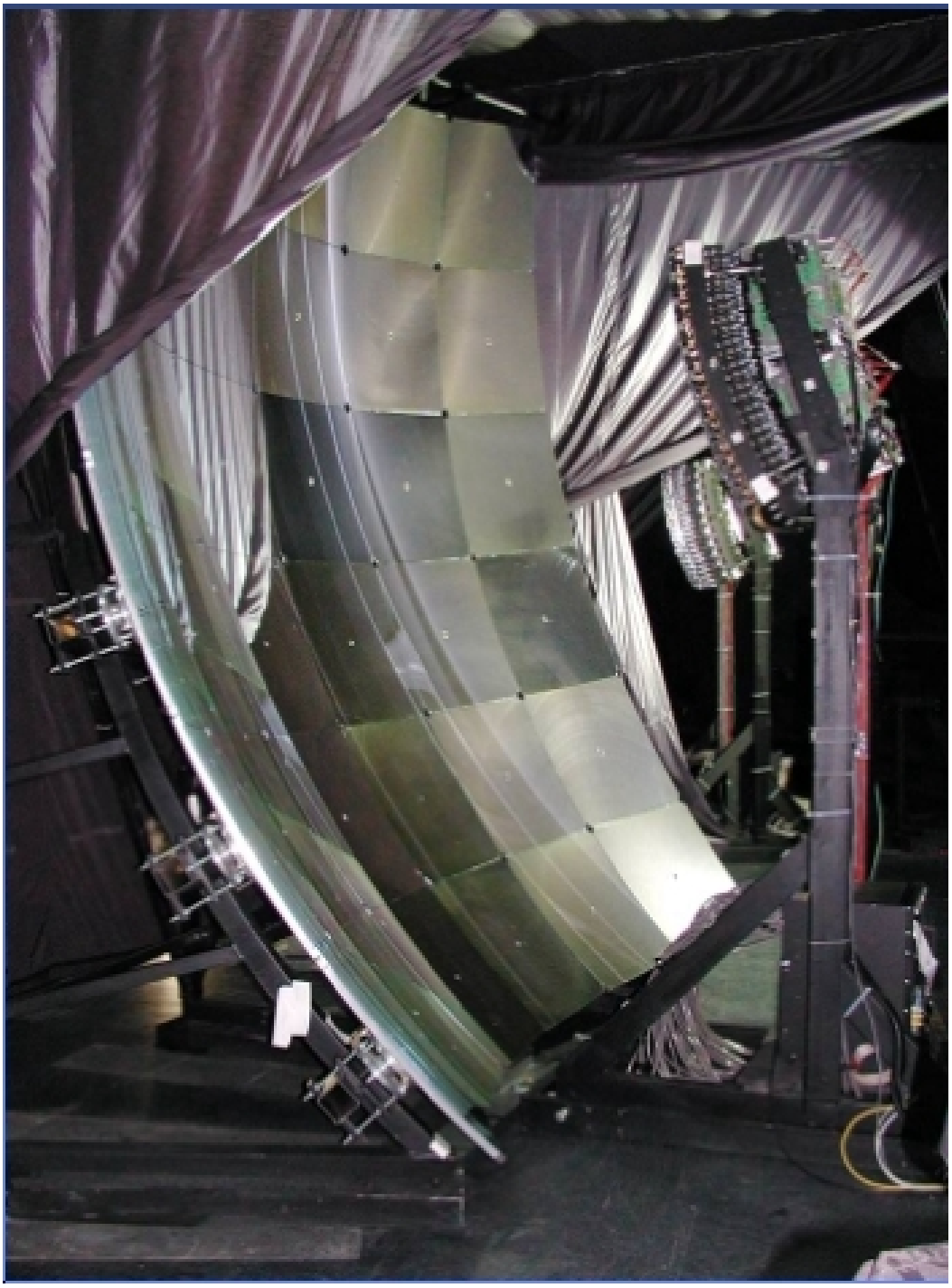

Figure 13: One of the six 11 m^2 mirrors in the FD stations. The mirror reflects fluorescent light from excited atmospheric nitrogen onto an array of 440 PMTs shown in the upper right of the figure.

Coincidence on multiple PMT serves as a trigger resulting in the information being sent to the Central Data Acquisition System (CDAS). At CDAS, the surface detector is also being monitored in order to find "hybrid" events, which are events seen by both the FD and the surface array. About 10% of events are hybrid.

3.2 PAO Surface Detector

Each of the red dots on Figure 11 of the surface detector (SD) is a water tank like the one shown in Figures 14 and 15. If the secondary shower particles happen to enter water moving faster than the speed of light in water, they will emit Cherenkov radiation. This emission of radiation will betray the presence of the secondary shower particle as it radiates in the water tank. Figures 14 and 15 show one of the 1,600 water tanks that make up the array of Cherenkov detectors of the Auger Observatory SD. Each station includes two car batteries that power the station. Solar panels are used to charge the batteries. Each tank has three nine-inch photomultiplier tubes. Timing and location of events are determined by the GPS at each station. The communications antenna allows communication with CDAS. The water inside the SD station is 1.2 meters tall and has an area of ten square meters.

One of the nine-inch photomultiplier tubes that detect the Cherenkov radiation deposited in the water tank by shower particles is shown in Figure 16. Each PMT has a low gain channel and a high gain channel from the anode and last dynode respectively, with the dynode gain ~32 times the anode[19]. Each channel's signal is passed through a 20MHz filter and digitized via a 40 MHz Flash Analog to Digital Converter (FADC)[19]. Each channels digitized voltage signal is stored as a 10-bit value. The two channels have 5 bits of overlap giving a large dynamic range able to measure from a few photoelectrons to ~20,000 photoelectrons [19][21]. The PMT voltage corresponds to a

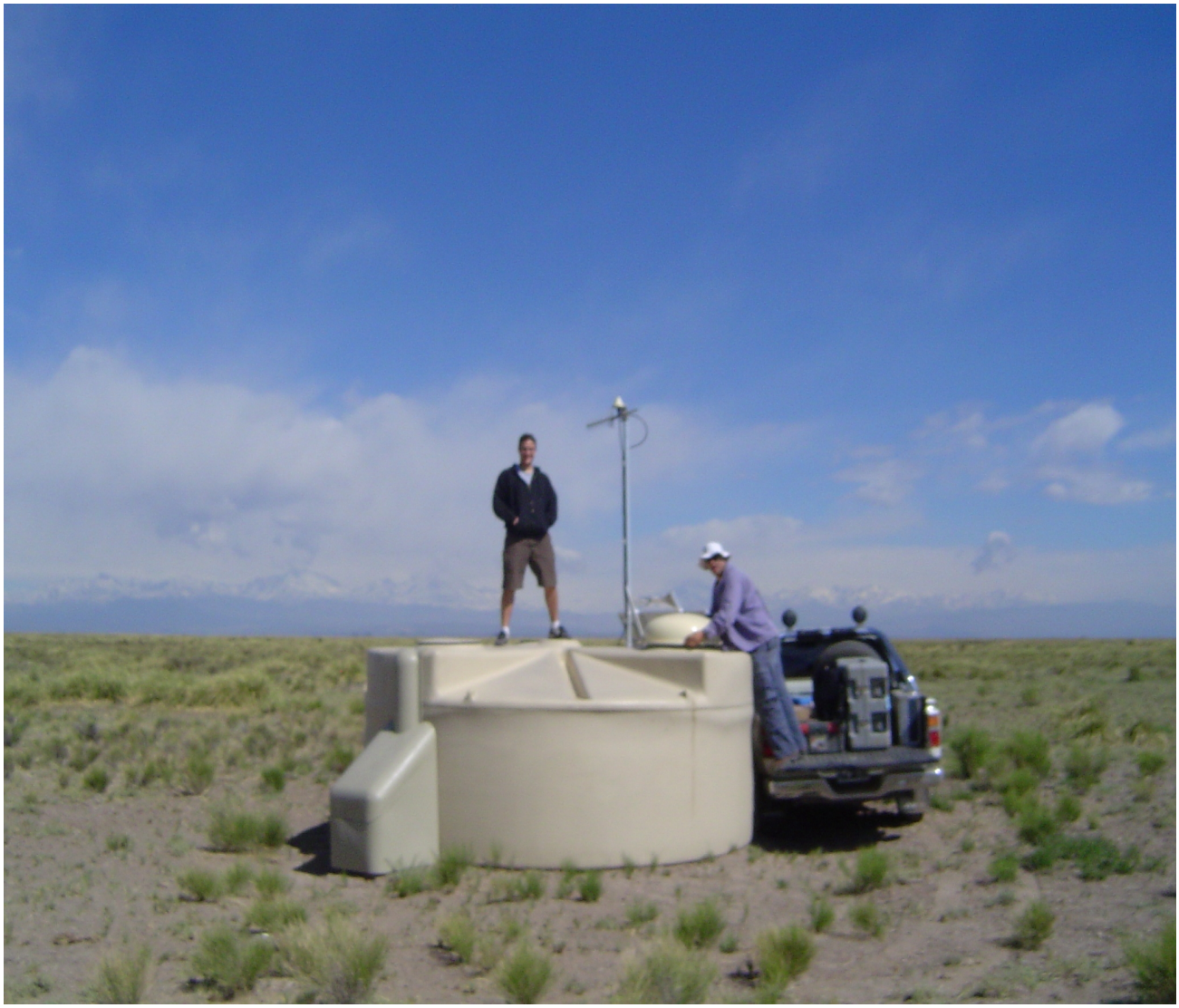

Figure 14: One of 1600 surface detectors on the Pampa in Argentina.

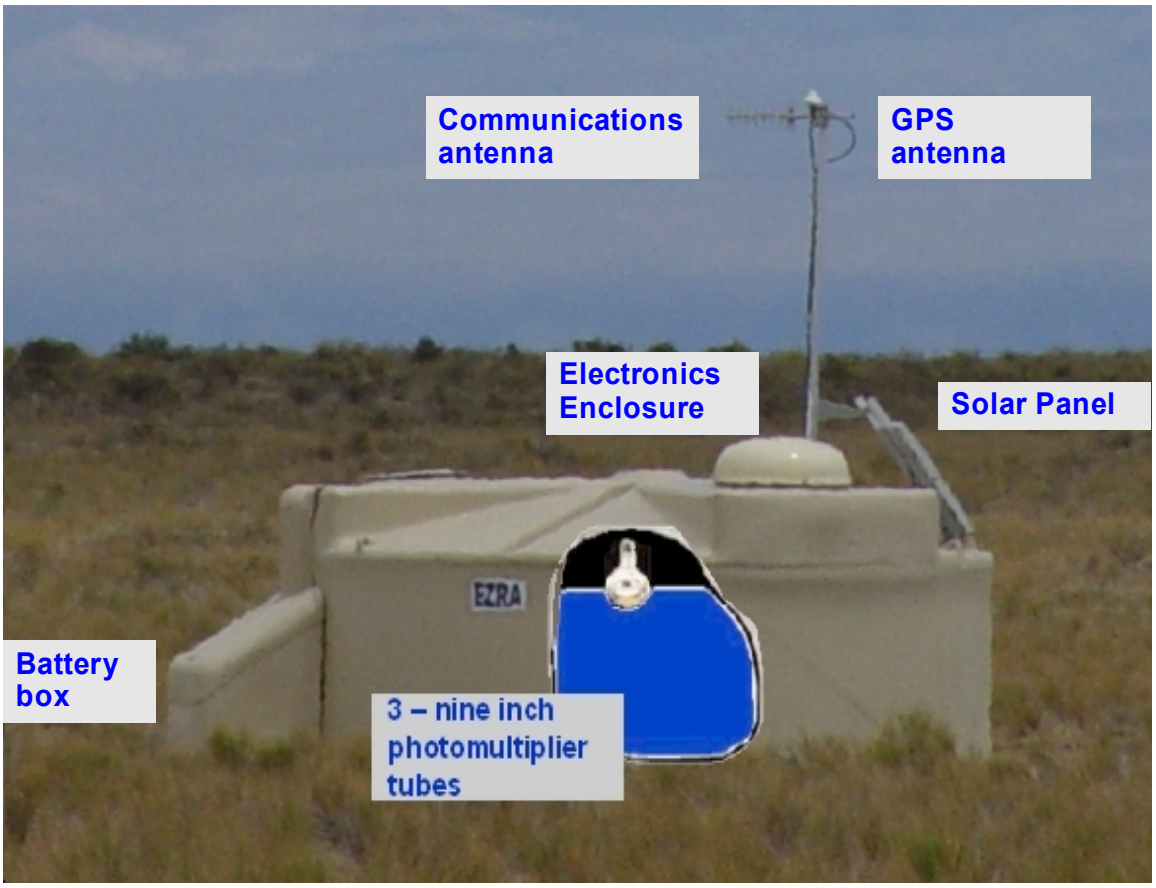

Figure 15: One of 1600 surface detectors on the Pampa in Argentina with components shown.

current whose time integral gives a charge, which gives the signal strength. The units used to measure the size of the signal on the SD is given in vertical equivalent muons. The unit is a convenient unit to use due to the abundance of atmospheric muons. The histogram of integrated charge of a threefold coincidence on a tank is shown in Figure 17. The second peak is due to vertical through-going muons [22], while the first peak is a triggering effect. The UHECR travel towards us for millions of years and by chance happen to cross Earth's path. They interact with the

particles in the atmosphere and create secondary particles, which also interact with the atmospheric molecules resulting in a massive cascading shower. A cartoon drawing of a shower cascade can be

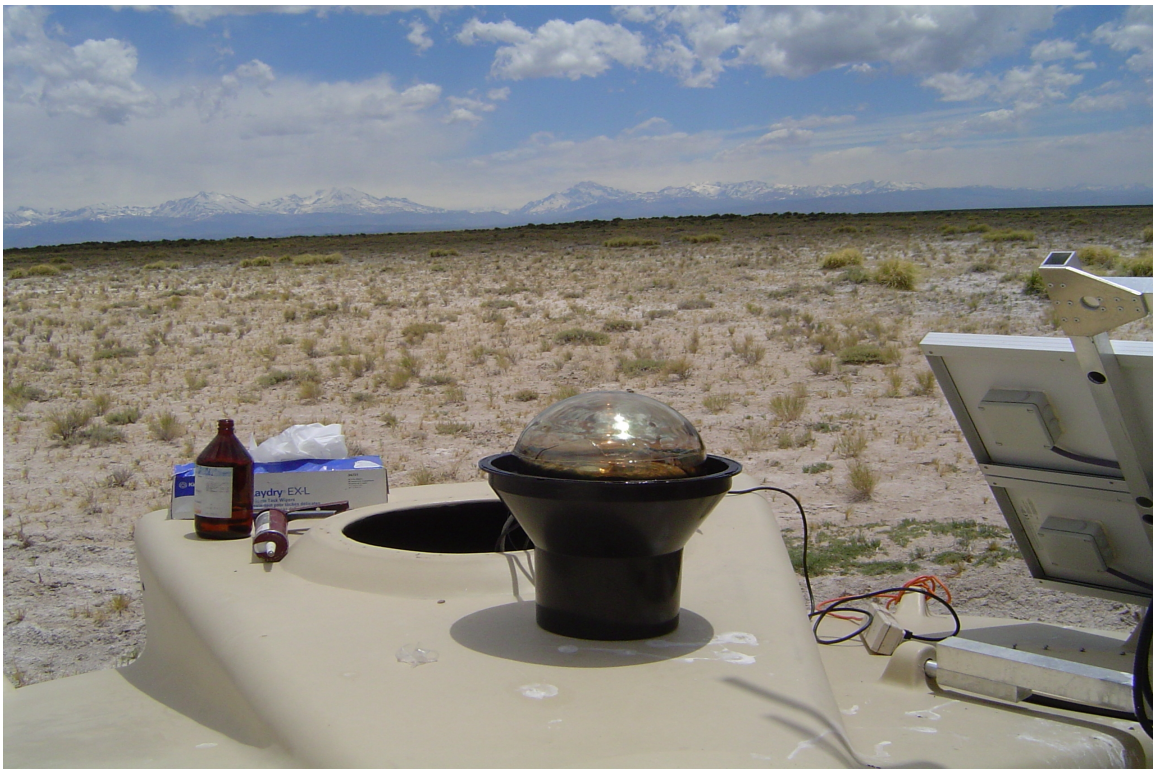

Figure 16: One of the three nine-inch PMTs in each SD tank.

seen in Figure 5. These particles are traveling close to the speed of light; and therefore, if they pass through a tank of water will lose energy via Cherenkov radiation, which will be seen by the PMT.

In order to distinguish between atmospheric muons in general and those associated with a shower, a five-step triggering scheme is required. The T1 and T2 triggers are done locally at each SD station based on the coincidence of at least 2 PMT [19]. The T3 trigger is not made at each station, but rather at CDAS. T3 requires that at least three non-aligned tanks correlate in time. At

least three tanks are required in order to recreate a plane shower front. There are about 1.3 T3 events a day per triangle of SD tanks [19]. T4 is satisfied, if the three non-aligned tanks are a true shower. This entails that the times and positions of the coincident tanks agree with that of a plane shower

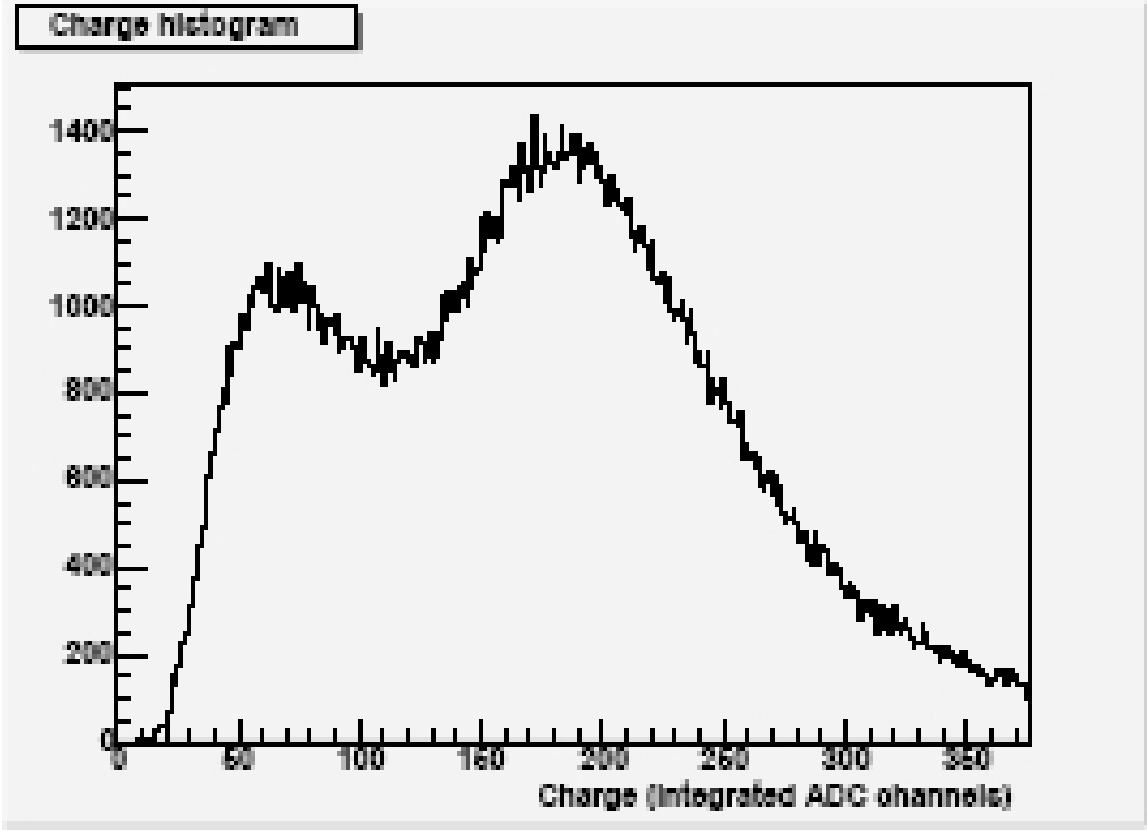

Figure 17: Integrated charge of threefold coincidence. The first peak is a triggering effect. The second peak corresponds to through-going muons. Taken from [22].

front moving at near the speed of light. The last trigger is a quality cut requiring that at least five tanks surrounding the tank with the largest signal be operational.

3.3 Reconstruction of UHECR Energy and Direction

The locations of each tank and the time that it registers a hit are used to determine the shower front plane and the pointing direction from which the primary UHECR came from. This direction will be perpendicular to the shower plane. Figure 18 illustrates how the shower front is observed by the SD. The graph in the upper left illustrates the signal size seen by the different SD stations, with the size of the dot corresponding to the magnitude of the signal. The x-y axis shows the position in kilometers of the SD station on the array grid. The time at which the signal was observed is indicated with color, red happening first and violet happening last.

The time ordering of the signals seen by the individual tanks is shown in the upper right of Figure 18. The x-axis shows time (ns), while the y-axis represents signal size. The time ordering of the signals along with the location of the tanks makes it possible to determine the plane of the shower front and the direction from which the shower came. A line can be reconstructed given at least two points on that line and analogously a plane can be reconstructed using at least three points on the plane. The direction from which the UHECR primary has come is perpendicular to this plane.

The lateral distribution function shown in the bottom left of the Figure 18 shows the signal strength in VEM versus the distance from the shower core in meters.

The signal strength, 1000 meters from the core, is used to determine the energy of the primary. The correlation between S1000 and the energy of the primary can be found from the comparison of hybrid events, which are events seen by both the SD and FD. Hybrid events allow the determination of the primary particle energy through the measurement of the fluorescence seen by the FD, while the SD measures S1000. FD makes a completely calorimetic measurement of the primary UHECR energy. This makes it possible to determine a map between S1000 and energy.

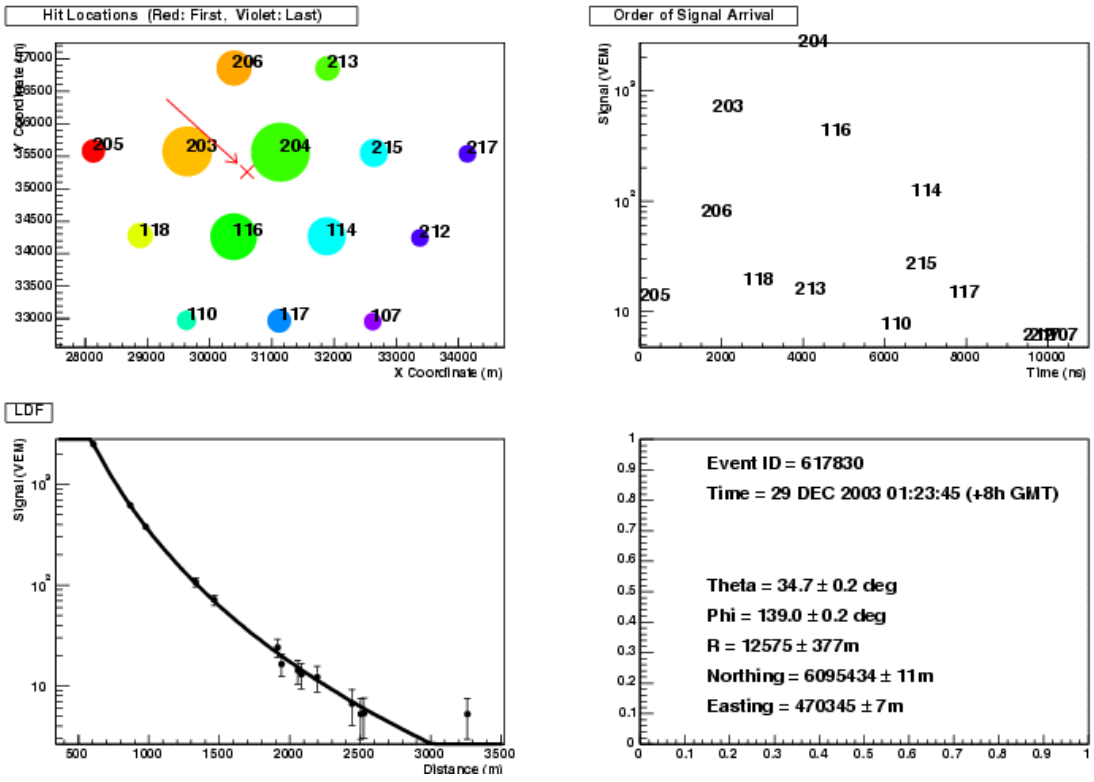

Figure 18: Auger SD Reconstruction of 35 degree zenith 70EeV shower. In the figure in the upper left, the x-y axis represents position on the grid of the array where each circle represents a SD station. The size of the circle corresponds to the energy deposited in the tank. The color indicates the time at which the signal was seen, with red occurring first and violet happening last. The time ordering of the tank signals is shown in the upper right, with signal strength in VEM shown on the y-axis, and time (ns) on the x-axis. The lateral distribution function for the event, gives the signal size as a function of the distance from the core (m), is shown in the bottom left. The timestamp of the event as well as the reconstructed values for its zenith and azimuth are given in the bottom right.

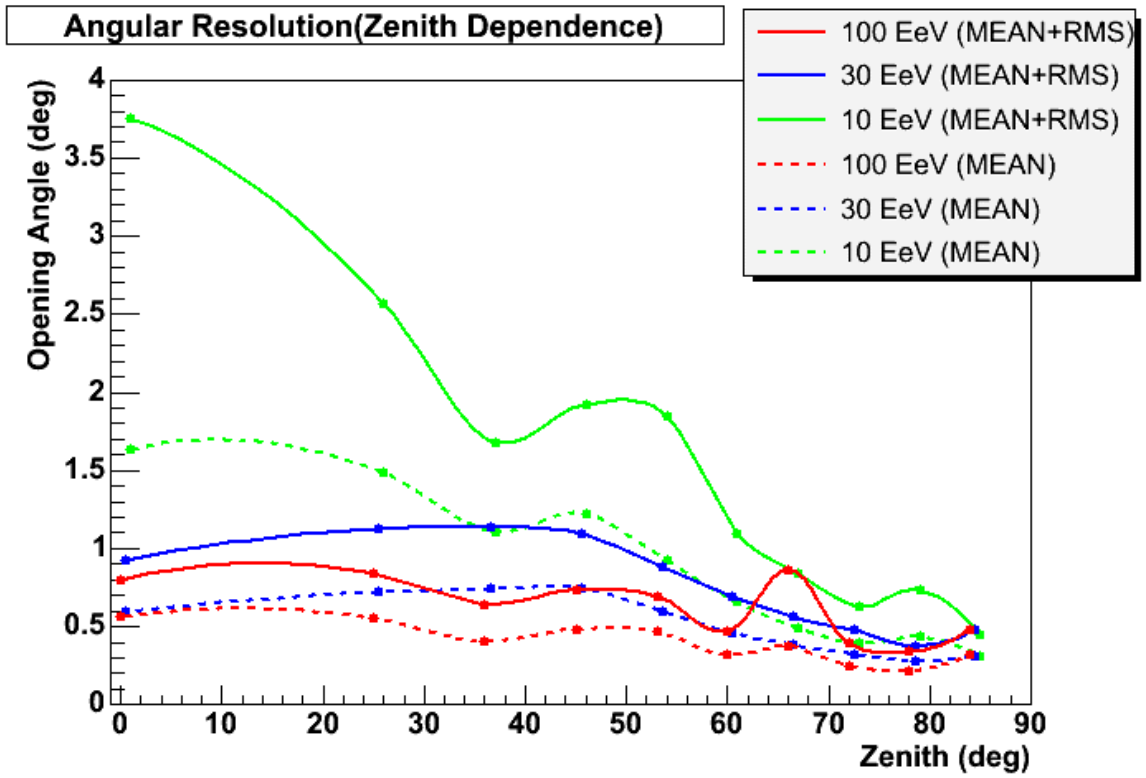

Figure 19: Opening angle error versus zenith. The dashed green line (solid line) shows the average error (average error plus standard deviation) in opening angle for 10EeV events. The dashed blue line (solid line) shows the average error (average error plus standard deviation) in opening angle for 30EeV events. The dashed red line (solid line) shows the average error (average error plus standard deviation) in opening angle for 100EeV events. More inclined events show less error than vertical events.

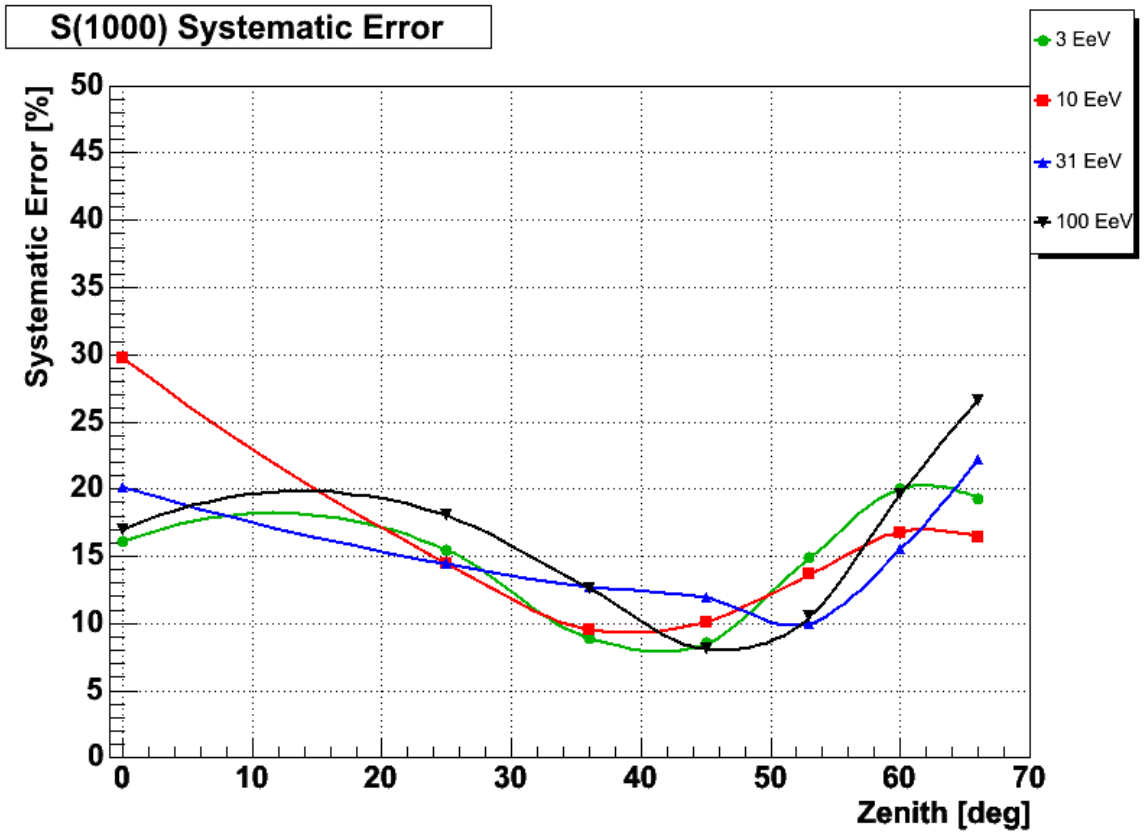

Figure 20: Percentage systematic uncertainty in S1000 for 3EeV, 10EeV, 31EeV and 100EeV, indicated in green, red, blue and black respectively, as a function of zenith angle.

Although only 10% of events are hybrid due to the inability of the FD to operate except during moonless nights, the information provided by the hybrid events carries over to instances when only the SD observes an event. This is good because the SD is always operational 24 hours a day; and therefore, allows us to collect more events. The same mapping between S1000 and energy can be done for events detected by only the SD [21][20][19].

The error on the opening angle is shown in Figure 19. This error corresponds to the error on the direction vector indicating the direction from which the particle has come. At the higher energies that are considered above 57EeV and the zenith angles below 60^0, the error on the opening angle is about 0.5^0 [23].

Additionally, the systematic uncertainty on S1000 is shown in Figure 20, which was taken from [19]. It shows that below 60^0 zenith, the systematic error on S1000 is about 15% at the energies we are concerned with above about 57 EeV.

3.4 Maintaining the Detector

While I was working shifts on the detector, I was able to meet some of the more than 280 people that contribute to the operation of the detector. I did shifts on the detector. These shifts entailed riding around off-road on the Pampa in Argentina, with a 4-wheel drive vehicle, through rivers and over whatever was in the way, searching for SD stations that were not operating correctly. We would search out broken stations using its GPS signal, which would lead us right to the station. Occasionally, we had to troubleshoot the detector in the field and make repairs. Making repairs entailed replacing any dead batteries, radio modules, PMT cables and occasionally a broken PMT. One such photomultiplier that was replaced because it was not giving the correct count rates is shown in Figure 16.

3.5 Data Set

The events collected above 10 EeV, within a zenith angle of 60^0, are shown in Figure 21. The purple illustrates the exposure of the Auger detector, which will be described in Section 4.3.

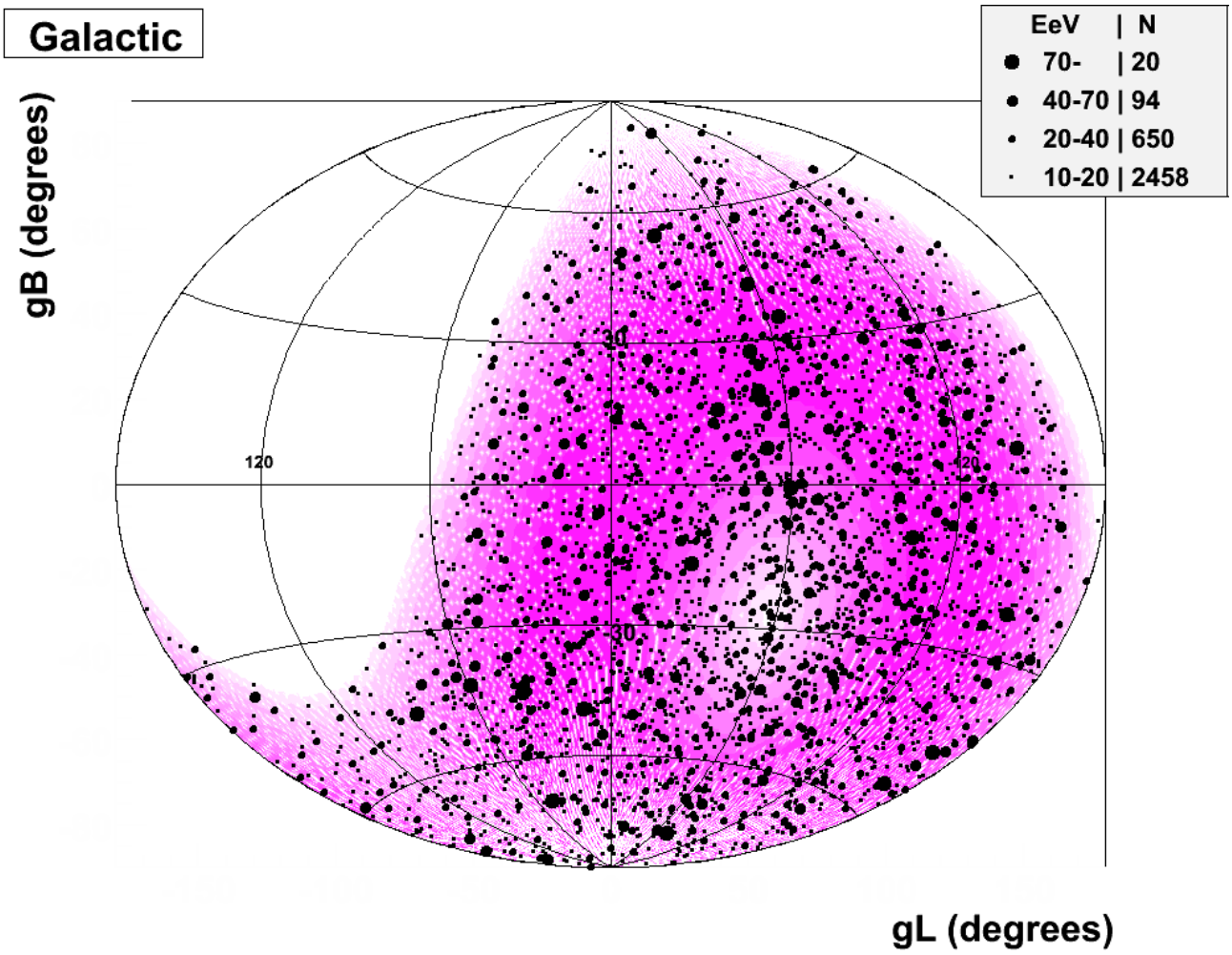

Figure 21: Auger events above 10EeV within 60^0 zenith between January 1, 2004 and June15, 2008. The sky map is in galactic coordinates with the galactic center at the center of the map. The legend in the upper right of the Figure shows the relationship between the dot size representing the event and the events energy. In addition, the number of events that fall between 10-20EeV, 20-40EeV, 40-70EeV and >70EeV is shown to be 2458, 650, 94 and 20 respectively.

The sky map is in galactic coordinates with the galactic center at the center of the plot. The Galactic Plane lies along the line with galactic latitude (gB) of zero degrees. The galactic longitude is labeled gL.

The UHECR energy is illustrated by the size of the dot; the larger the dot, the larger the energy. The legend in the upper right of Figure 21 illustrates the dot size with its corresponding energy range and the number of events found in the energy range. Between January 1, 2004 and June 15, 2008, 2458 events between 10-20EeV were seen. The integrated exposure for this period is ~10,000 km^2.sr.year. Between 20-40EeV, 650 events were seen. Between 40-70EeV, 94 events were seen, and 20 events above 70EeV were seen. These results are shown in Table 1.

	Integrated Exposure km^2.sr.year	10-20EeV	20-40EeV	40-70EeV	>70EeV
January 1, 2004-May 26, 2006	4,000	781	226	36	7
May 26, 2006-August 31, 2007	3,000	891	229	31	7
August 31, 2007-June 15, 2008	3,000	786	195	27	6
January 1, 2004-June 15, 2008	10,000	2458	650	94	20

Table 1: Count of UHECR between 10-20EeV, 20-40EeV, 40-70EeV and larger than 70EeV for stated time intervals.

Additionally, the number of events collected during three other time periods is shown for reasons described in Section 6.1. The integrated exposure of the detector on May 26, 2006 is ~4000 km^2.sr.year. On August 31, 2007, the integrated exposure is 7000 km^2.sr.year while on June 15, 2008, it is ~10,000 km^2.sr.year. All of these events fall within a zenith angle of 60^0. The spectrum

of UHECR seen by the Auger Detector is shown in Figure 22. The spectrum has been multiplied by E^3 to make any subtle change in the spectrum more apparent. The flux of UHECR at the highest end of the spectrum is suppressed. This feature is in agreement with the GZK effect. Therefore, any UHECR that are seen should have originated from a nearby source.

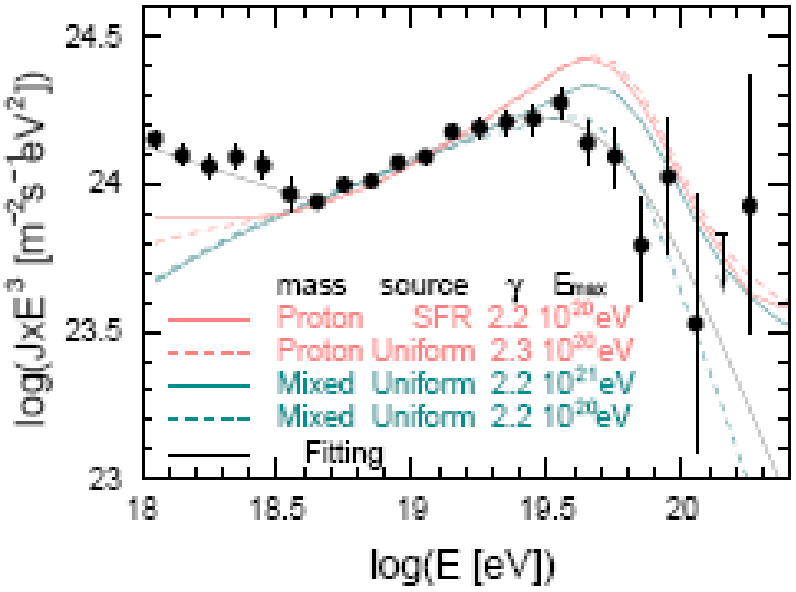

Figure 22: Auger Spectrum multiplied by E^3. The flux at the highest energies is suppressed in agreement with the GZK effect. Taken from [24].

3.6 Pierre Auger Detector Summary

In the end, up until June 15, 2008, a total of 3222 events were seen above 10EeV within a zenith angle of 60^0. The integrated exposure for this period is 10,000 km^2.sr.year. With these events, a sky map and spectrum were constructed as shown in Figures 21 and 22, respectively.

The sky map indicates that the distribution of the lower energy UHECR appears isotropic. These lower energy events can wash out any sign of anisotropy with noise. This motivates the consideration of only the highest energy UHECR for the purpose of our charged particle astronomy.

The Pierre Auger Observatory's UHECR spectrum indicates a rapid drop in flux at the highest end of the spectrum as would be expected from the GZK effect. Therefore, the UHECR at the highest end of the spectrum are expected to have come from nearby extragalactic sources. This allows us to narrow our search and only consider the nearest source candidates among AGN and radiogalaxies.

CHAPTER 4

Analysis Method

In our search for UHECR sources, we will employ two different methods that search for clustering among the UHECR. The first method is named autocorrelation and searches for clustering among the events themselves. The second method searches for correlations between the UHECR and astronomical objects. In both cases, we will test against the null hypothesis that the distribution of our UHECR are completely isotropic.

4.1 Autocorrelation Analysis for Small Scale Clustering

Autocorrelation analysis will search for small scale clustering among the cosmic rays themselves and determine if the clustering found in the real data deviates significantly from what we would expect from an isotropic sky. Clustering will be associated with the occurrence of pairs of cosmic rays. Pairs are defined as two events within a specified angular separation of each other. The significance of the clustering will be determined by counting the number of pairs of events in a sample set; and then, counting the relative number of isotropic Monte Carlo skies that give the same or greater number of pairs. If we generate N Monte Carlo skies, and N_{pairs} of those skies have an

equal or greater number of pairs than the real data; then, the chance of getting the number of pairs in the real data by chance will be given by:

$$\frac{N_{pairs}}{N} \tag{6}$$

The smaller this value is, the more our set of cosmic rays deviates from isotropy. This will allow us to find potential hot spots of UHECR production.

4.2 Correlation with Likely Source Candidates

This second method will search for correlations between our cosmic ray event set and event sets for various sets of astronomical objects that fit the profile of a possible UHECR source. The deviation from isotropy in this case will be found by first determining the relative exposure weighted area within some angle x surrounding a set of possible source candidate objects to the total exposure weighted area of the sky visible to the detector. This value will be used as the probability for a single correlation to occur randomly. The total significance of the signal will be found using the integrated binomial probability of getting an equal or greater number of correlations within angle x than that found in the real data. Suppose that the probability of a single success assuming isotropy is given by:

$$p = \frac{A_{astro}}{A_{total}} \tag{7}$$

Where A_{astro} is the total exposure weighted area of the sky within angle x of our source candidates and A_{total} is the total exposure weighted area of the sky seen by the detector. The binomial

probability P of getting an equal or greater number of correlations within angle x than seen in the real data set can be found by:

$$P = \sum \binom{n}{n_{corr}} p^{n_{corr}} (1-p)^{n-n_{corr}} \tag{8}$$

Where n is the total number of cosmic rays in the real data set and n_{corr} is the number of correlations in the real data , while p is given by (7). The sum is taken from n_{corr} to n.

In both of these methods, some problems arise due to our lack of knowledge of the traversed magnetic fields and our ignorance of the exact nature of our primary. For the case of autocorrelation, what angular separation between two cosmic rays should characterize them as a pair? Should a pair be two events within 1^o or should we instead choose 2^o or perhaps something else? In the case of correlations with astronomical objects, the relative exposure weighted area of sky covered by our astronomical objects also requires that we define the angular separation between source and cosmic ray within which the two are considered correlated, and outside which a cosmic ray is not considered correlated. We will overcome the problem of ambiguity for our angular separation that should distinguish between correlation and no correlation by considering a range of angular separations and calculating deviations from isotropy for all values in the range.

Another problem arises concerning our energy. High-energy protons deflect less than low-energy ones. Therefore, a high-energy event will more likely point back towards its source, while a lower energy event (which has undergone large deflections) may not. These lower energy events can wash out our signal, so we would like to exclude them when looking for anisotropies. Above what critical energy E_c should we focus our attention to avoid masking any interesting signal? This

value is also hard to pin down exactly. Again, we will scan through all of our possible choices for E_c.

By doing these scans, it is hoped that any potentially interesting signal can be found and characterized by a critical angular separation δ_c and energy E_c . Doing these scans has a down side though, in that it turns the probabilities described in Expression 6 or 8 into posteriori values. To remove any bias introduced into the analysis by the scan, a prescription will be proposed using δ_c and energy E_c and tested. To get an apriori probability that gives the true significance of a signal at δ_c and $E_{c,}$, we must use an independent data set to confirm the hypothesis laid out in the prescription.

4.3 Exposure

In order to determine if the number of events detected in a certain area of the sky is different from expectations under isotropy, we need to determine the exposure of the detector. For detectors that are fully efficient up to some zenith angle θ_m located at latitude a_0, the relative exposure $\omega(\delta)$ in declination δ is [25]:

$$\omega(\delta) \propto \cos(a_0)\cos(\delta)\sin(\alpha_m) + \alpha_m \sin(a_0)\sin(\delta)$$

$$where\ \alpha_m \begin{pmatrix} 0\, if\ \xi > 1 \\ \pi\, if\ \xi < -1 \\ \cos^{-1}(\xi)\, otherwise \end{pmatrix} \tag{9}$$

$$\xi = \frac{\cos(\theta_m) - \sin(a_0)\sin(\delta)}{\cos(a_0)\cos(\delta)}$$

For the SD, which is fully efficient up to 60^0 and located at -35.2^0 latitude, and so the exposure in declination is as shown in Figure 23. Detectors that operate all day have constant exposure in right

ascension. The exposure in right ascension for the Auger detector over the full 360^0 in right ascension will be a constant value equal to unity.

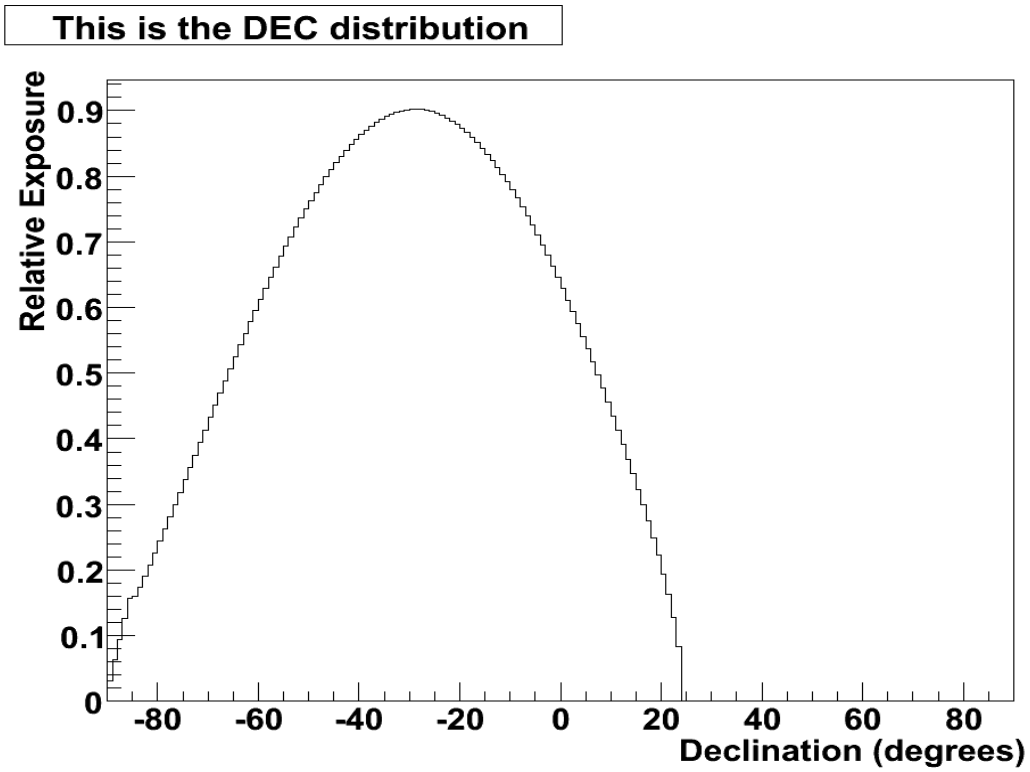

Figure 23: Relative Exposure in declination for Auger SD $\omega(\delta)x\cos(\theta)$ at latitude -35.2^0 where θ is zenith angle.

The Monte Carlo skies used in the autocorrelation analysis will have the right ascension and declination of their events randomly selected from these distributions. The relative exposure weighted area surrounding astronomical objects (Expression 7) will be determined using the distribution in Figure 23 to weight each $1^o x1^o$ pixel at each right ascension and declination on the sky. The magnitude of the product of the relative exposure in declination and relative exposure in right ascension is illustrated in Figure 21 as the magnitude of the purple shading. The regions with

zero exposure are shown as white. Blockage by the Earth is what causes these regions to be unseen by the detector.

4.4 Analysis Methods Summary

Given the relative exposure at different points on the sky, the number of events expected from that point on the sky under the assumption of isotropy is known. Deviations from this number of events will determine the amount of anisotropy for any position on the sky. With the relative exposure at each location on the sky determined, autocorrelation analysis can be performed, as well as correlation studies with likely source candidates in order to search for anisotropy.

CHAPTER 5

Autocorrelation

An UHECR emitter's location on the sky may coincide with an abundance of pairs of cosmic rays. This abundance of pairs will be associated with a small value for Expression 6. Due to our lack of knowledge of composition and the magnetic fields traversed by the primary particle, it is hard to specify apriori what angular separation between two events should be considered a pair or doublet. Expression 6 will be found for a range of angular separations. Also, it is hard to know above what energy we should focus our attention to avoid having the signal washed out by noise. Noise will be caused by lower energy events that have undergone large angular deflection and are scattered isotropically across the sky. To get around this problem, a range of energies will be considered, each energy defining the lowest energy event in a set of highest energy events. Starting from 40 EeV, up to the highest energy event are considered, and the value of Expression 6 is found for all of these different sets of highest energy events.

5.1 Autocorrelation Analysis

Figure 24 shows the relative number of random Monte Carlo skies having the same or greater number of correlations than the real data (Expression 6) as a function of the angular separation

defining a doublet, and the number of highest energy events. The scan in the energy is done to exclude lower energy events that could wash out the signal. In other words, Figure 24 shows the value of Expression 6 on the z-axis for a range of different angular separations and lowest energy that defines sets of highest energy events.

In [26], events up until August 31, 2007 are shown to exhibit an auto correlation signal. The reason events up until August 31, 2007 are considered first is described in Chapter 7.

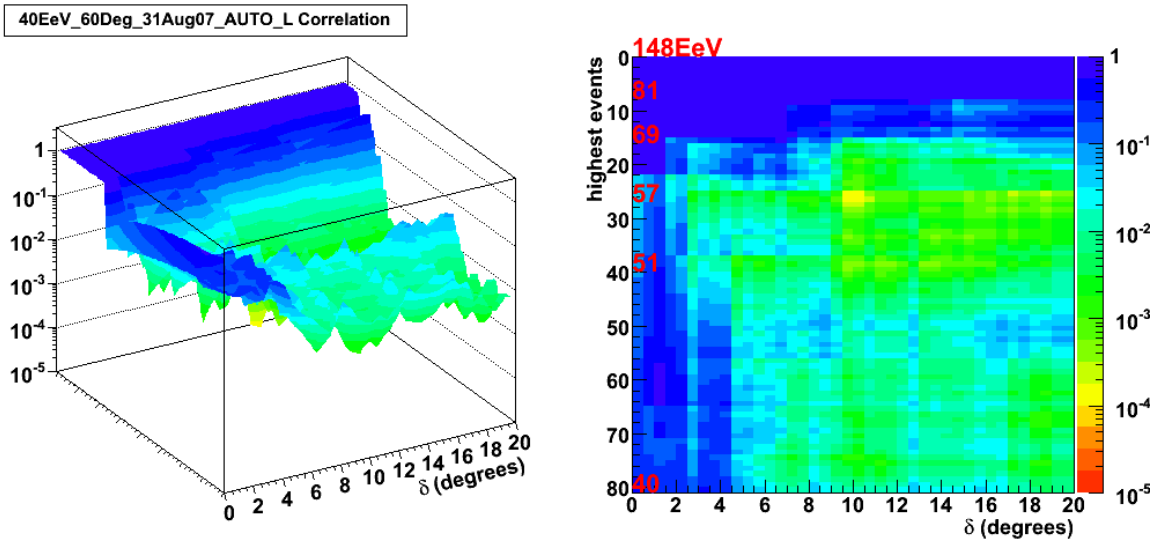

Figure 24: Scan of events above 40 EeV collected until August 31, 2007. Location showing maximum possible clustering occurs at 10.5^0 among 27 highest energy events. The vertical axis on the graph on the left shows the value of Expression 6 indicating the number of Monte Carlo skies with equal or greater number of pairs than the real sky, divided by the total number of Monte Carlo skies ($N=10^5$).

In short, August 31, 2007 was when the hypothesis of AGN correlation was found at less than 1%

confidence as described in Chapter 7. This analysis shows deviation from an isotropic sky for larger angles between about 10^0-30^0. Figure 24 shows the scan of Expression 6 for events above 40 EeV over a range of angular separations that define a pair from 0.5^0 to 20^0 until August 31, 2007. The location showing maximum possible clustering occurs at 10.5^0 degrees among 27 highest energy events above 57.5 EeV.

The projection at the minimum of this scan is shown in Figure 25 and indicates that only one in 10^4 Monte Carlo skies produced equal or greater numbers of pairs. These results agree with the results of [26] in that among the set of UHECR with energies larger than 57 EeV, autocorrelation at larger angles may exist.

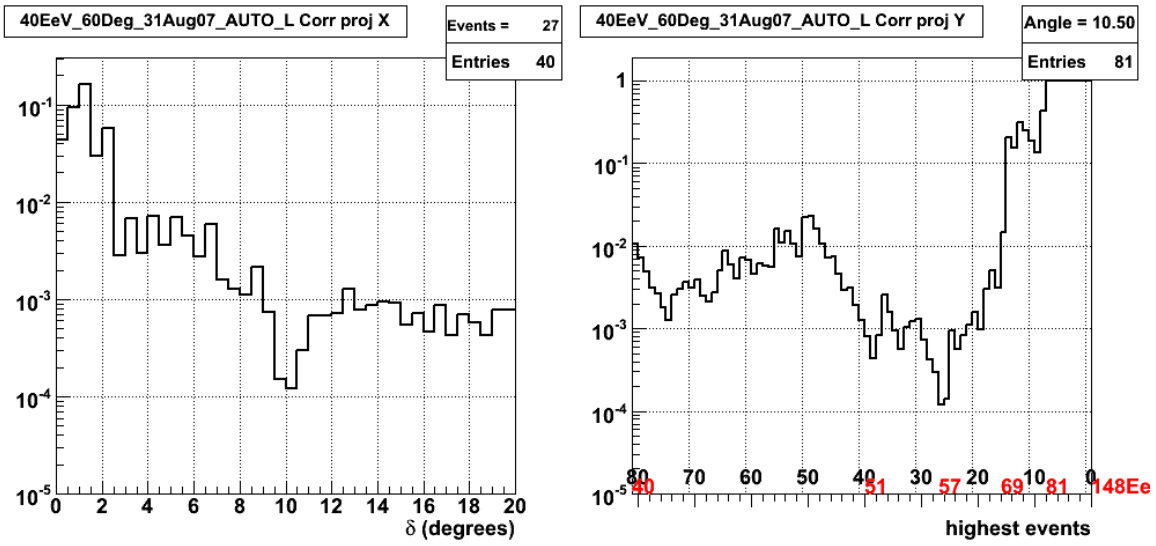

Figure 25: Projection of position of maximum possible signal from scan of events above 40 EeV within 60 degrees zenith collected until August 31, 2007. Location showing maximum possible clustering occurs at 10.5 degrees among 27 highest energy events.

Figure 26 shows the galactic sky map of 14 events above 57 EeV collected until August 31, 2007.

The blue shading indicates the exposure of the detector for all locations of the sky. The locations of the sky that are not visible are due to obstruction by the Earth. The reason events above 57 EeV

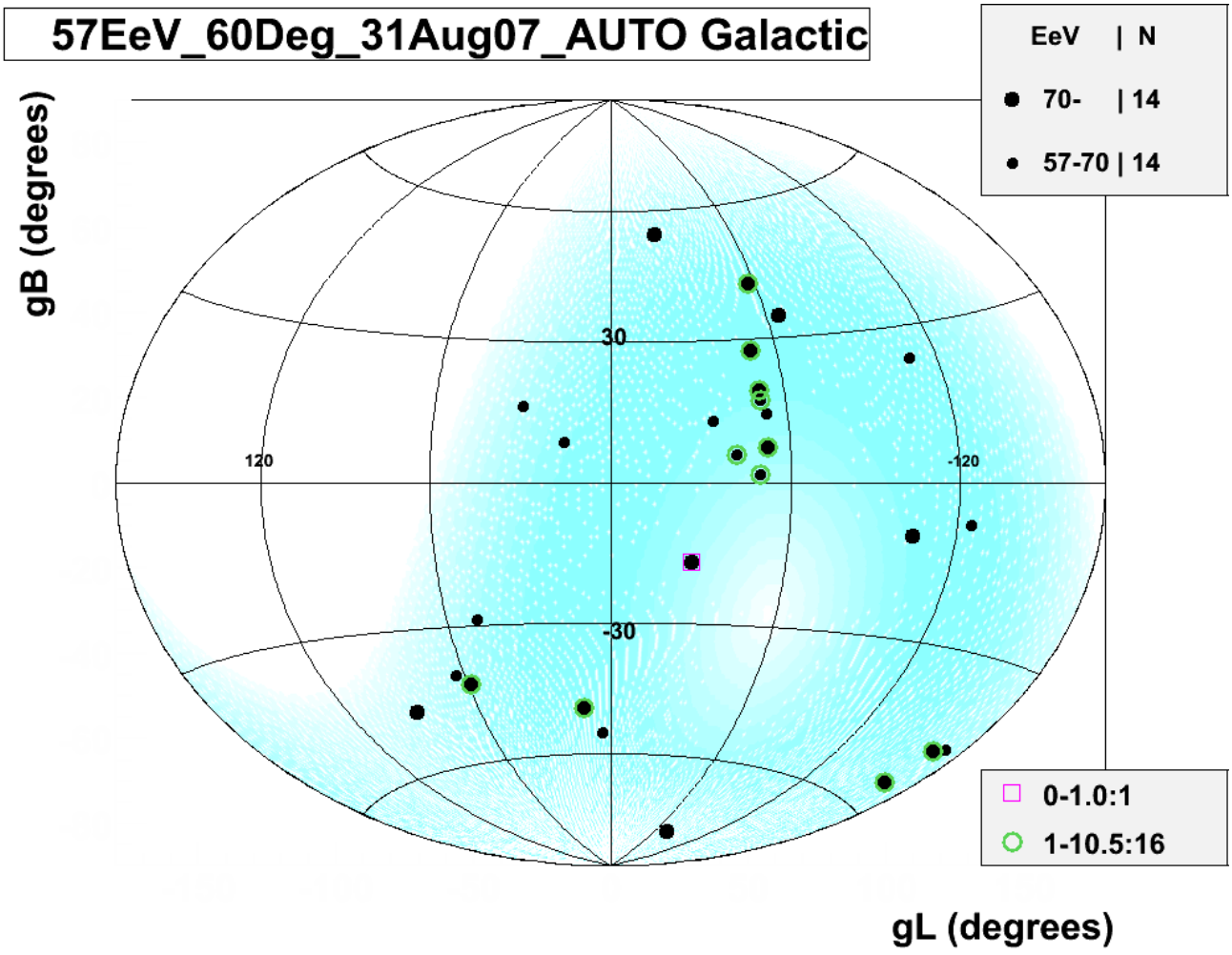

Figure 26: Galactic sky map of 14 events above 57 EeV (within 60^0 zenith) collected until August 31, 2007. Galactic center is at center. Clustering among events within 1^0 are shown in red squares. Only one of these is found. Clustering between 1^0 and 10.5^0 are shown as green circles of which 16 are found.

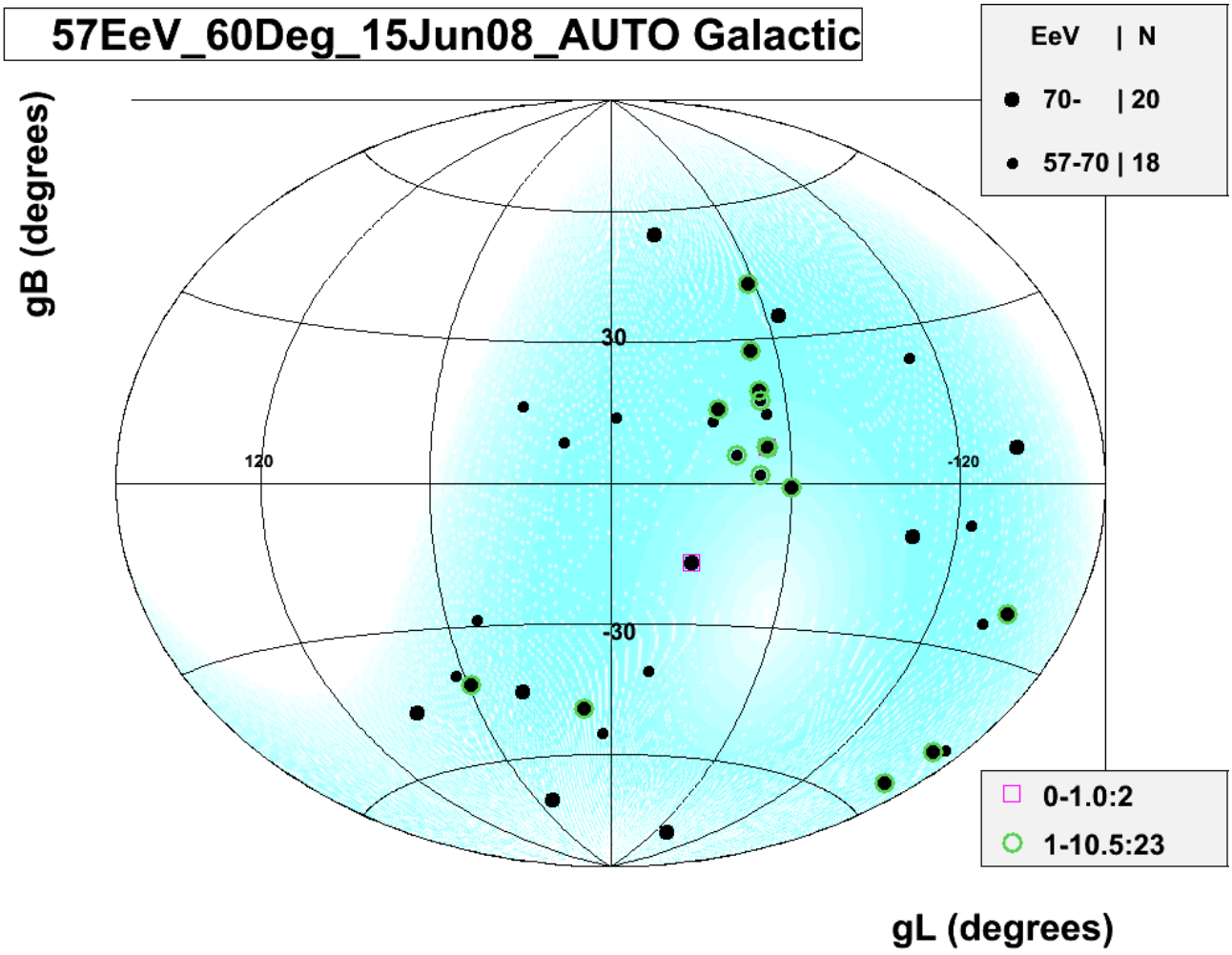

Figure 27: Galactic sky map of events above 57 EeV (within 60^0 zenith angle) up until June 15, 2008. Among these top 38 events, there are 25 correlations within 10.5^0 angular separation.

are plotted as opposed to say 57.5 EeV is because the hypothesis described in Chapter 6 concerning the correlation of UHECR with AGN is for events above 57 EeV. Events above 57EeV are plotted for consistency and ease of comparison with the AGN hypothesis. Seventeen doublets are found within an angular separation of 10.5^0. The event at galactic longitude of 29.5^0 and 16.1^0 galactic latitude has an energy of 57.1 EeV, which is the lowest energy event among the set. The set with the maximum deviation from isotropy is among the top 27 events, which does not include this lowest energy event. Therefore, there are 17 pairs among the top 27.

This information is illustrated in the legend in the bottom right of the figure. The legend in the upper right shows that 14 events between 57-70EeV are represented by small black dots. It also shows that 14 events above 70EeV are represented with larger black dots.

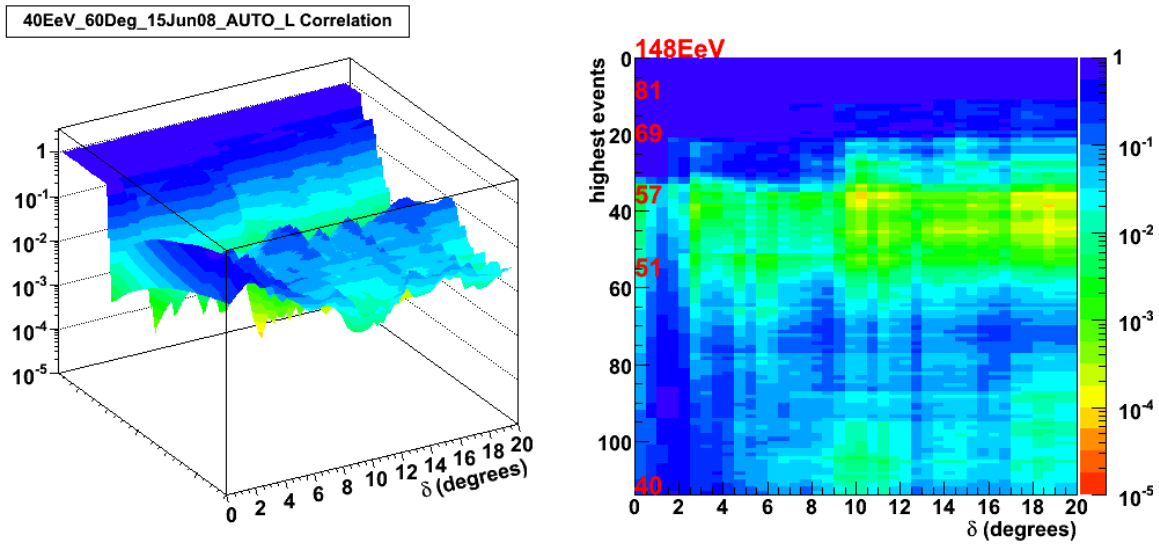

Figure 28: Scan of relative number of Monte Carlo skies that had equal or greater number of pairs than in the real sky for events above 40EeV up until June 15, 2008.

Let us look at all the events collected up until June 15, 2008 and check to see if the autocorrelation signal increases with the inclusion of this new data. The galactic sky map of events above 57 EeV up until June 15, 2008 are shown in Figure 27. Among these top 38 events, there are 25 correlations within 10.5^0 angular separation. The scan of relative number of Monte Carlo skies that had equal or greater number of pairs than in the real sky for events above 40EeV until June 15, 2008 is shown in Figure 28. The projection at the scans minimum at 18.5^0 among the top 36 events is shown in Figure 29.

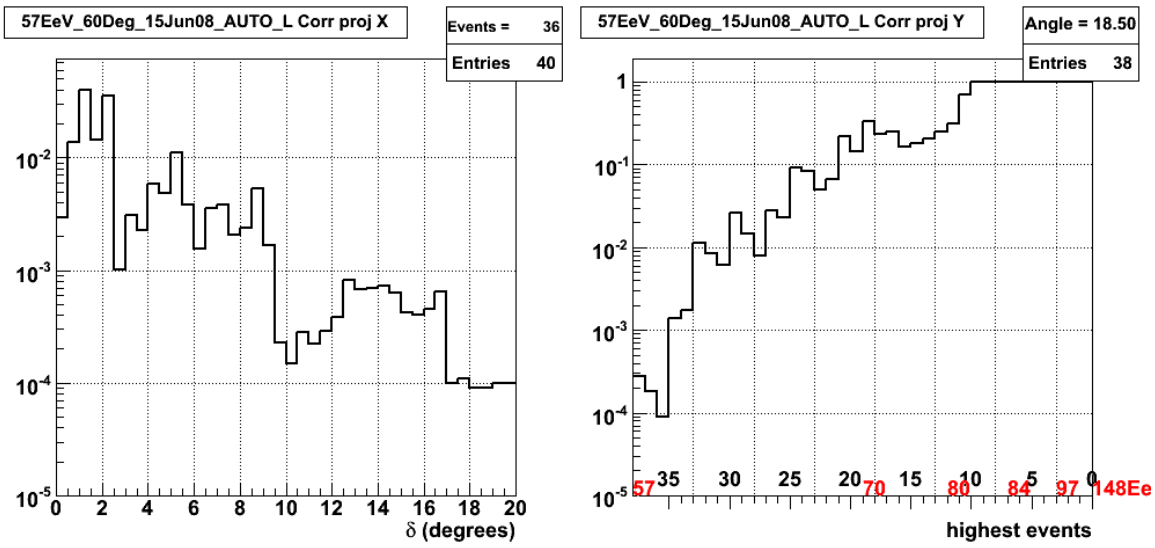

Figure 29: Projection at minimum of Figure 28.

5.2 Autocorrelation Analysis for Three Independent Data Sets

To get an impression of how the autocorrelation signal varies in time, the events above 57 EeV collected up until June 15, 2008 will be split into three time periods; between January 1, 2004 to May 26, 2006 (Period A); from May 26, 2006 to August 31, 2007 (Period B); and from August 31, 2007 to June 15, 2008 (Period C). These dates correspond to the dates that the AGN hypothesis

described in Chapter 6 were prescribed by the collaboration on May 26, 2006, and the date the hypothesis was fulfilled at less than 1% on August 31, 2007. June 15, 2008 is of no real significance. The number of UHECR events between 57-70EeV and greater than 70EeV for these time periods is shown in Table 2.

		57-70EeV	>70EeV
January 1, 2004-May 26, 2006	Period A	7	7
May 26, 2006-August 31, 2007	Period B	7	7
August 31, 2007-June 15, 2008	Period C	4	6

Table 2: Events between 57-70EeV and greater than 70EeV for specified time periods.

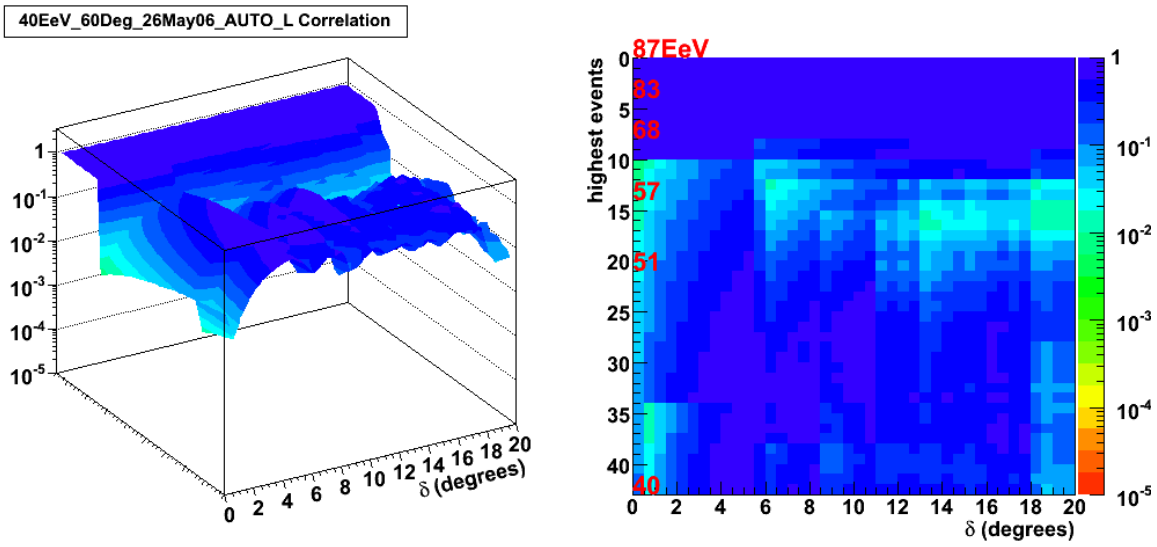

Figure 30: Scan of relative number of Monte Carlo skies that had equal or greater number of pairs than the real sky for events above 40 EeV (within 60^0 zenith angle) for Period A.

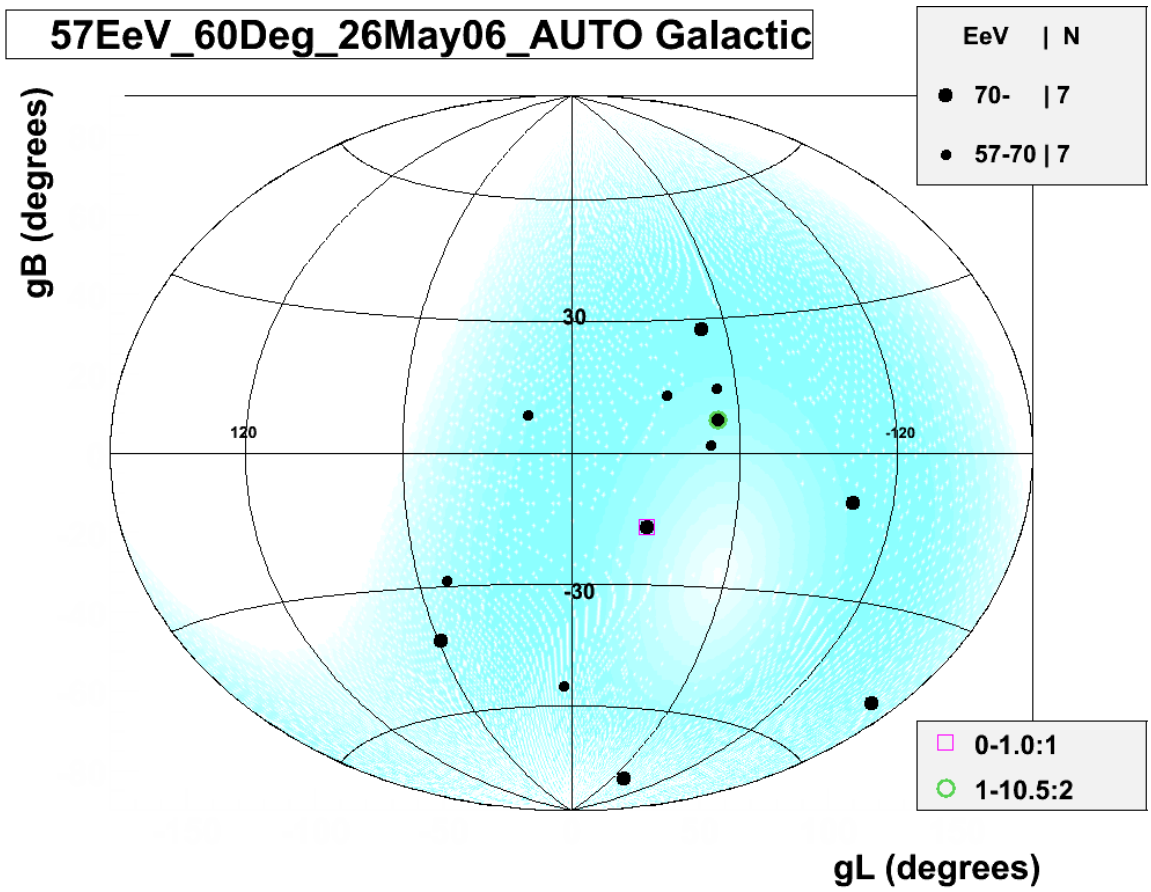

Figure 31: Galactic sky map of events above 57EeV (within 60^0 zenith angle) for Period A. There are seven events between 57 and 70 EeV (shown as smaller black dots) and another seven events above 70 EeV (shown as larger black dots). There are three correlations within 10.5^0.

The galactic sky map of events above 57EeV for Period A is shown in Figure 31. There are seven events between 57 and 70 EeV (shown as smaller black dots) and another seven events above 70 EeV (shown as larger black dots). There are three correlations within 10.5^0. The scan of the relative number of randomly generated Monte Carlo skies as a function of angular separation and

lowest energy event is shown in Figure 30. The scan starts at 40EeV and proceeds up until 87EeV. The angular separation defining a pair is scanned from 0.5^0 to 20^0.

The total number of Monte Carlo skies generated is 10^5. Projection at the minimum of Figure 30 occurs at 0.5 degrees angular separation defining a pair among the top 11 events. The projection of this scan's minimum is shown in Figure 32.

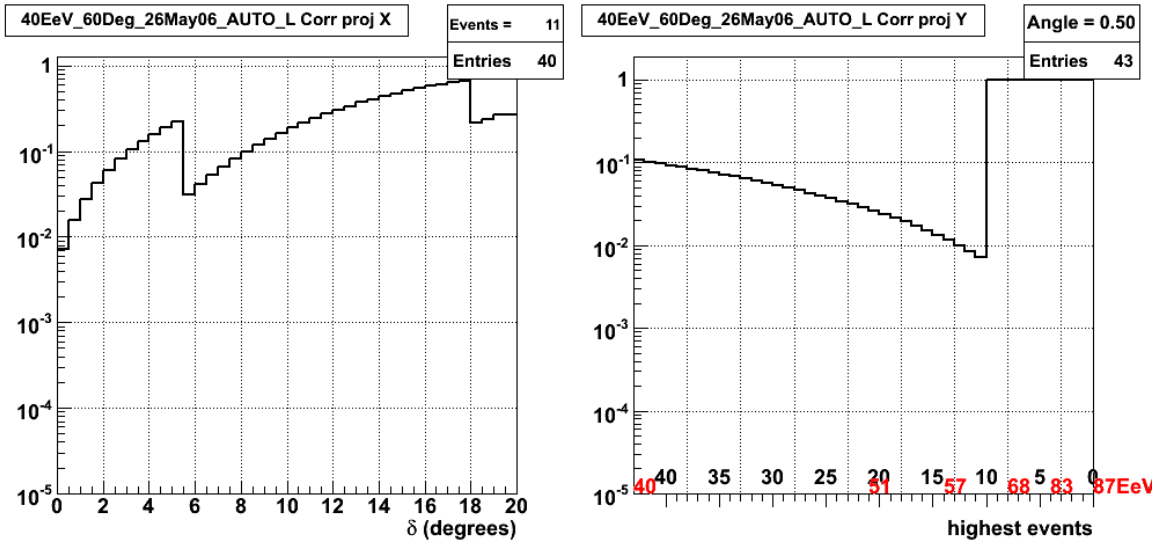

Figure 32: Projection at the minimum of Figure 30 at 0.5^0 angular separation among the top 11 events.

The galactic sky map of events above 57EeV (within 60^0 zenith angle) for Period B is shown in Figure 33. There are seven events between 57 and 70 EeV (shown as smaller black dots) and another seven events above 70 EeV (shown as larger black dots). There are three correlations within 10.5^0. The scan of the relative number of Monte Carlo skies that had equal or greater number of pairs than the real sky for Period B is shown in Figure 34.

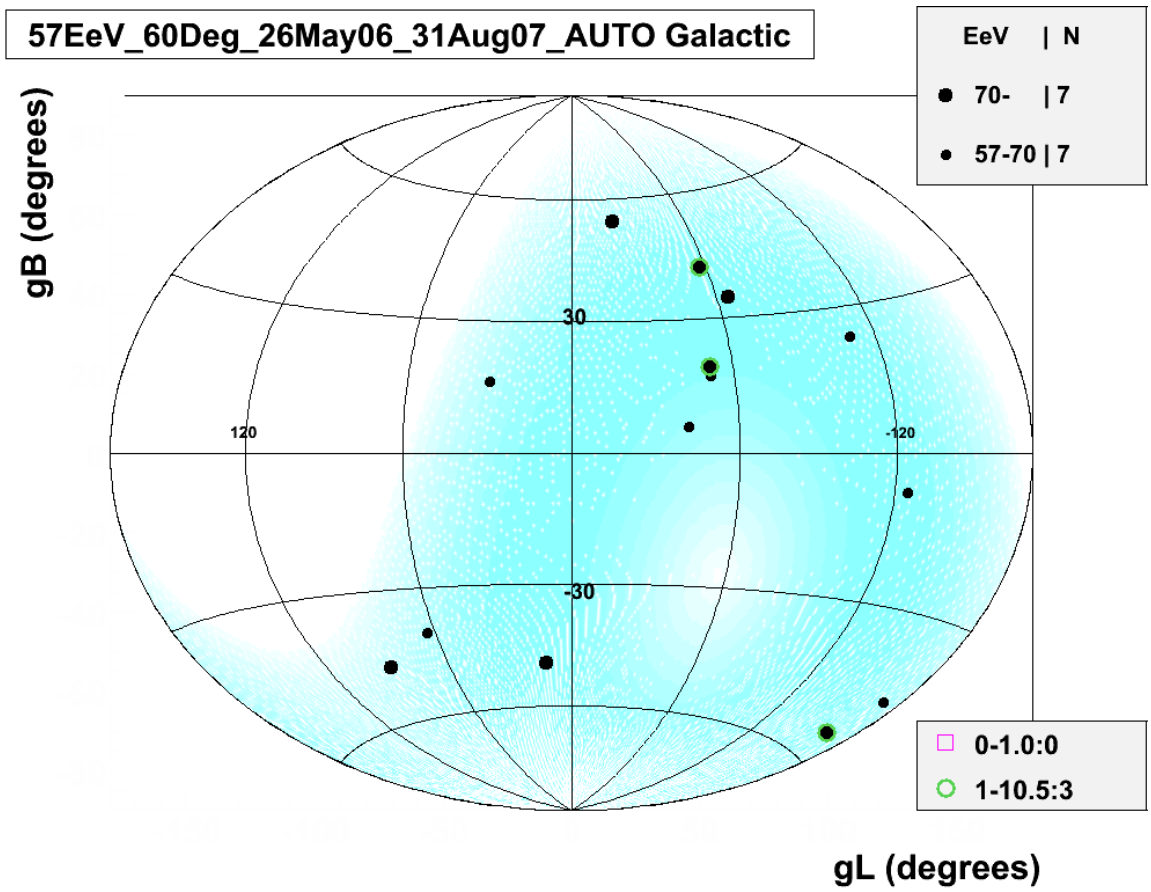

Figure 33: Galactic sky map of events above 57EeV (within 60^0 zenith angle) for Period B. There are three correlations within 10.5^0.

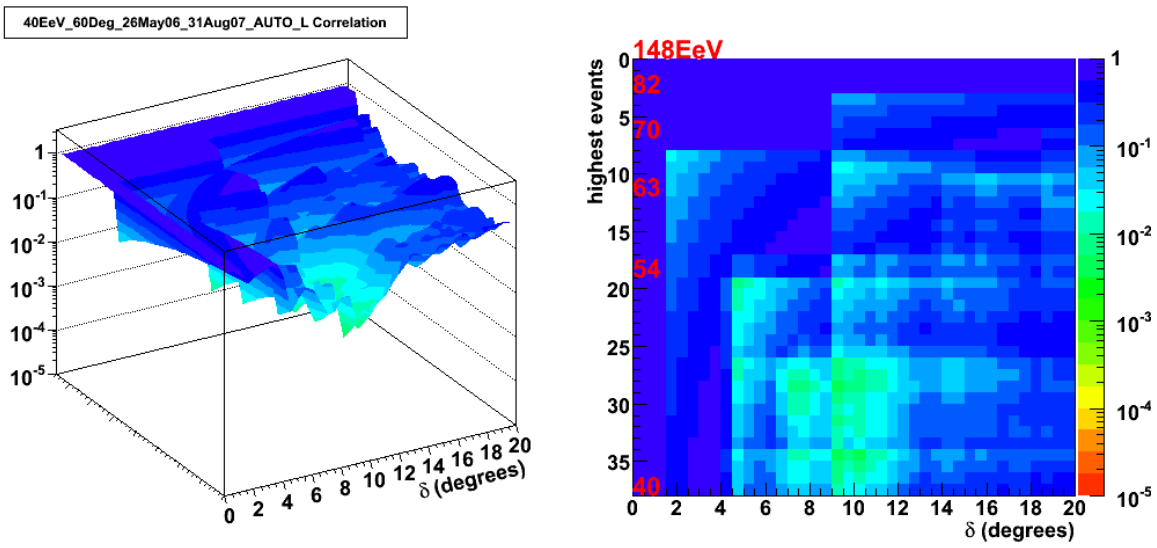

Figure 34: Scan of relative number of Monte Carlo skies that had equal or greater number of pairs than the real sky for events above 40 EeV (within 60^0 zenith angle) for Period B.

The galactic sky map of events above 57EeV for Period C is shown in Figure 35. There are four events between 57 and 70 EeV (shown as smaller black dots) and another six events above 70 EeV (shown as larger black dots). There is one correlation within 10.5^0.

The scan of the relative number of Monte Carlo skies that had equal or greater number of pairs than the real sky for events above 40 EeV (within 60^0 zenith angle) for Period C is shown in Figure 36. In this case, signs of an excess of pairs appear at lower energies around 40EeV and 9^0 defining the maximum distance between two events and still be considered a pair. About two out of one hundred Monte Carlo skies were able to reproduce the same or greater number of pairs as that seen in the real sky for events above 40 EeV, with separations of less than nine degrees defining two cosmic ray events as a pair or doublet.

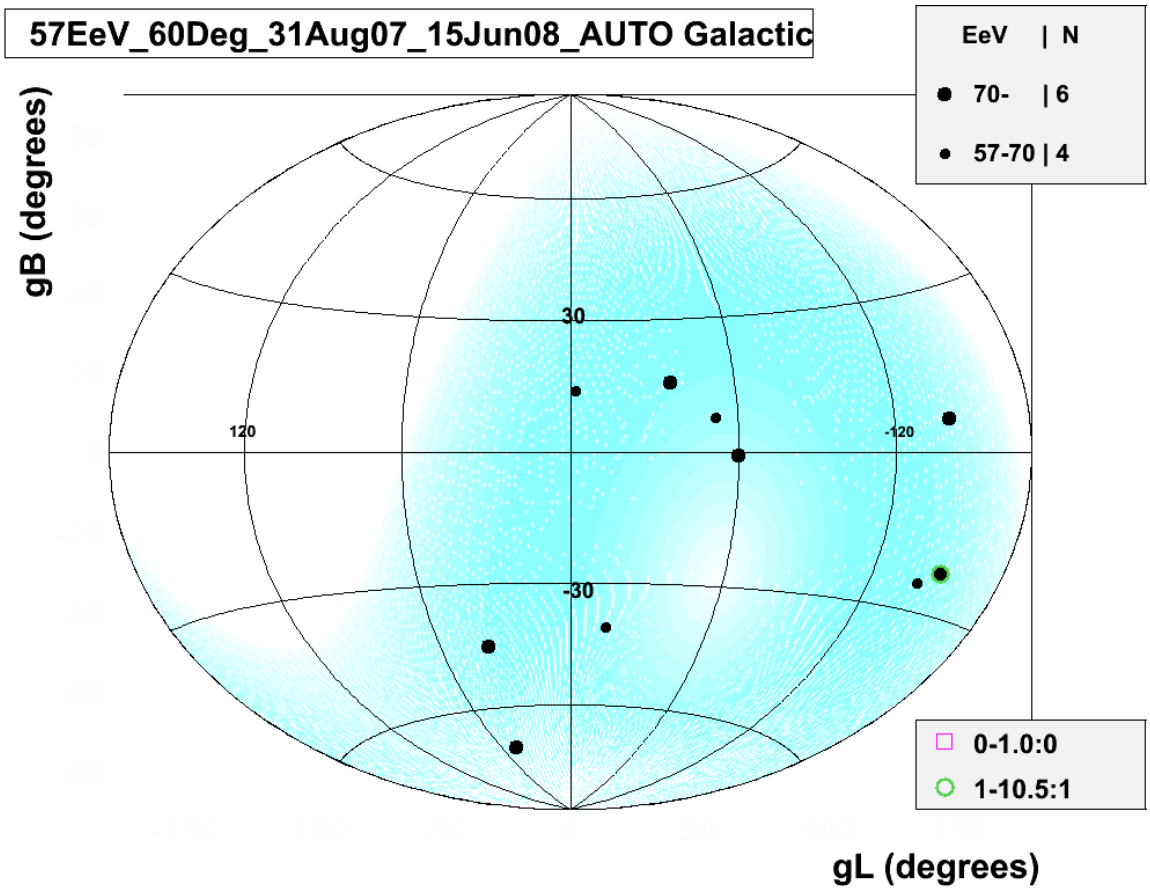

Figure 35: Galactic sky map for events above 57 EeV within 60^0 zenith for Period C. Only one doublet is found within 10.5 degrees.

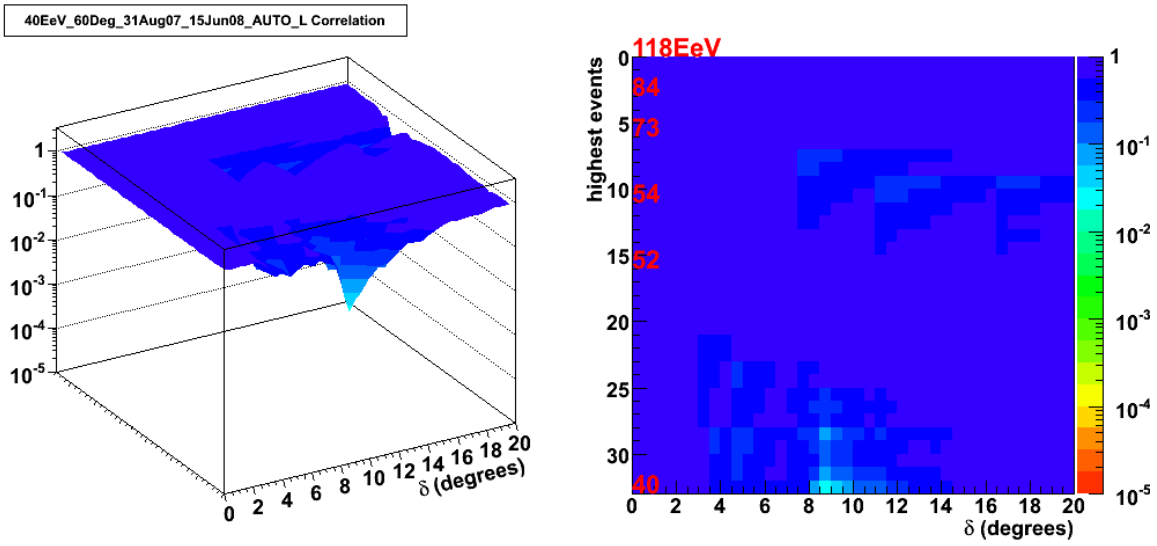

Figure 36: Scan of relative number of Monte Carlo skies that had equal or greater number of pairs than the real sky for events above 40 EeV (within 60^0 zenith angle) for Period C.

If the flux from a single source is low and pairs of events are found only after observing the source for a long time, it might be expected that an autocorrelation signal will not be found for the events collected over too short a time, for example for Period C.

5.3 Autocorrelation Analysis Summary

The Autocorrelation analysis does suggest that clustering among the UHECR for energies >57EeV does exist for larger angular separations of 10^0-20^0. However, this signal does not appear in the three independent time periods, possibly because the source flux is too low. The autocorrelation signal should continue to be monitored.

CHAPTER 6

Large Scale Structure

Determining what locations of the sky have an over abundance of UHECR can be accomplished by finding the value of Expression 6 for each location of the sky. The sky is pixelized, and the number of events within 15^0 (20^0) of the pixel is found; then 10^5 random Monte Carlo skies are generated and the number of these skies with equal or greater number of events within 15^0 (20^0) of the pixel are counted. The amount of anisotropy associated with that pixel of the sky is then determined as the ratio of the number of skies that had equal or greater number of correlations than the real sky to the total number of Monte Carlo skies which is 10^5.

6.1 Large Scale Structure Analysis

Figure 28 shows that the set of highest energy events larger than 57 EeV have an excess of pairs, if a pair is defined as two events within angular separations of about 10^0-20^0. Figure 37 shows 15^0 large scale structure and Figure 38 (which was presented by the UCLA Auger Group in September 2006 at the Auger South Analysis Meeting in Chicago, Illinois) shows 20^0 large scale structure for events above 56EeV. The deviation from isotropy is represented with color coding according to the

legend to the right of Figures 37, 38 and 39. Figure 37 shows that the area around the position of Cen A deviates from isotropy with a chance probability of 10^{-4}. An update of Figure 38, with events up until June 15, 2008 included, is shown in Figure 39.

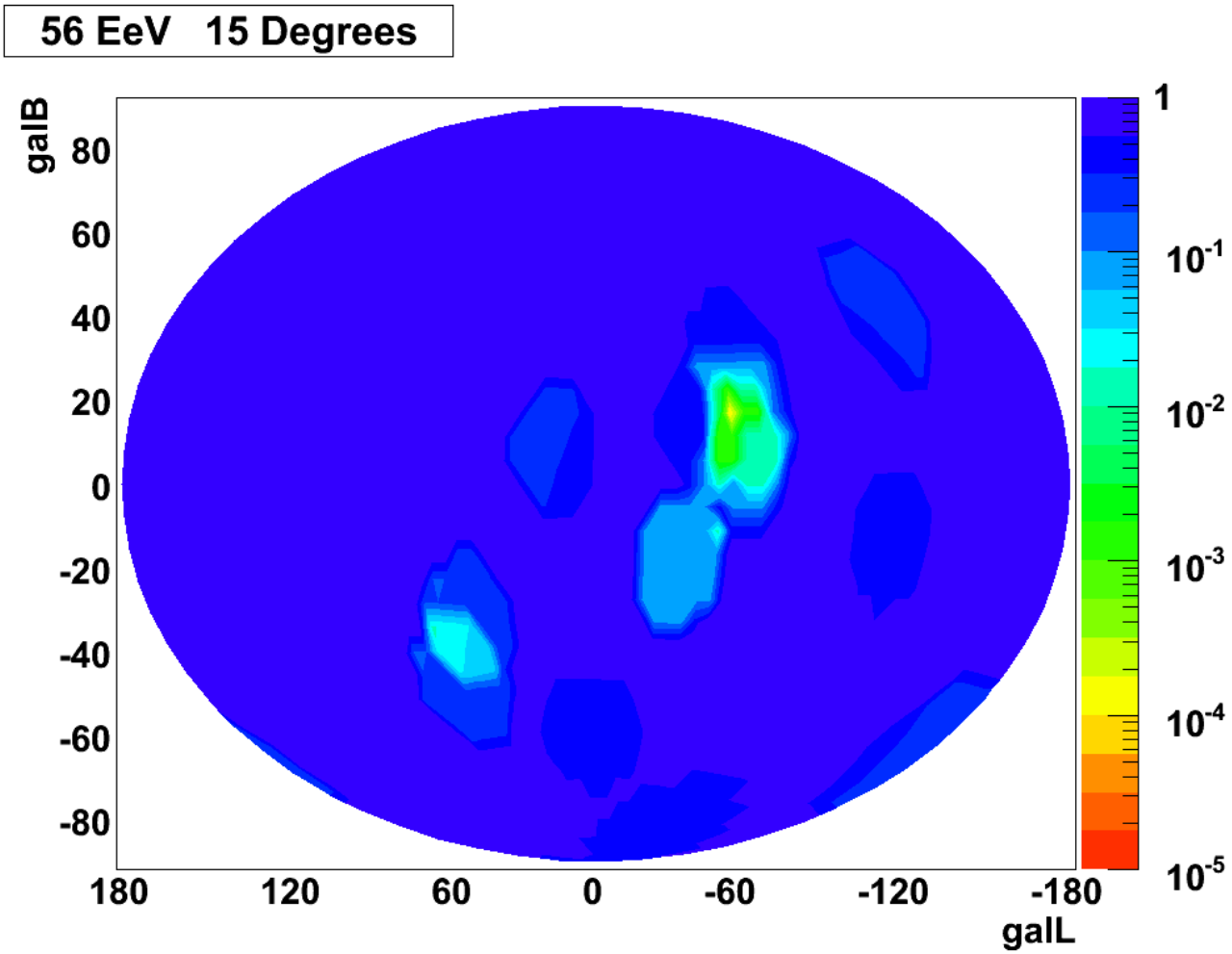

Figure 37: 15^0 Large scale structure for events above 56EeV. The sky map is in galactic coordinates with the galactic center at the center. The region around Cen A shows the location with minimum chance probability of 0.0001.

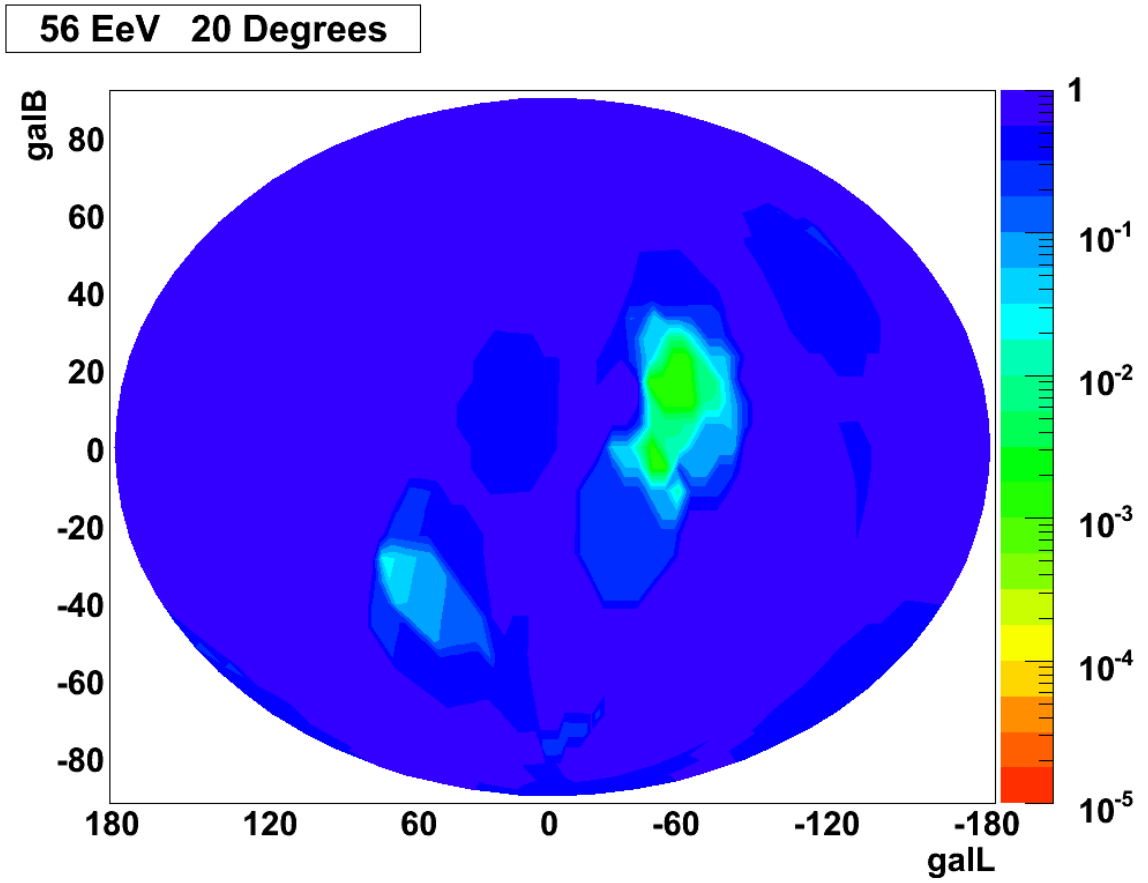

Figure 38: 20^0 large scale structure presented by the UCLA team at the collaboration meeting in Chicago, September 2006. The sky map is in galactic coordinates with the galactic center at the center. The region around Cen A and the Great Attractor shows the maximum chance probability.

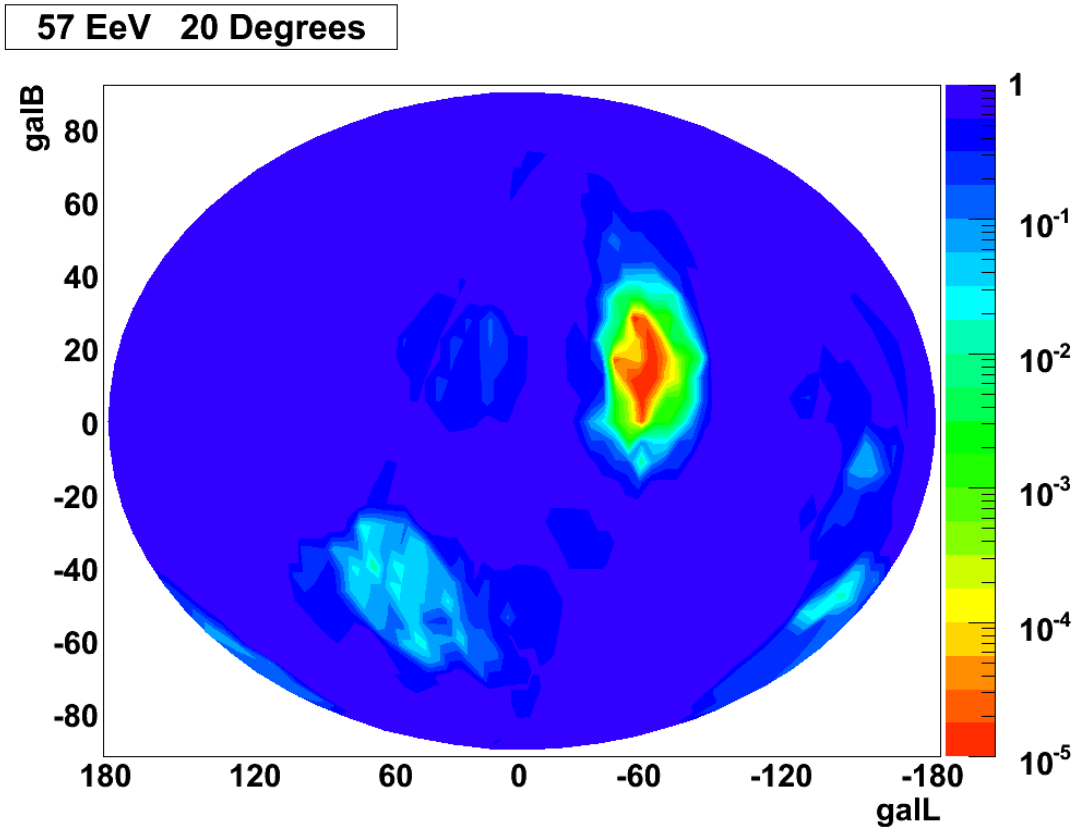

Figure 39: 20^0 large scale structure for events collected up until June 15, 2008. The sky map is in galactic coordinates with the galactic center at the center. The region around Cen A and the Great Attractor shows the maximum chance probability.

6.2 Large Scale Analysis Summary

Large scale analysis shows that the signal in the region around Centaurus A and the Great Attractor has increased. A real signal is expected to increase in time, while a statistical fluctuation is expected

to fade away. Comparing Figures 38 and 39 indicates that the signal has increased, lending support to the possibility that the region around Cen A may be a hot-spot.

CHAPTER 7

Active Galactic Nuclei

Specific criteria must be met in order for an astronomical object to qualify as a source candidate for UHECR. They must be able to accelerate charged particles up to very high energies. They also need to be close by because of the GZK affect, which causes UHECR energies to decrease rapidly as a result of interactions with the CMB. One such candidate is nearby active galactic nuclei (AGN).

AGN are thought to be super-massive black holes at the center of galaxies. As dust and stars are pulled into the black hole, tremendous energy is released as roughly two solar masses of material falls down the gravitational potential well of the black hole every year and converted into energy. These objects can spew tremendous jets of material, including charged particles, into space. As shown in Figure 2, AGN have sizes on the order of 10^9 km with magnetic fields of about 10^4 G and are capable trapping charged nuclei in its acceleration regions. Electromagnetic forces in these regions can then accelerate the particle up to UHECR energies.

The luminosity of AGN can range from 10^{11} times the luminosity of the Sun up to hundreds of times this value [27]. The mass of the central nucleus can range from 10^8 to 10^{10} solar masses [27]. Therefore, AGN are extraordinary objects with the luminosity of an entire galaxy in a region

the size of the solar system. The region around the nucleus of the object is expected to contain large amounts of matter and radiation, which would cause heavier nuclei like iron to photo disintegrate and lose their energy. Therefore, if UHECR are seen to correlate with these regions then their composition is expected to be lighter nuclei and protons.

7.1 Time-Line of Auger's AGN Findings

The time periods under consideration were chosen based on a time line followed by the Auger collaboration, while determining that an excess of events above 57EeV was shown with AGN. In May 26, 2006, a scan in angular separation (defining a correlation with AGN), the lowest energy event (defining the UHECR set), and a redshift (defining the set of nearest AGN) found that the maximum value for Expression 8 occurred for AGN within a redshift of 0.018 and UHECR energies above 57 EeV, with a correlation defined as angular separations within 3.2^0 between an UHECR and the AGN.

Figure 40 shows the scan in energy, angular separation and redshift done in [28] showing that the redshift of around 0.018 gives the maximum deviation from isotropy. This analysis was first done by the PAO group at Bariloche.

The value of Expression 8 for these parameter values was 1.7×10^5, but does not represent a true deviation from isotropy. The significance of this value is biased by the scans performed and in order to find the true significance of this signal, a penalty factor needs to be considered. In order to get around having to find this penalty factor, a hypothesis will be stated apriori that UHECR above 57EeV correlate within 3.2^0 of AGN within a redshift of 0.018. This hypothesis that is stated apriori will be tested with an independent data set collected after May 26, 2006.

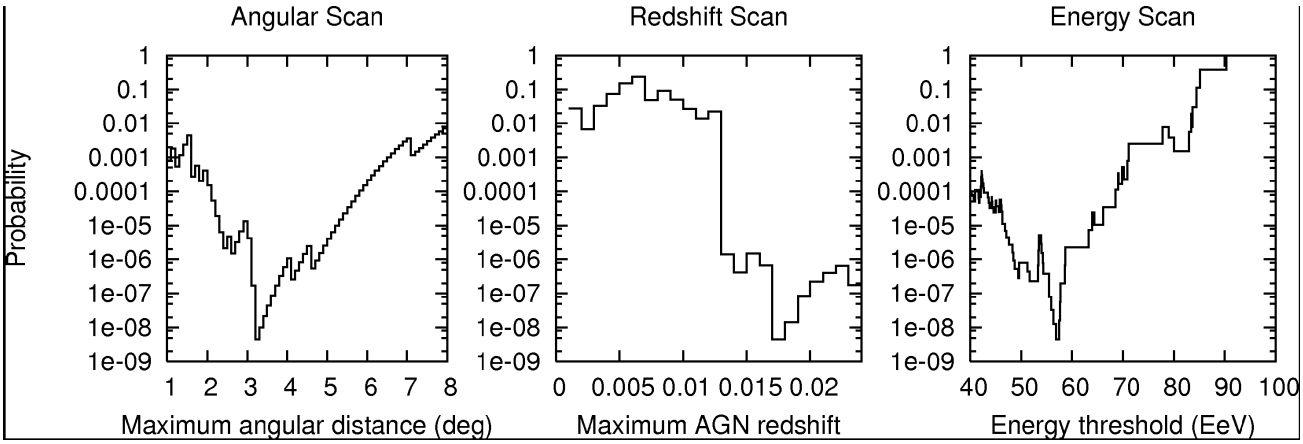

Figure 40: Scan in energy, angular separation and redshift giving the maximum deviation from isotropy. Taken from [28].

A prescription will be created indicating that the hypothesis is satisfied at less than 1%, when the value of Expression 8 becomes less than 0.01 for UHECR energies above 57EeV and AGN within a redshift of 0.018 with a correlation defined by an angular separation of less than 3.2^0. On August 31, 2007, the hypothesis was confirmed at less than 1%.

To reiterate, the Period between January 1, 2004 and May 26, 2006 will be named Period A. The Period between May 26, 2006 and August 31, 2007, will be named Period B. Finally, the Period between August 31, 2007 and June 15, 2008 will be named Period C.

7.2 AGN Correlation Analysis

In order to determine if a possible correlation exists between UHECR events and AGN, deviations from isotropy are calculated with the integrated binomial probability shown in Expression 8. The

scan of Expression 8 in energy and angular separation defining a correlation is shown in Figure 41. The scan in angular separation is required because apriori it is not known what kind of deflection the UHECR will undergo before they reach us. The scan over energy is required because apriori it is not known below what energy the events are scrambled over the sky and isotropic. The values of energy and angular separation that result in the lowest value of Expression 8 show the greatest deviation from isotropy. For Period A, the minimum value of Expression 8 in this scan occurs at 3.3^0 angular separation for the top 14 events above 57 EeV. The projection at the minimum from Figure 41 can be seen in Figure 42.

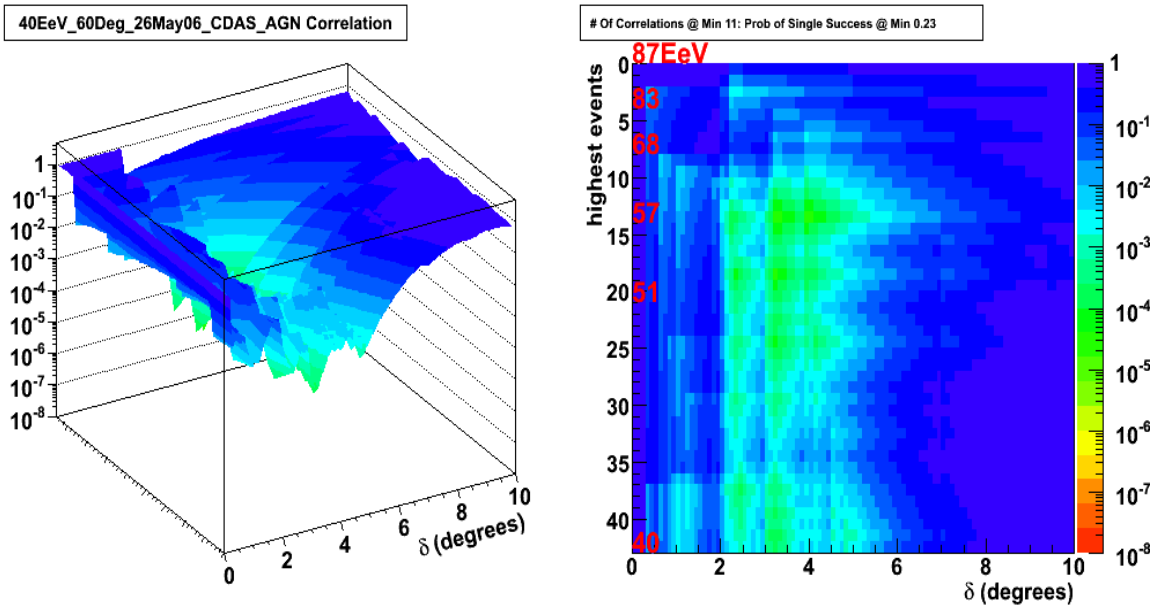

Figure 41: Scan of possible deviation from isotropy for events above 40EeV within 60^0 zenith found for Period A.

The relative exposure weighted area 3.3^0 around the AGN covers 0.23 of the sky; therefore, the binomial probability of getting 11 correlations out of 14 given a chance probability of 0.23 is about 2.0×10^{-5}. The galactic sky map of these 14 events is shown in Figure 43. Therefore, it appears that events above 57 EeV may come from AGN and are deflected up to 3.3^0. However, it must be remembered that this is not an apriori prediction because a scan over energy and angular separations was performed; and so, it is not a true measure of the signal's significance. Perhaps the low value of Expression 8 was an accident, a statistical fluctuation.

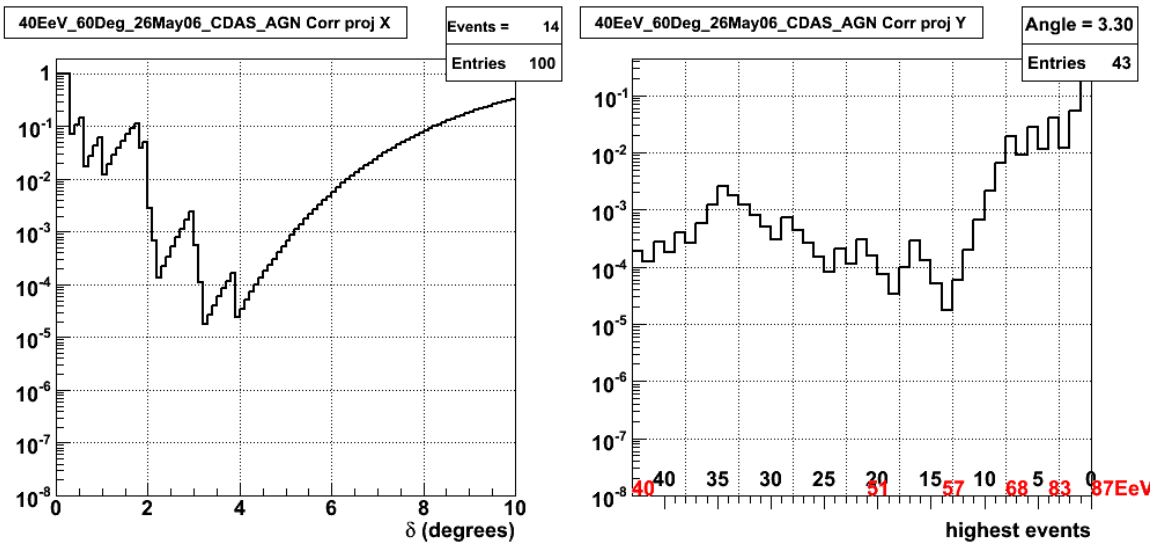

Figure 42: Maximum potential deviation from isotropy occurs among the top 14 events at an angular separation of 3.3 degrees for events above 40EeV for Period A.

Rather this hypothesis must be tested with an independent data set. A prescription will be proposed as a means of determining the true significance of the correlation with AGN. The hypothesis that events above 57 EeV come from AGN within a redshift of 0.018 and correlate

within 3.3^0 is proposed and events after May 26, 2006 will be considered as an independent data set that will be used to confirm this apriori hypothesis. The prescription will be satisfied when at less than 1% confidence when Expression 8 becomes less than 0.01. The prescription was then found to be satisfied on August 31, 2007, at less than 1% confidence.

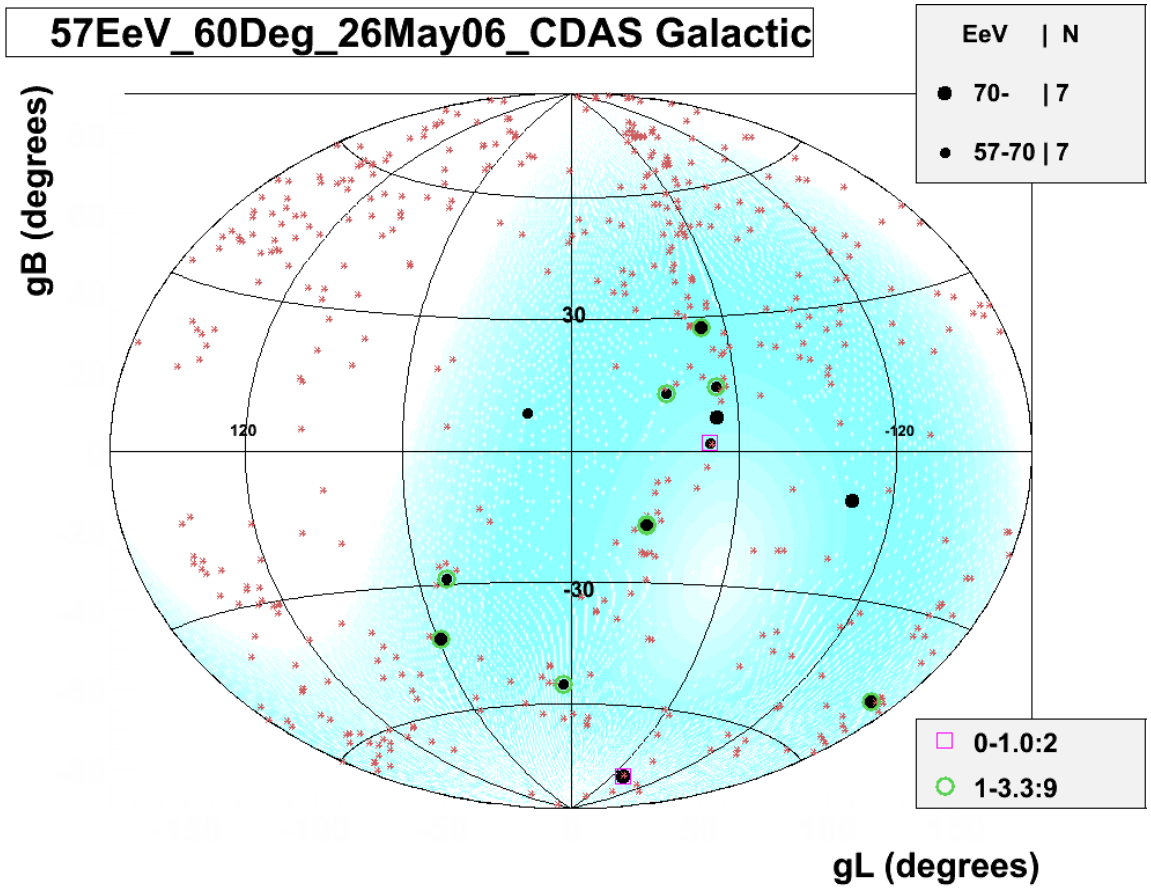

Figure 43: Galactic sky map of Auger events above 57EeV (within 60^0 zenith) shown as black dots with size of dot indicating energy. AGN are shown in red. Among these top 14 events collected up until May 26, 2006, we find 11 correlations within 3.3^0. Correlations shown in red squares correspond to separations less than 1^0 degree and green circles for correlations within 1^0-3.3^0.

The galactic sky map for events above 57 EeV within 60^0 zenith for Period B is shown in Figure 44. Among these 14 events, eight are correlated within 3.3^0 of an AGN. The chance probability for a single event from an isotropic distribution to correlate with an AGN is 0.23. Therefore, the chance probability of this occurring is about 6.0×10^{-3} from Expressions 7 and 8. This is a true measure of deviation from isotropy.

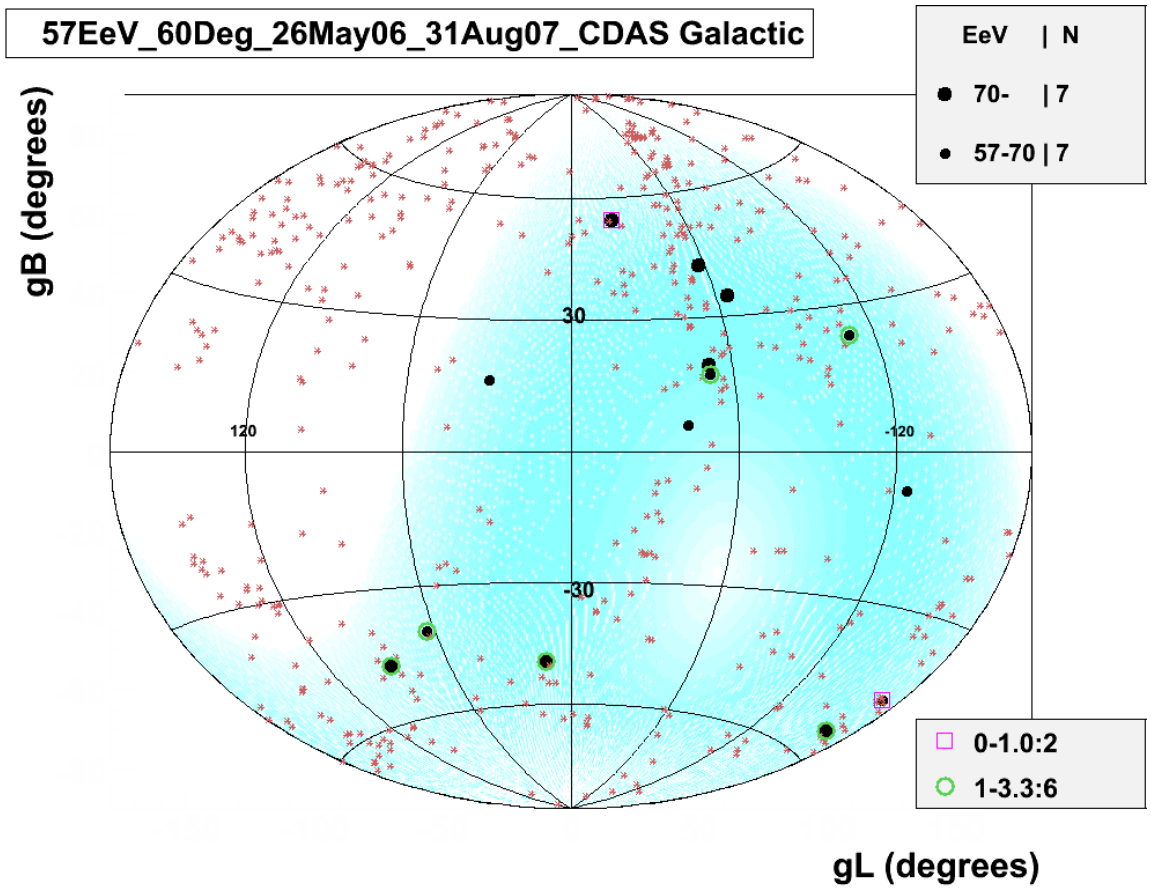

Figure 44: Galactic sky map for events above 57 EeV (within 60^0 zenith) for Period B. AGN are shown in red. Among these 14 events, 8 are correlated within 3.3^0.

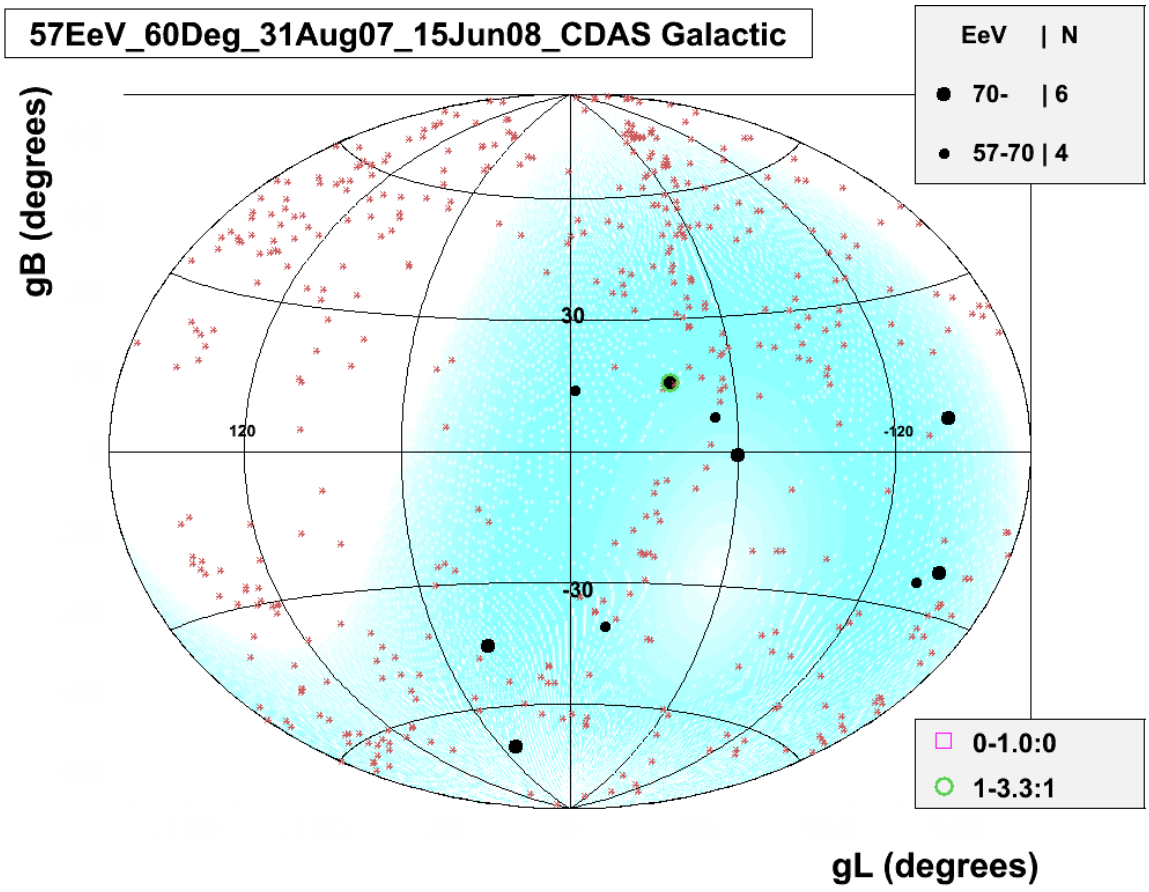

Figure 45: Galactic sky map for events above 57 EeV (within 60^0 degrees zenith) for Period C. The size of the black dot corresponds to the event's energy. AGN are shown in red. Among these ten events, one is correlated within 3.3^0. The chance probability of getting one or more correlations out of ten is found to be 0.927 using Expression 8.

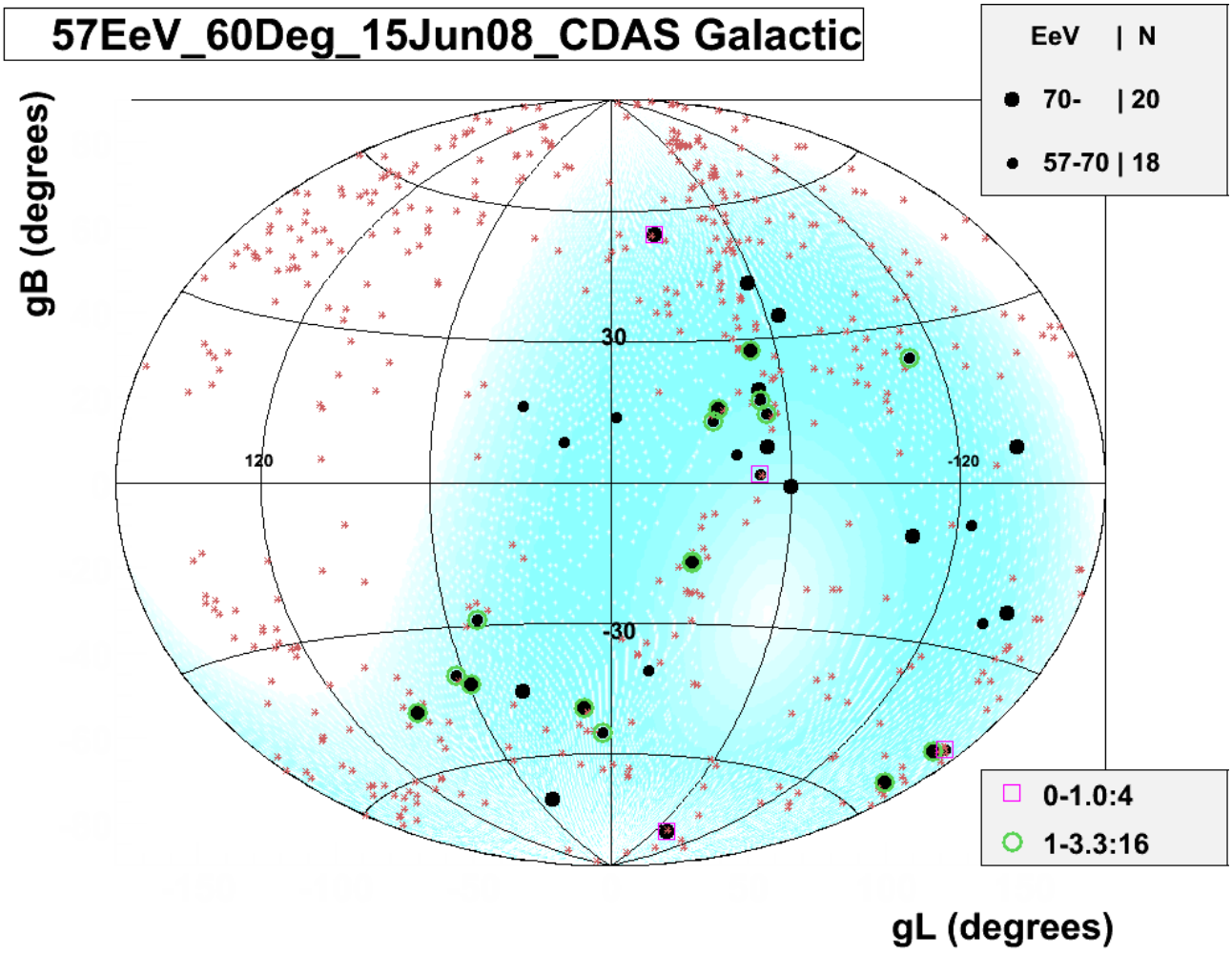

Figure 46: Galactic sky map of events above 57 EeV (within 60^0 zenith) collected between January 2004 and June 15, 2008 (Periods A, B, C). AGN are shown as red stars. Correlations within 1^0 are shown with red squares of which there are four, while correlations between 1^0 and 3.3^0 are shown with green circles of which there are 16.

Let us also consider events for Period C. This also serves as an independent data set allowing another test of the hypothesis as described in the prescription with blind analysis. Figure 45 shows that for Period C, Auger sees ten events above 57 EeV. Of these ten events, only one is correlated with an AGN within 3.3^0. The average number of expected correlations among ten isotropically distributed events is 2.3 events. This appears to refute the claim of the correlation with AGN within a redshift of 0.018.

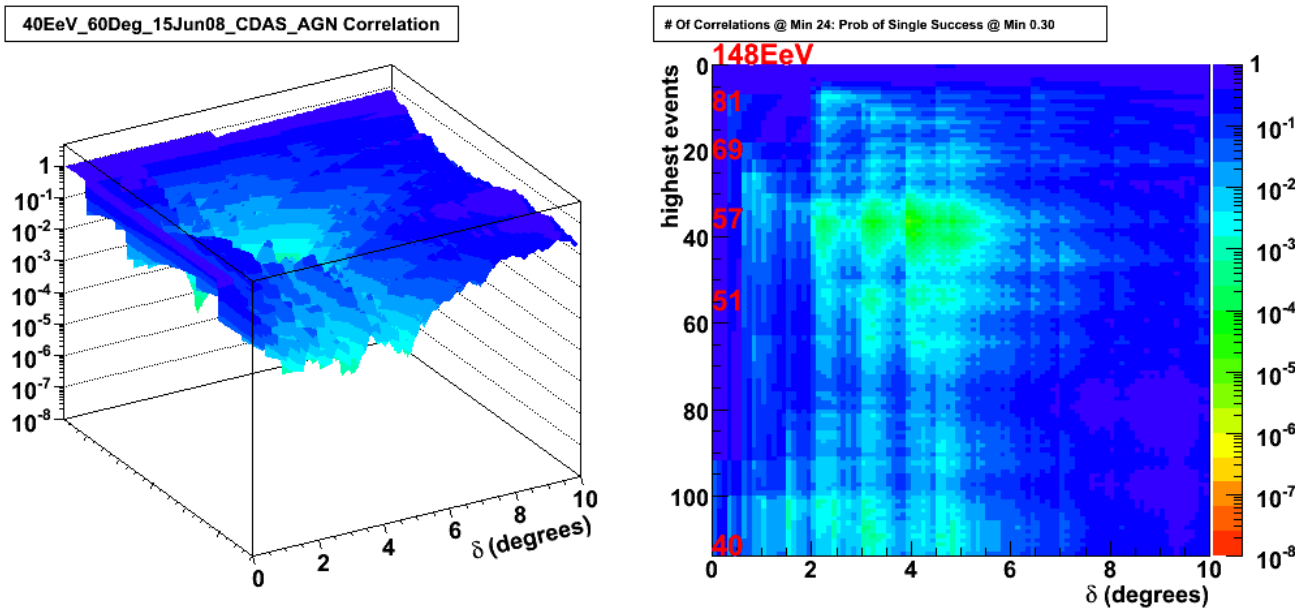

Figure 47: Scan of Expression 8 for events above 40 EeV (within 60^0 zenith) collected between January 1, 2004 and June 15, 2008 (Periods A, B, C).

The galactic sky map of events above 57 EeV (within 60^0 zenith) collected between January 1, 2004 and June 15, 2008 is shown in Figure 46. The scan of Expression 8 in energy and angle is shown in Figure 47, while the projection at the minimum of this scan is shown in Figure 48.

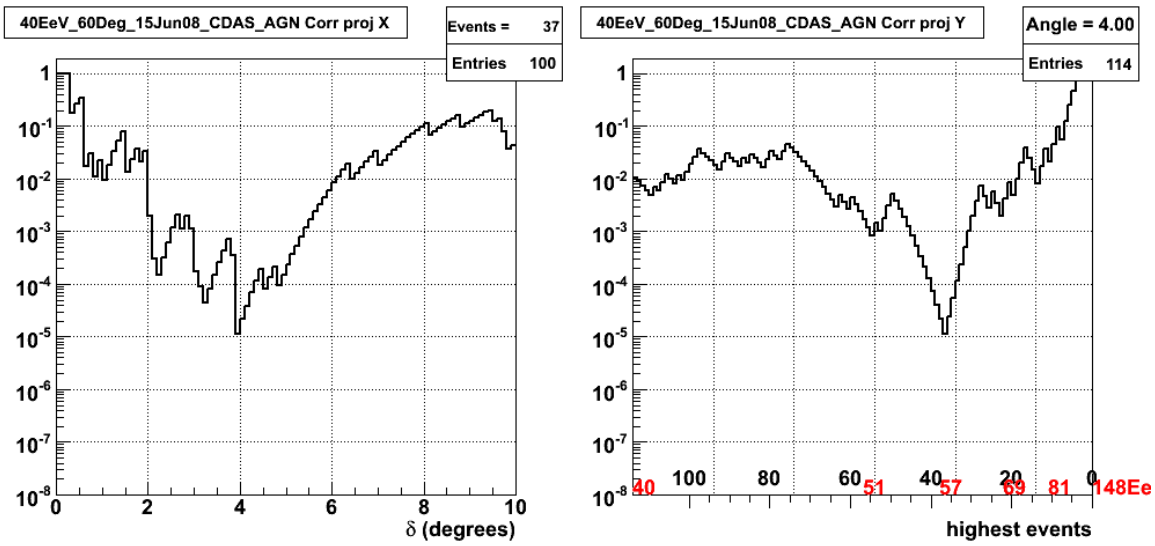

Figure 48: Minimum of scan of Figure 47 for events collected between January 1, 2004 and June 15, 2008 (Periods A, B, C).

7.3 AGN Analysis Summary

The region 3.2^0 around AGN within a redshift of 0.018, covers 23% of the sky; and so, an isotopic sky is expected to give 2.3 correlations among every ten events. Ten events above 57EeV are collected during Period C; and so for an isotropic sky, at least 2.3 events on average are expected to correlate within 3.2^0 of an AGN. However, only one correlation is found. This casts doubt on the validity of the hypothesis that UHECR above 57EeV correlate within 3.2^0 of AGN within a redshift of 0.018.

CHAPTER 8

Radio Galaxies

Another type of object, which is also thought to be powered by a super-massive black hole, are the radio galaxies. The size of these objects is on the order of hundreds of kpc, while their magnetic field strength is on the order of 10^{-6} G. These objects serve as possible source candidates because their magnetic fields are able to trap charged particles in the very large acceleration regions of the radio galaxy. These regions can include very large radio lobes that shoot out of the central galactic nucleus. Charged particles can be accelerated electromagnetically in these regions. The radio features of the radio galaxies fall into two categories called FRI and FRII [27] depending on whether the intensity of the radio signal decreases away from the core (FRI) or increases away from the core (FRII). Figure 49 shows FRI type in the top row and intermediate FRI-FRII type in the bottom two rows.

8.1 Radio Galaxy Correlation Analysis

In [29], it is shown that among Auger's high energy cosmic rays that showed correlation with AGN, a strong correlation with nearby radio galaxies within about 70 Mpc also exists. The scan of

possible correlation signal, for events above 40 EeV within 60^0 zenith until August 31, 2007, is shown in Figure 50. The most significant point in the scan occurs at 3.5^0 among the top 20 events, the projection at the minimum of the scan as shown in Figure 51. This corresponds to energies >64EeV

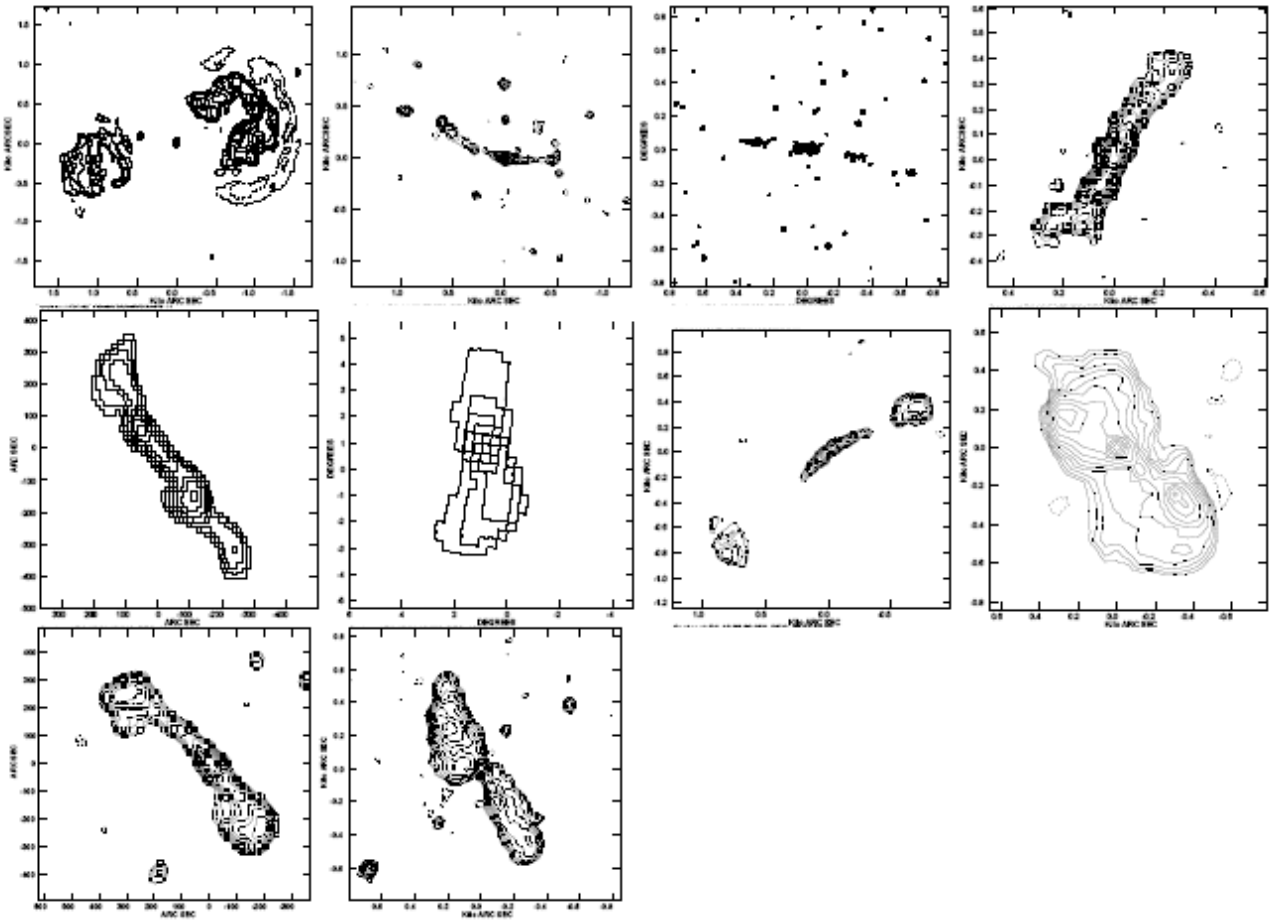

Figure 49: Radio morphologies of ten nearest radio galaxies. FRI radio galaxies on top row. Intermediate FRI-FRII radio galaxies on bottom two rows. Cen A is in the middle row 2nd from left. Taken from [29].

Therefore, the claim that radio galaxies are a significant source of UHECR may be true [29].

However, this claim must be used to set a prescription, which can be checked with an independent data set. This independent data set will correspond to events collected during Period C.

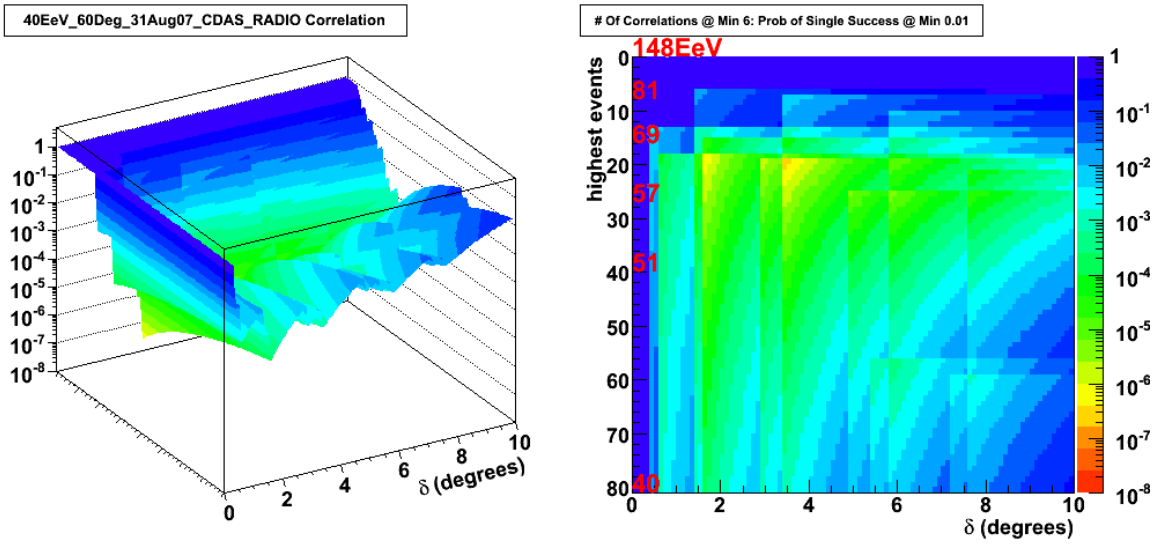

Figure 50: Scan of Expression 8 for correlations with radiogalaxies for events above 40 EeV until August 31, 2007.

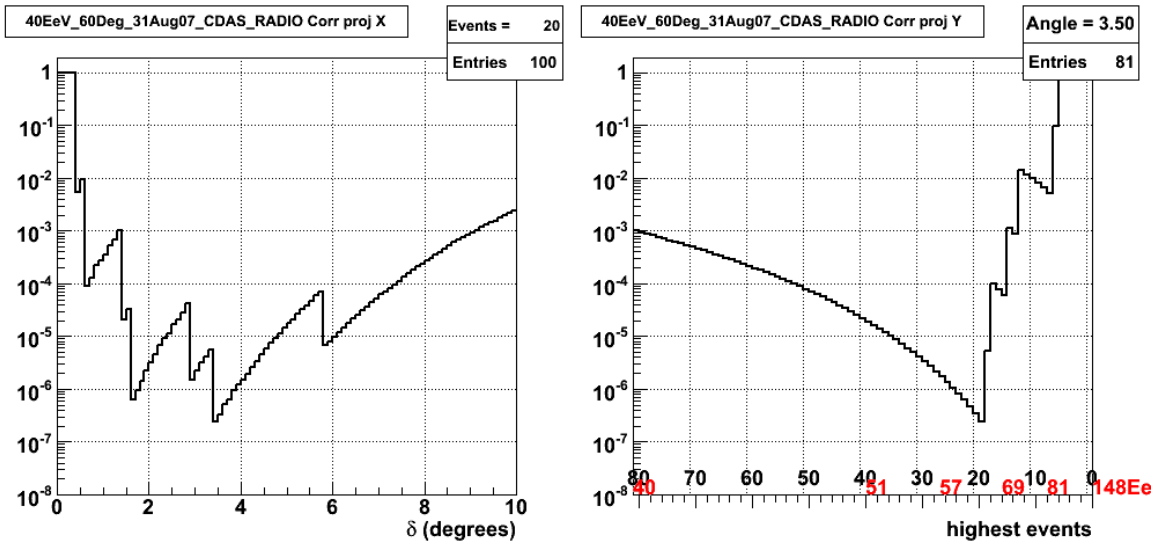

Figure 51: Location of maximum possible significance from scan of Figure 50. The maximum correlation occurs at 3.5^0 among the top 20 events above 64 EeV.

Figure 52 shows the scan of events above 40 EeV (within 60^0 zenith) for Period C. It shows that the high energy events, which were claimed to be correlated within 3.5^0 of radio galaxies, may in fact not be true and rather a statistical fluctuation. The independent data set is consistent with isotropy; and therefore, casts doubt on the claim of [29].

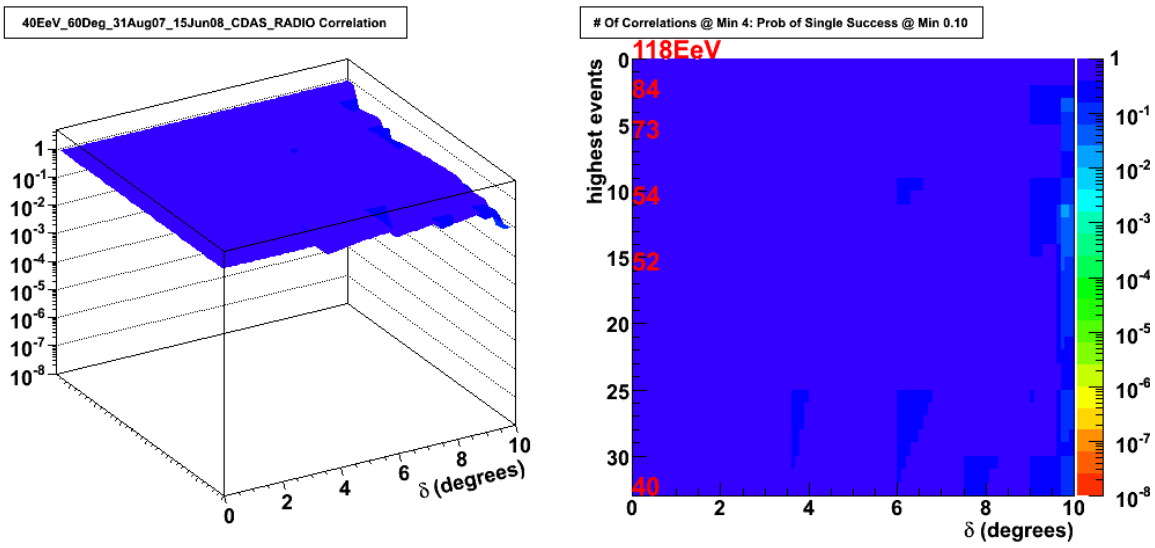

Figure 52: Scan of events above 40 EeV (within 60^0 zenith) for Period C. The sky above 57EeV with 3.5^0 corresponding to a correlation is shown to be consistent with isotropy.

Another test is done to study the claim that UHECR correlate with nearby radio galaxies as made in [29] by splitting up the time between January 1, 2004 and June 15, 2008 into three time Periods A, B, C. This allows us to do blind analyses on three independent data sets.

Figure 53 shows the galactic sky map for events above 57 EeV (within 60^0 zenith) for Period A. The nearby radio galaxies are shown in red. Among these 14 UHECR events, two are correlated within 3.5^0. Given the chance probability of a single success as 0.1, the chance probability of getting two events is found to be 0.008.

Figure 54 shows the galactic sky map for events above 57 EeV (within 60^0 zenith) for Period B. Among these 14 events, four are correlated within 3.5^0 corresponding to a chance probability of 9.2×10^{-6}.

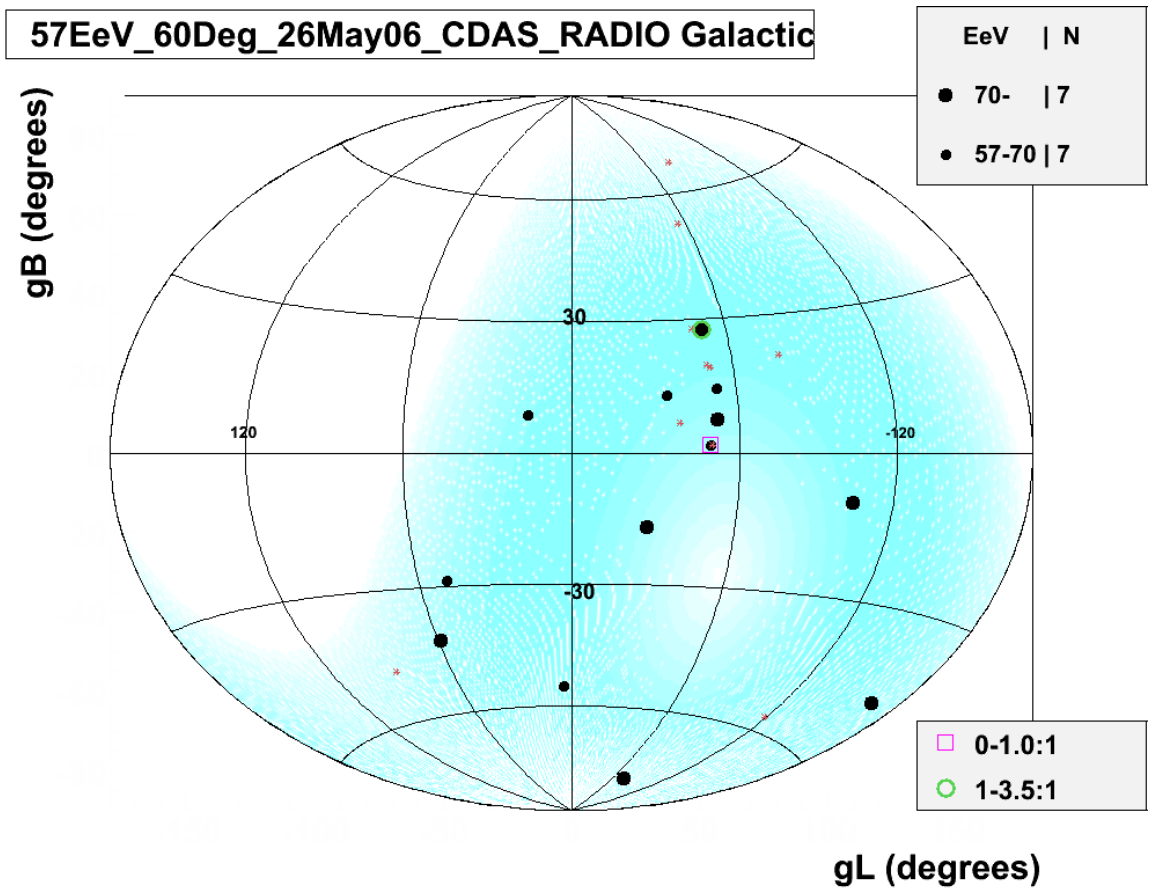

Figure 53: Galactic sky map for events above 57 EeV (within 60^0 zenith) for Period A. Nearby radio galaxies are shown in red. Among these 14 events, two are correlated within 3.5^0.

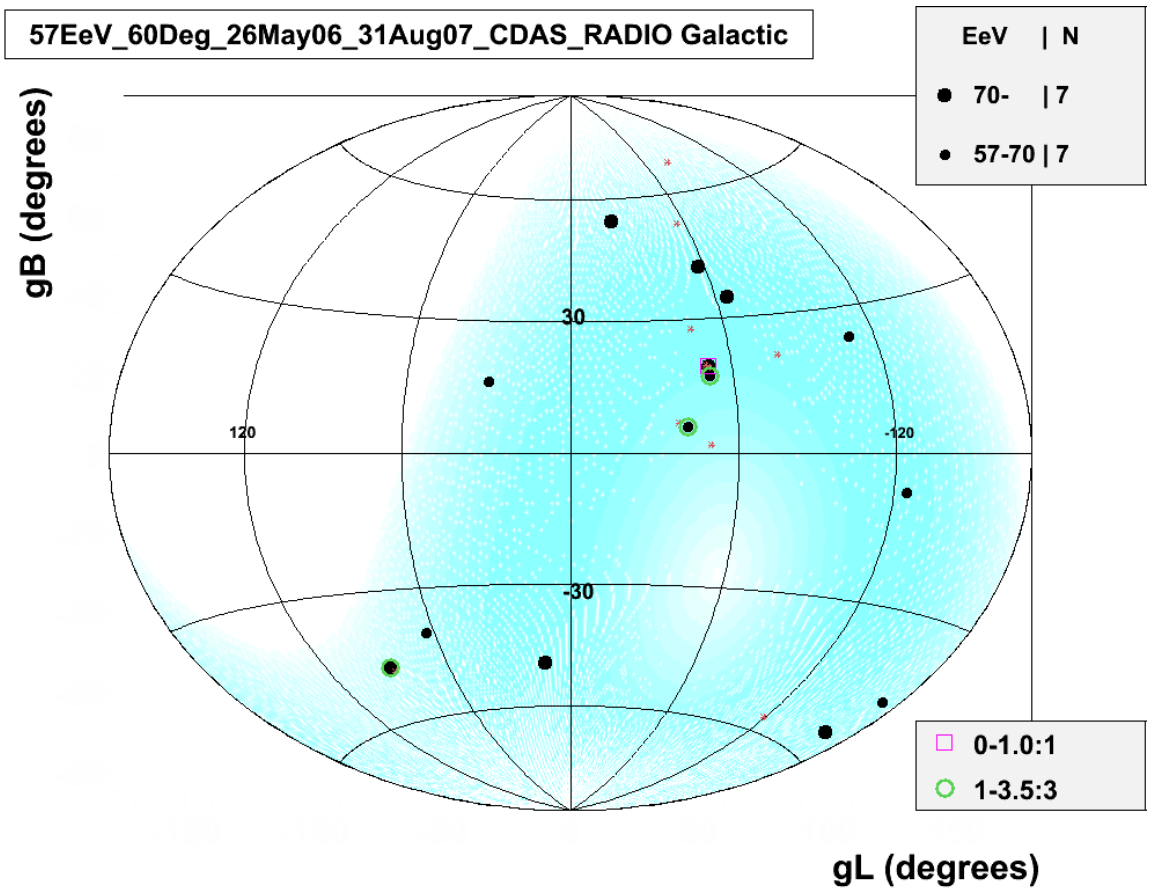

Figure 54: Galactic sky map for events above 57 EeV (within 60^0 zenith) for Period B. Nearby radio galaxies are shown in red. Among these 14 events, 4 are correlated within 3.5^0.

Figure 55 shows the galactic sky map of Auger events with energies greater than 57 EeV (within 60^0 zenith) for Period C. The lowest energy event at galactic latitude of 7.6^0 and galactic longitude of -51.8^0 is the lowest energy event at 60 EeV. Of these ten events, none are correlated within 3.5^0 of a nearby radio source.

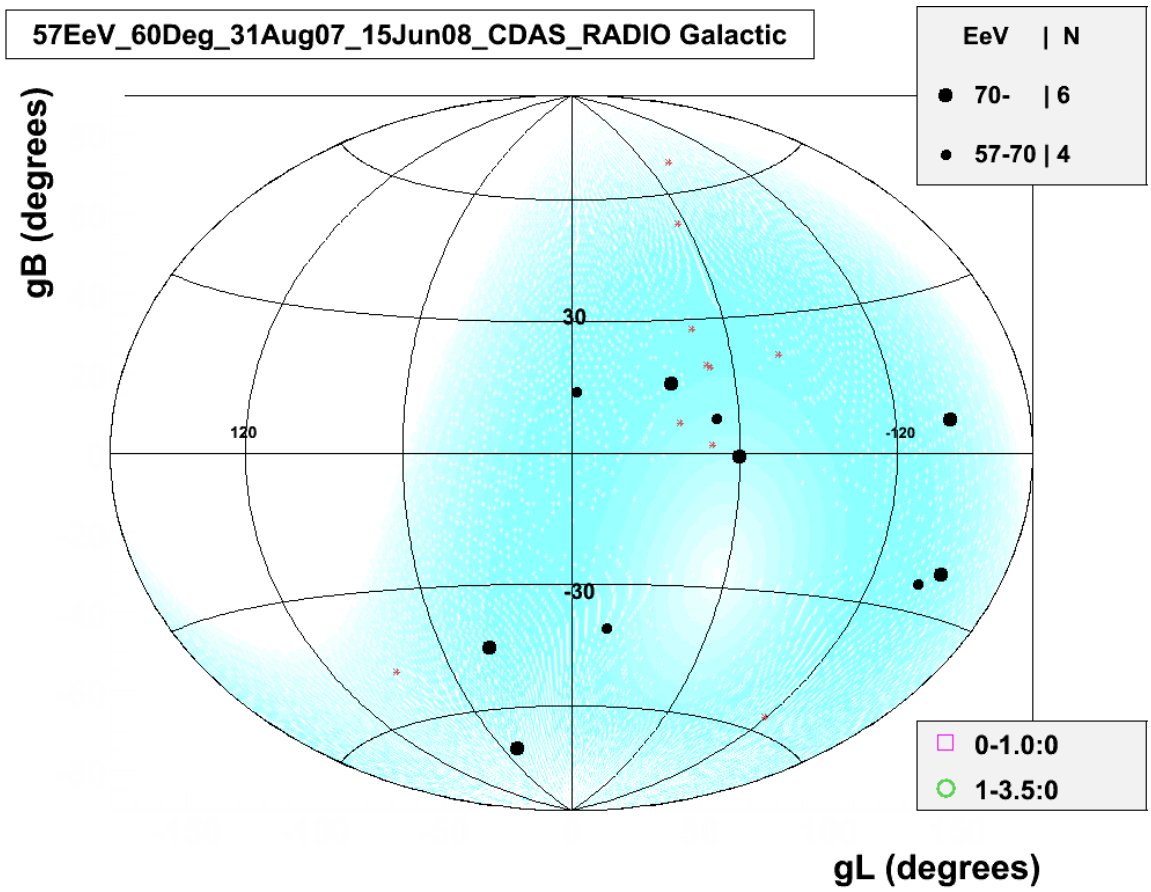

Figure 55: Galactic sky map of Auger events with energies greater than 57 EeV (within 60^0 zenith) for Period C.

It is interesting to note that two of the events in Period B are correlated with Cen A; and if these two events are removed, the chance probability decreases substantially. One of these events correlates within 1^0 and the other is between 1^0 and 3.5^0. The scan over energies above 40EeVand angular separation is shown in Figure 56 for all events June 15, 2008 and shows that the correlation signal has decreased compared to the signal of May 26, 2006.

8.2 Radio Galaxy Correlation Analysis Summary

The region 3.5^0 around radio galaxies covers 10% of the sky, and so under the assumption of isotropy, we expect one correlation on average among the ten events found during Period C. However, no correlations were found. This disfavors the hypothesis laid out in [29].

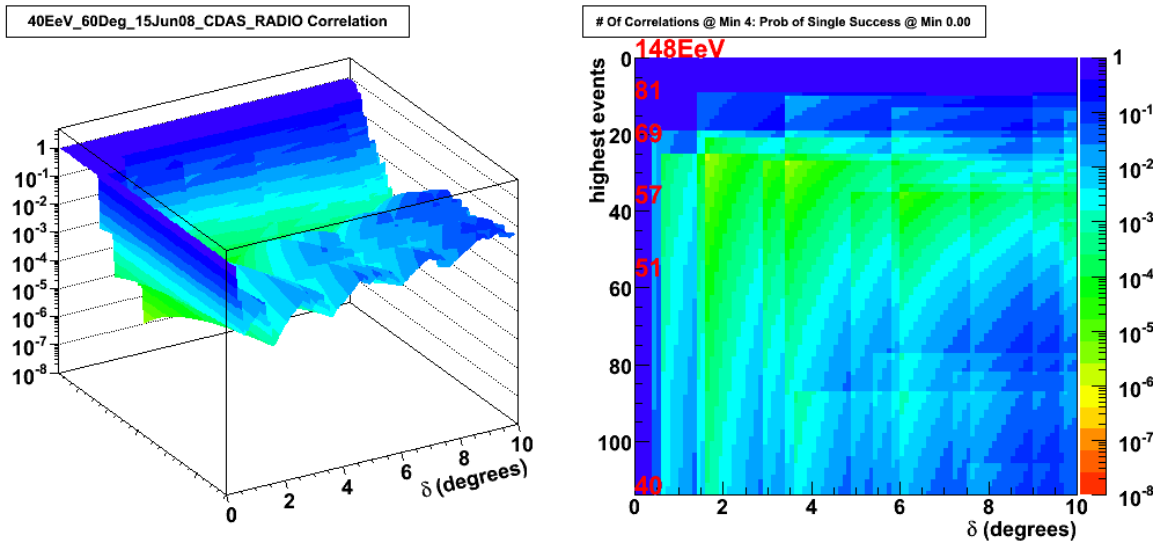

Figure 56: Scan of events above 40 EeV (within 60^0 zenith) until June 15, 2008.

CHAPTER 9

Cen A

NGC5128 or Centaurus A (Cen A) is included in both the radio galaxy set and the AGN set. Its radio morphology is shown in Figure 49 in the middle row second from the left. It is the closest of the nearby radio galaxies at a distance of 3.4 Mpc. Cen A has two jets shooting out of its core region, which are thought to be the result of a galaxy merger that yielded a high-mass and high-spin central black hole.

Figure 57 shows the galactic sky map of the radio sky at 408MHz, the galactic center of the galaxy is at the center. Cen A can be seen in the upper right quadrant of the sky map near the inner part of the galaxy. It is the object that is extended north-south with a size of about 10^0 [30]. The radio lobes and the galaxy's plane can be seen in Figure 58, which shows Cen A's image in the optical and radio regimes. The radio lobes visible in the radio regime indicate that the jet's axis and the perpendicular to the dust plane of the galaxy are not aligned. This is thought to be the result of a galaxy collision indicating that Cen A is a collision remnant [31]. The central nucleus of this active galaxy is less than a parsec in size, while huge radio plumes extend away from the core for about

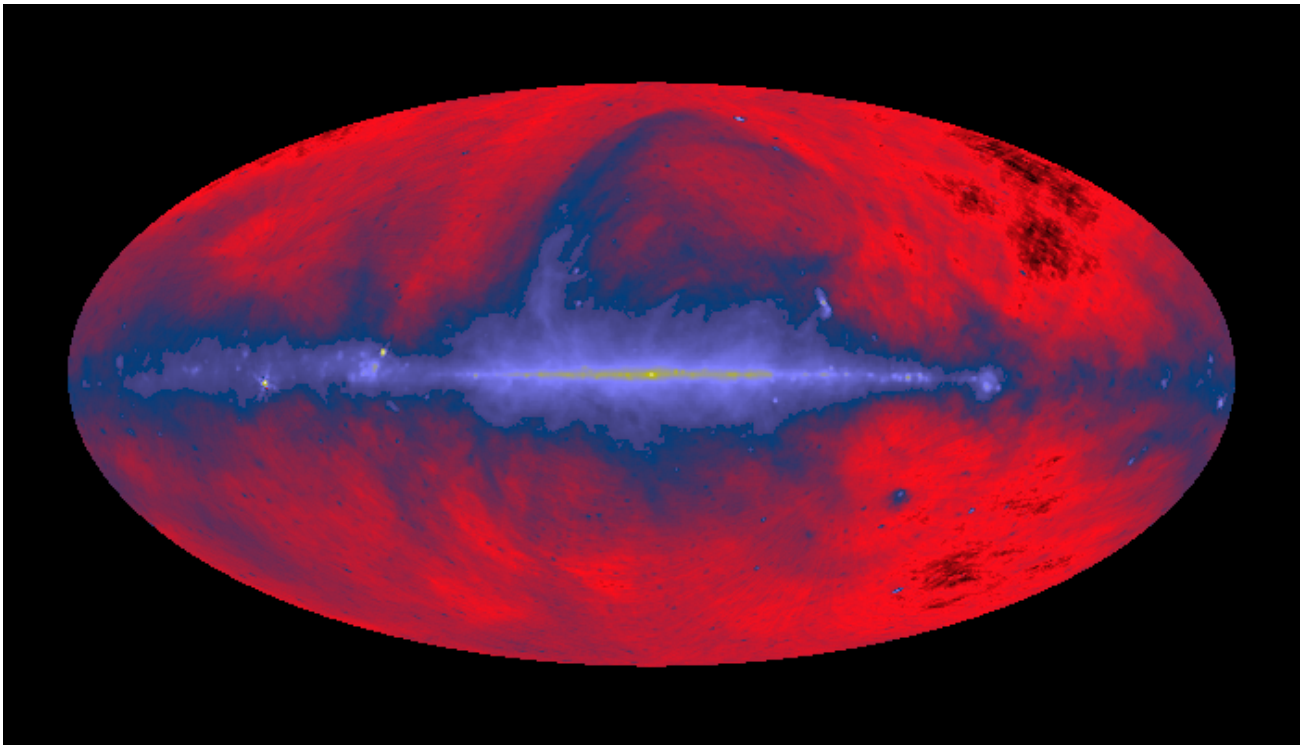

Figure 57: Galactic sky map from Max Planck Institute. Cen A is in the upper right quadrant close to the inner galaxy but separate from it.

250 kpc [32]. Relativistic jets emanate from the central core out to a few parsecs; beyond this, the jets are non-relativistic. Figure 37 shows the locations in the sky with the largest UHECR anisotropy occurs in the region around Cen A.

Figure 58: Radio and optical image of Cen A from STScl and NASA.

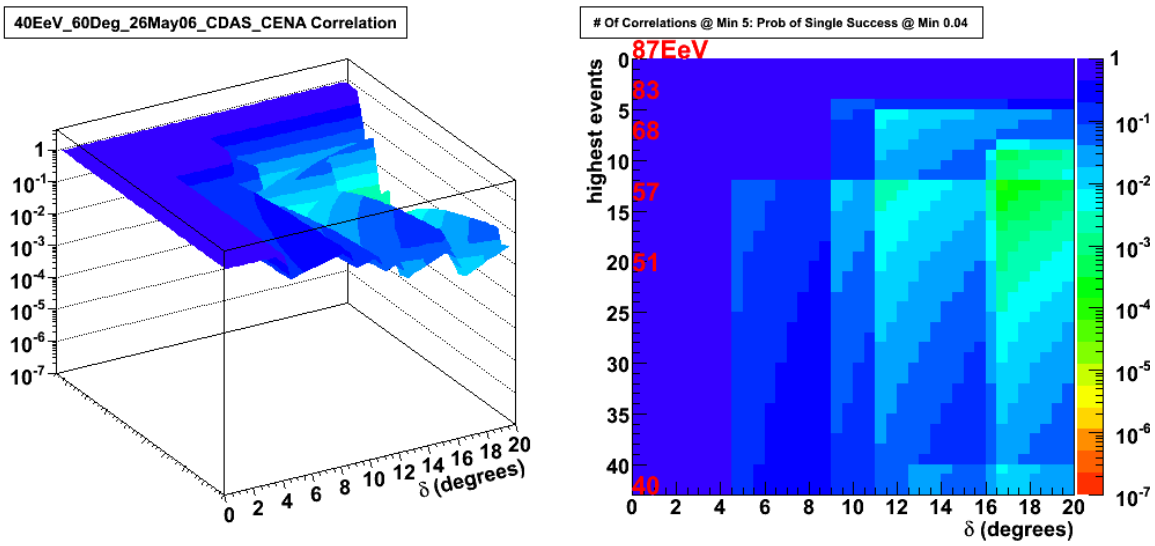

Figure 59: Scan in energy and angular separation for events above 40 EeV (within 60^0 zenith) for Period A. Maximum possible correlation signal occurs at 17 degrees for top 13 events.

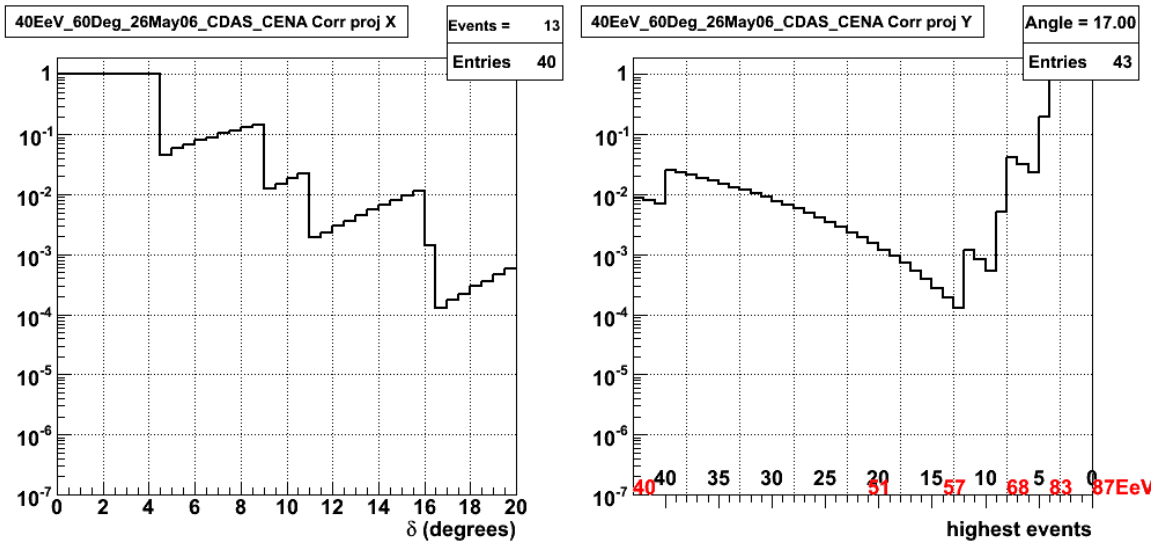

Figure 60: Projection of location of maximum possible correlation from scan in energy and angular separation for events above 40 EeV within 60 degrees zenith for Period A. Maximum possible correlation signal occurs at 17^0 for top 13 events.

9.1 Cen A Correlation Analysis

The scan of Expression 8 for events greater than 40EeV with Cen A is shown in Figure 59 and the projection at the minimum of 10^{-4} is shown in Figure 60. The minimum of the scan occurs at 17^0 among the top 13 events or for energies above 57.5 EeV.

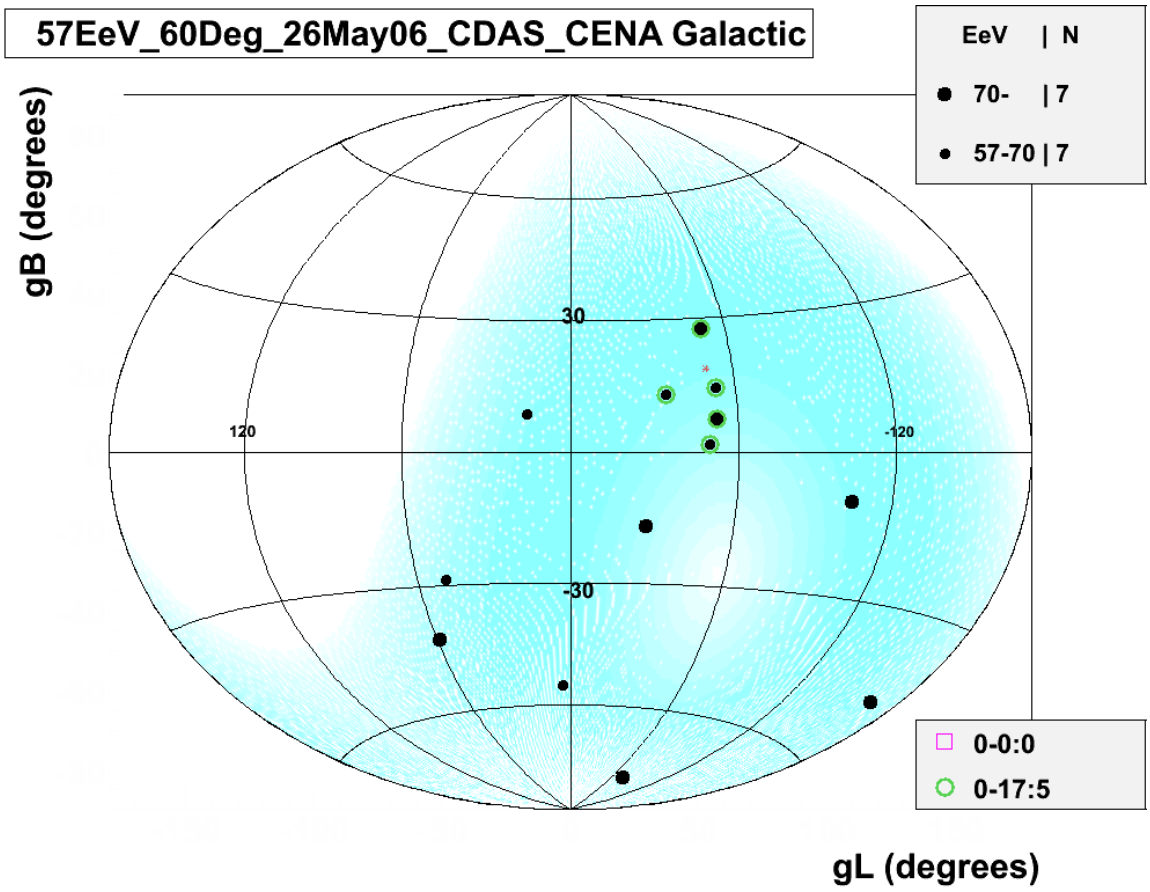

Figure 61: Galactic sky map for events above 57 EeV (within 60^0 zenith) until May 26, 2006. Cen A is shown in red. Among these 14 events, five are correlated within $17^{0.}$

The galactic sky map for events above 57 EeV for Period A is shown in Figure 61. Cen A is shown in red. The lowest energy event in the set with an energy of 57.45 EeV at 4.2^0 galactic longitude

and galactic latitude of -54.8^0 is not included in the event set, which gives the maximum deviation from isotropy. Excluding this event, we have five events correlated among the top 13 energy events above 57.5 EeV.

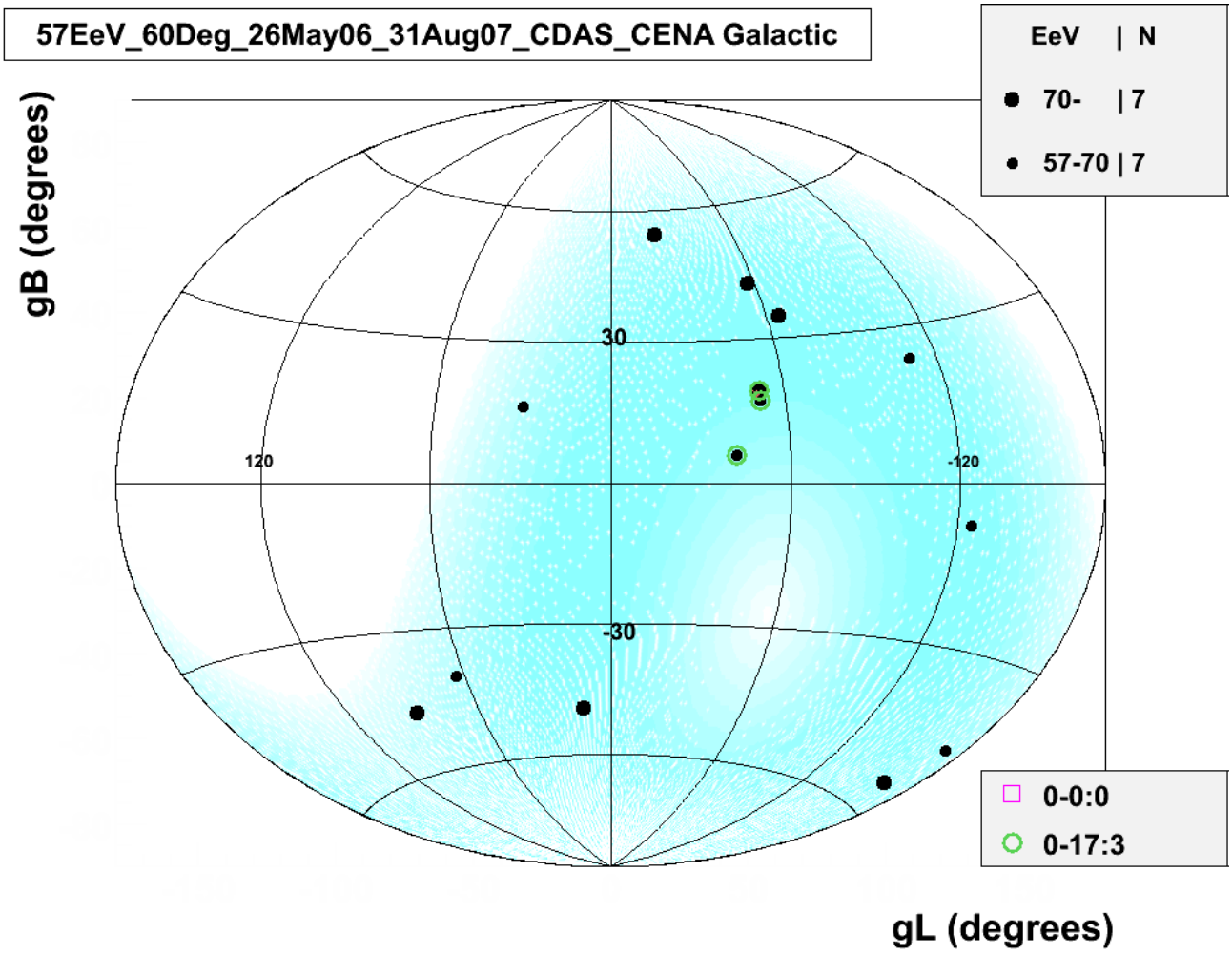

Figure 62: Galactic sky map for events above 57 EeV (within 60^0 zenith) for Period B. Size of black dot corresponds to events energy. Cen A is shown in red. Among these 14 events, three are correlated within 17^0.

We will also look for the correlation signal with Cen A with two other independent event sets collected between May 26, 2006 and August 31, 2007 (Period B); in addition to August 31, 2007 and June 15, 2008 (Period C). The galactic sky map for events above 57 EeV collected during Period B is shown in Figure 62. Among these 14 events, three are correlated within 17^0 of Cen A. The scan of Expression 8 for these events is shown in Figure 63. The projection at this scan minimum is shown in Figure 64, which indicates that the minimum occurs among the top nine events above 69 EeV at an angular separation of 2^0. Among these nine events, there are two correlations. However, we are more concerned with events above about 57 EeV at 17^0 in order to test if the original signal can be corroborated. Given a chance probability of 0.04 for a single event

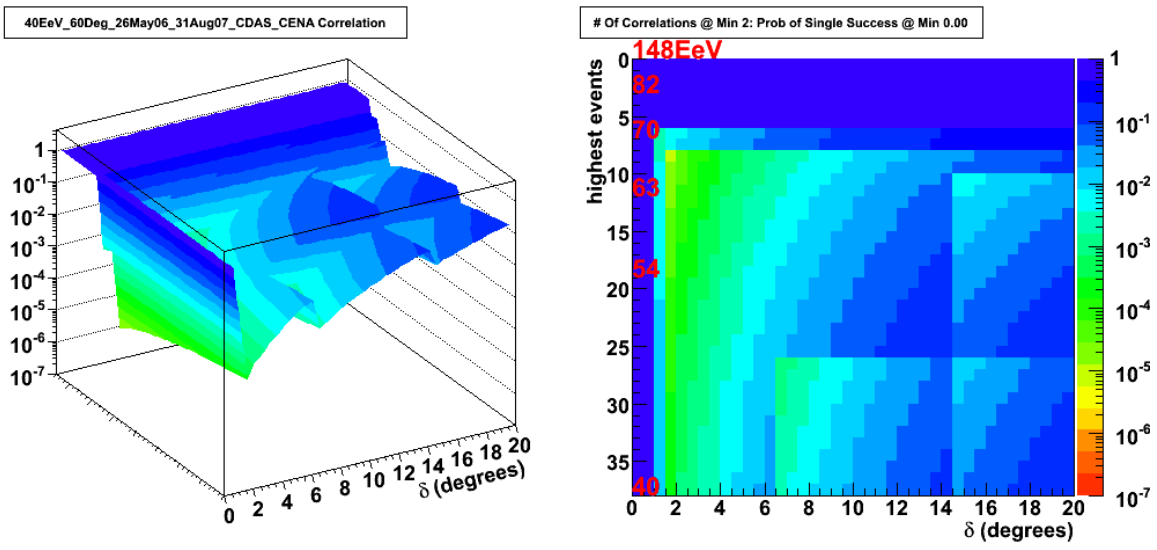

Figure 63: Scan in energy and angular separation for events above 40 EeV (within 60^0 zenith) for Period B. Maximum possible correlation signal occurs at 2^0 for the top nine events.

to fall within 17^0 of Cen A, Expression 8 gives chance probability for three events out of 14 to land

within 17^0 of Cen A as 0.02. The galactic sky map for events above 57 EeV for Period C is shown in Figure 65. The scan of Expression 8 for this sky is shown in Figure 66, while the projection of the minimum occurs among the top 11 events above 54.5 EeV at 18^0. Again, we are concerned with the correlation signal with Cen A for events above 57 EeV at 17^0 angular separation. Using Expression 8, with a chance probability of a single success at 0.04, the probability of getting two out of ten correlations is 0.06.

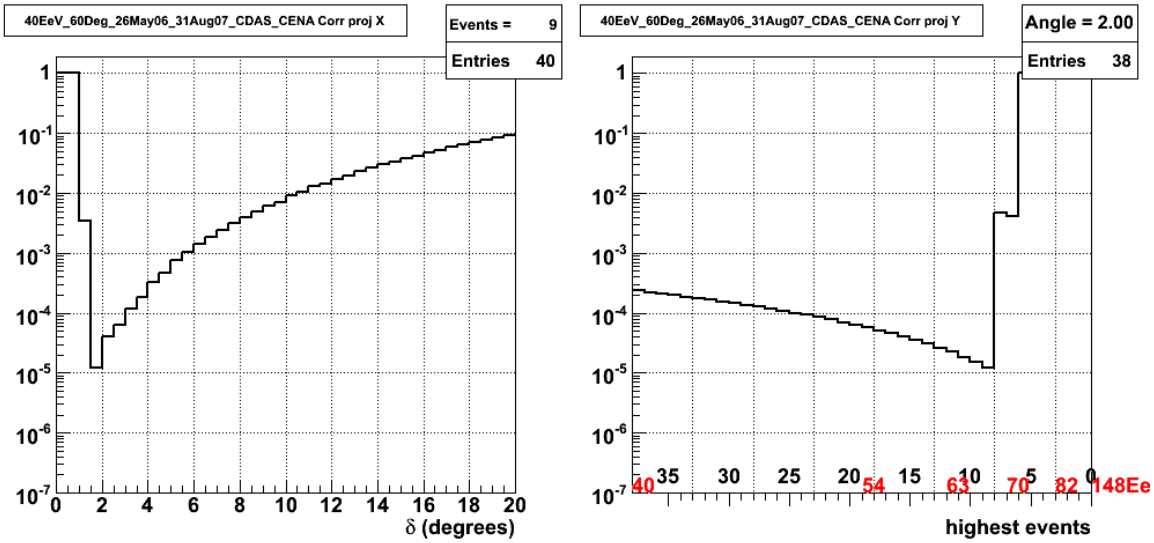

Figure 64: Projection of position of maximum possible deviation from isotropy from scan in energy and angular separation for events above 40 EeV (within 60^0 zenith) for Period B. Maximum possible correlation signal occurs at 2^0 for top nine events above 69 EeV.

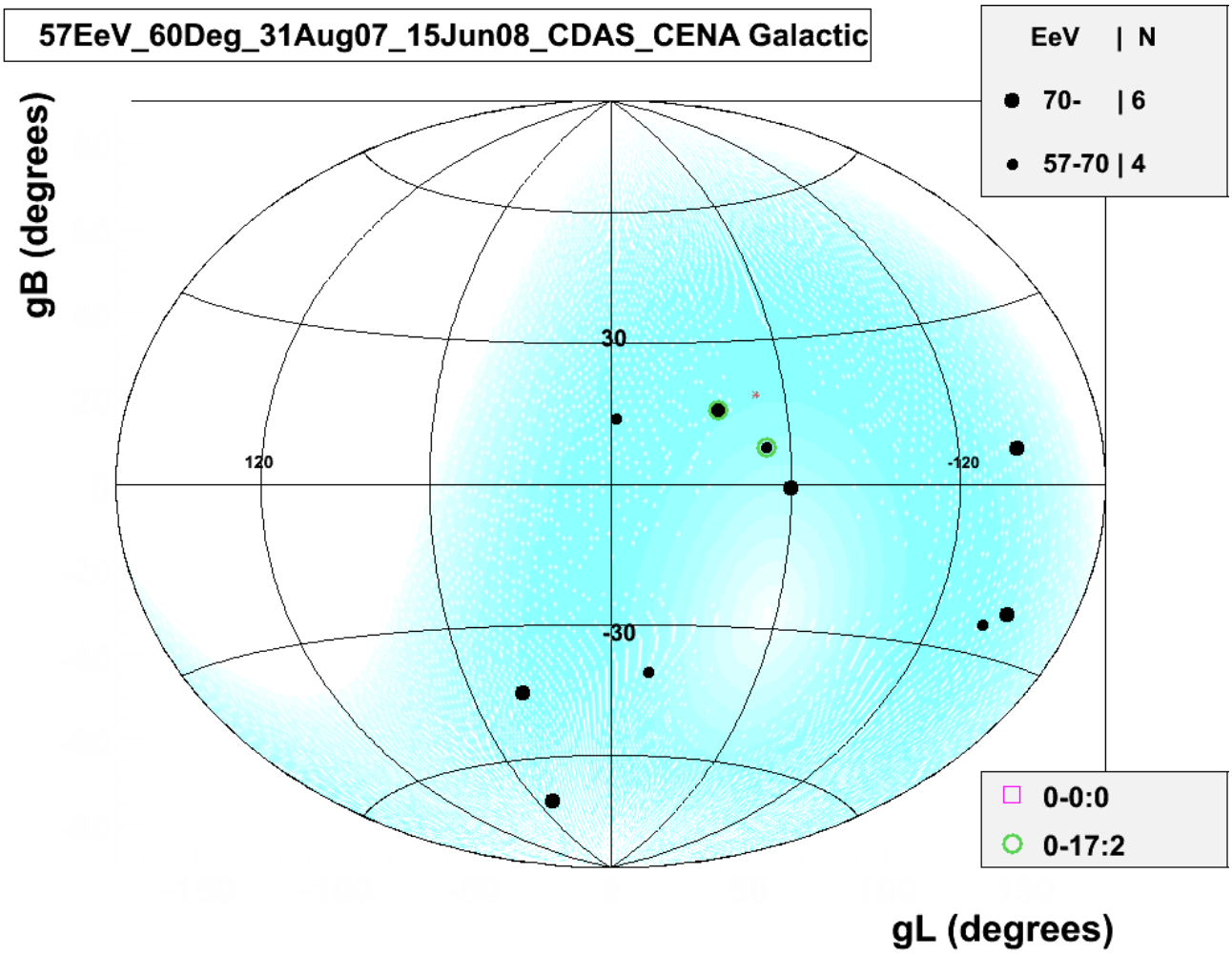

Figure 65: Galactic sky map for events above 57 EeV (within 60^0 zenith) for Period C. The size of the black dot corresponds to events energy. Cen A is shown in red. Among these ten events, two are correlated within 17^0.

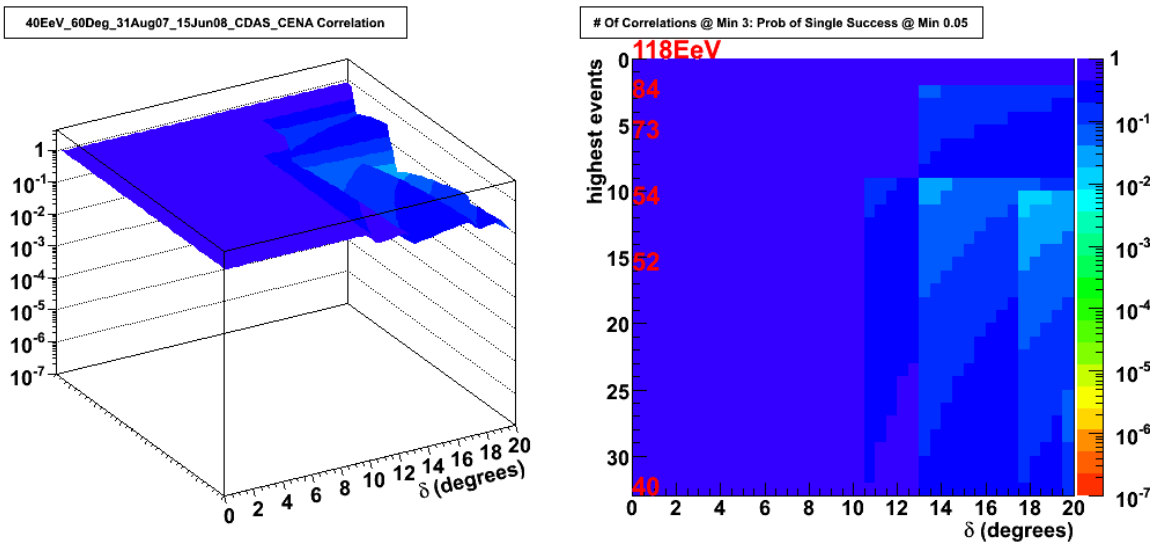

Figure 66: Scan in energy and angular separation for events above 40 EeV (within 60^0 zenith) for Period C.

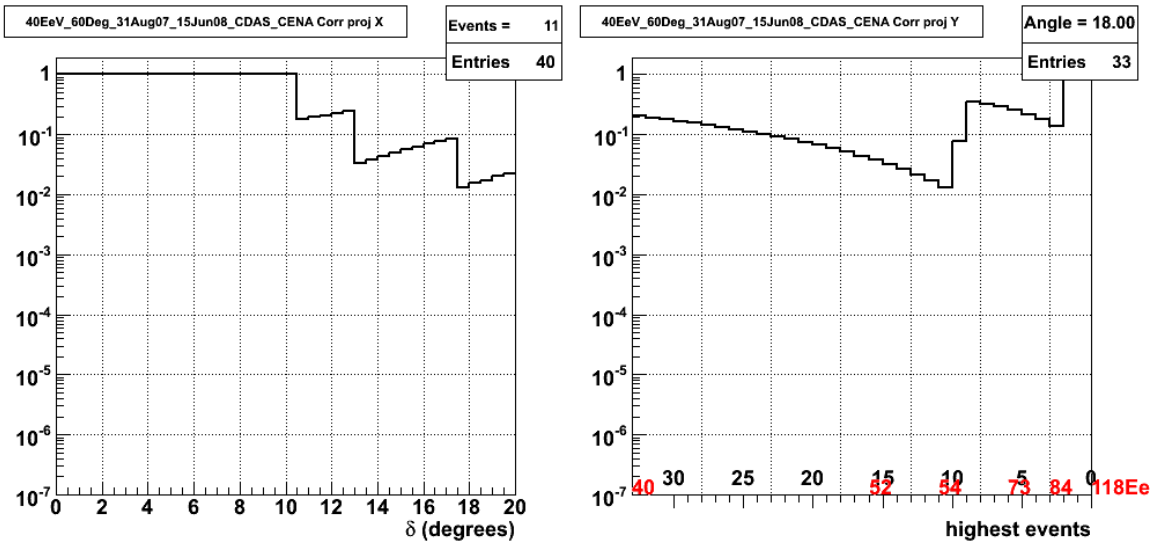

Figure 67: Projection at minimum of Figure 66.

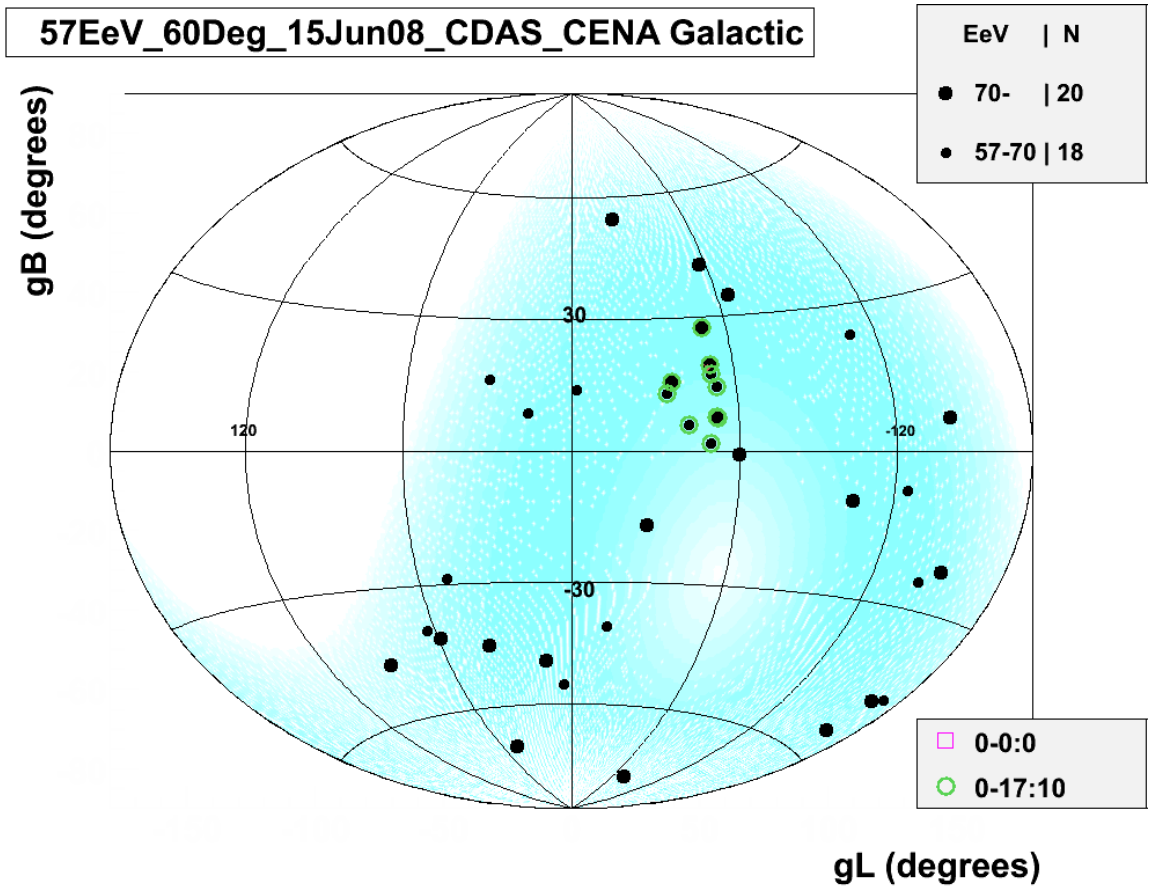

Figure 68: Galactic sky map of events above 57 EeV up until June 15, 2008 (Periods A,B,C). Cen A is marked in red.

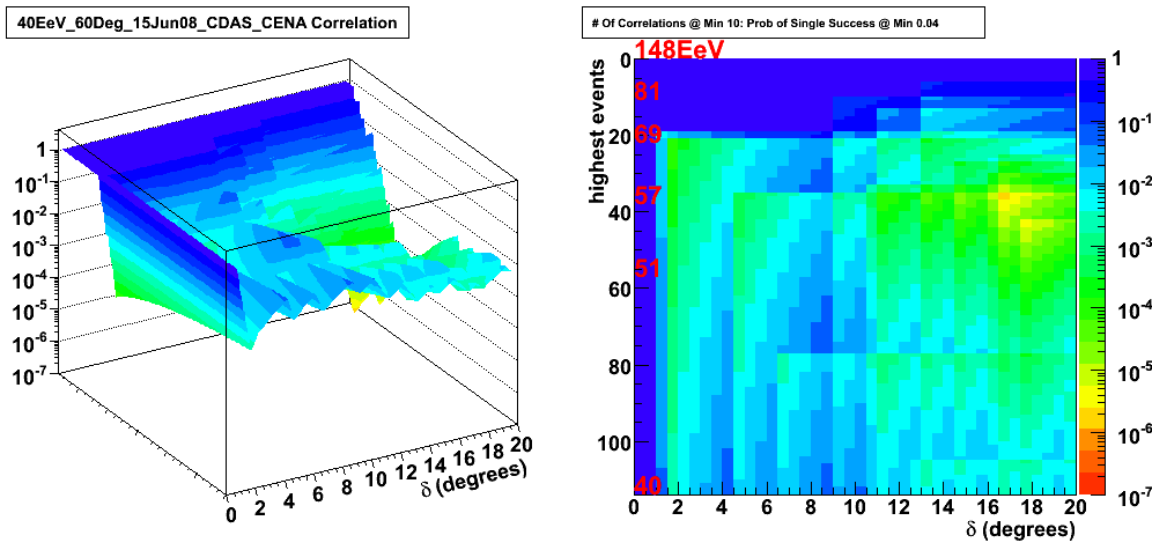

Figure 69: Scan of Expression 8 for events above 40 EeV (within 60^0 zenith) up until June 15, 2008.

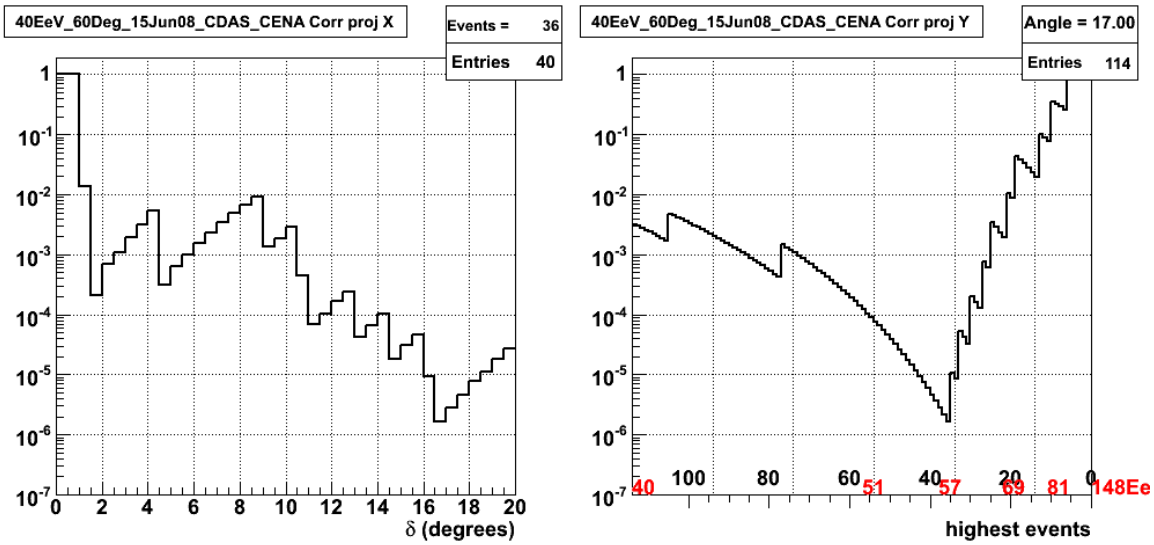

Figure 70: Projection of minimum of scan of Figure 69

The projection of the position of maximum possible deviation from isotropy from the scan in Figure

66 is shown in Figure 67. The maximum possible correlation signal occurs at 18^0 among top 11 events.

Doing the scan of Expression 8 for all events collected until June 15, 2008 is shown in Figure 69. The projection of the scan maximum is shown in Figure 70 to be among the top 36 events above 57.5 EeV at 17^0.

9.2 Composition

If all events after the initial observation of the signal on May 26, 2007 are considered as an independent data set, then to get five out of 24 events to correlate (with a 0.04 chance probability of a single success) within 17^0 of Cen A is 2.3×10^{-3}. Although the results conclude that the region around Cen A deviates from isotropy with a confidence of 2.3×10^{-3}, it does not indicate Cen A to be the source unambiguously. Despite this, Cen A is the closest radio galaxy and the most likely source.

Energy	proton (Z=1)	carbon (Z=6)	nitrogen (Z=7)	oxygen (Z=8)	Ne (Z=10)	Fe (Z=26)
50EeV	50	8	7	6	5	2
100EeV	100	17	14	13	10	4

Table 3: Larmor radii for 50-100EeV proton, carbon, nitrogen, oxygen, neon and iron. Larmor radii are given in Mpc.

Knowing the source of the cosmic rays will allow us to study the composition of the UHECR through spectroscopy, which describes the bending of a particle moving through a magnetic field as a function of its charge. The magnetic fields traversed by the charged particles are not well known and make this task difficult.

Let us proceed under the assumption that the source is Cen A and the traversed magnetic fields between the Earth and Cen A is uniform and on the order of 10^{-9} G. For a 50-100EeV proton, carbon, nitrogen, oxygen, neon and iron nucleus, the Larmor radius is given in Table 3. The Larmor radii of the charged primary are found from Expression 2.

The coherent length of the magnetic fields is assumed to be about one Mpc. The lighter charged nuclei have Larmor radii that are much larger than the coherent length; and therefore, the expected deflection for a proton, carbon, nitrogen, oxygen and neon can be found with Expression 3. Those angular deflections are shown in the Table 4.

	deflection (degrees) for 50EeV	deflection (degrees) for 100EeV
proton	2	1
carbon	12	6
nitrogen	14	7
oxygen	16	8
neon	20	10

Table 4: Light nuclei angular deflections

As the charge of the primary is increased, its Larmor radius decreases and gets closer to the coherent lengths. The Larmor radius of iron is approaching the coherent lengths of the magnetic fields; and so, Expression 4 will be used to determine its angular deflection. These values are shown in Table 5.

	Deflection (degrees) 50EeV	Deflection (degrees) 100EeV
iron	52^0	26

Table 5: Deflection of 50-100EeV iron.

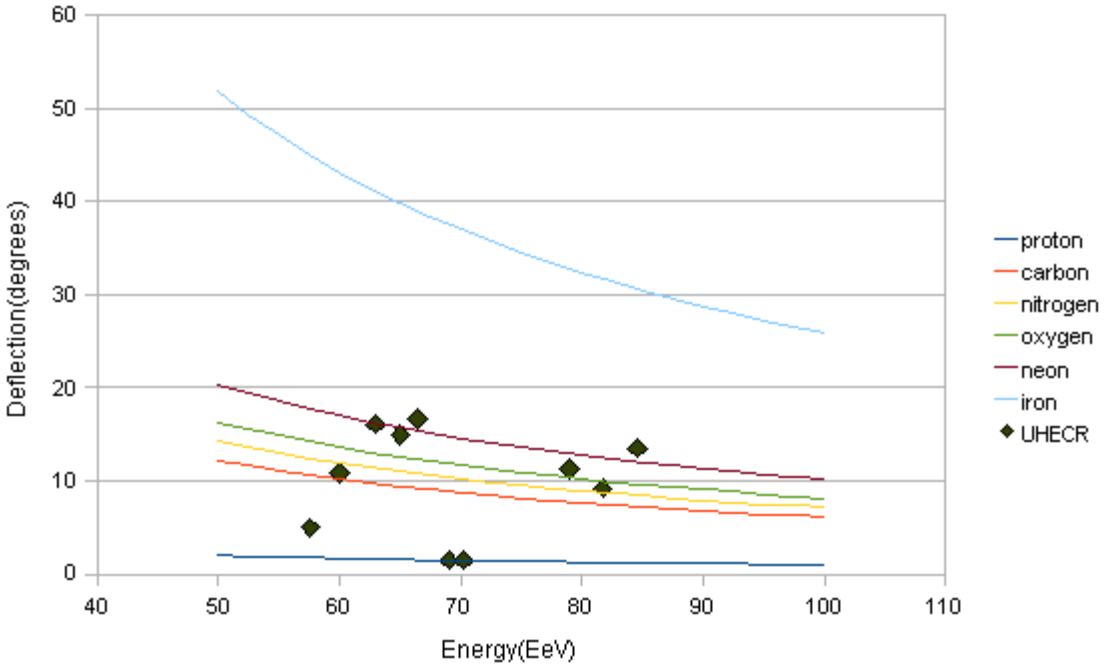

Figure 71: Deflection of UHECR that are within 17 degrees of Cen A. The lines represent the deflections versus energy for the stated nuclei. It appears that the UHECR are CNO and some protons.

The angular separation versus energy for the events that correlate with the region surrounding Cen A are shown in Figure 71. Given that only ten events are now correlated with the region surrounding Cen A, it is difficult to see any pattern in Figure 71. Also, the lack knowledge pertaining to the magnetic fields traversed by each of the UHECR adds to the difficulty in determining composition. Despite this, given the angular deflections observed, if Cen A is the source, then the composition of the UHECR is likely a mixture of carbon, nitrogen and oxygen (CNO). Some protons are also possible.

9.3 Cen A Analysis Summary

Considering events in Periods B and C as independent data sets to test the hypothesis determined in Period A, the region 17^0 around Cen A has an excess of UHECR with energies larger than 57EeV with a confidence of 0.0023. If Cen A is the source of these UHECR, it is likely that their composition are CNO and some protons.

CHAPTER 10

Conclusions

The results of autocorrelation analysis along with the results of correlation analysis with AGN, radio galaxies and Cen A are summarized in Table 6 for different time periods from January 1, 2004 to May 26, 2006; and from May 26, 2006 to August 31, 2007; and from August 31, 2007 to June 15, 2008, in addition to all events up until June 15, 2008.

Date	AGN	RADIO	AUTO	CEN A
January 1, 2004-May 26, 2006 (Period A)	11/14	2/14	3/14	5/14
May 26, 2006-August 31, 2007 (Period B)	8/14	4/14	3/14	3/14
August 31, 2007-June 15, 2008 (Period C)	1/10	0/10	1/10	2/10
January 1, 2004-June 15, 2008 (Periods A, B, C)	20/38	6/38	25/38	10/38
p probability of single chance correction	0.23	0.1	N/A	0.04
Angle defining correlation or pair	3.3	3.5	10.5	17

Table 6: Numbers of pairs and correlations among UHECR with energy larger than 57EeV.

Table 6 values correspond to the number of events above 57EeV that correlate with the corresponding astronomical object, or in the case of autocorrelation, the number of pairs. The last row of the table shows the angular separation that defines two events as a pair for autocorrelation

and a correlation for the astronomical objects. The second to last row shows the chance probability of a single correlation to occur assuming an isotropic sky or the value of Expression 7. The value of Expression 6 (for autocorrelation) and Expression 8 (for correlation with astronomical objects) found from Table 6 is shown in the table below.

Date	AGN	RADIO	AUTO	CEN A
January 1, 2004-May 26, 2006	$1.7\text{x}10^{-5}$	$8.0\text{x}10^{-3}$	0.2	$1.5\text{x}10^{-4}$
May 26, 2006-August 31, 2007	$6.0\text{x}10^{-3}$	$9.2\text{x}10^{-6}$	0.2	$1.7\text{x}10^{-2}$
August 31, 2007-June 15, 2008	0.927	1	1	$5.8\text{x}10^{-2}$
January 1, 2004-June 15, 2008	$6.9\text{x}10^{-5}$	0.2	$3.0\text{x}10^{-4}$	$1.8\text{x}10^{-6}$

Table 7: The value of Expression 6 (for autocorrelation) and Expression 8 (for correlation with astronomical objects) .

10.1 UHECR Source

The events above 57 EeV within 60^0 zenith collected up until May 26, 2006 show a strong possible correlation with AGN. This correlation signal of $1.7\text{x}10^{-5}$ is not a true measure of the deviation from isotropy due to the bias introduced by the scan in energy and angular separation. A prescription was set to confirm that AGN are the true source by searching for this signal in an independent data set. Between May 26, 2006 and August 31, 2007 (Periods A and B), fourteen new events above 57 EeV were found of which eight correlate within 3.3^0 of an AGN. Given a 0.23 chance for a single event to correlate with an AGN, it is found that the prescription is satisfied at $6.0\text{x}10^{-3}$. However, between August 31, 2007 and June 15, 2008 (Period C) only one out of ten of the events correlate with an AGN, while 2.3 are expected from an isotropic distribution of UHECR. This appears to refute the AGN correlation hypothesis. Indeed, if one considers all events until June 15, 2008, the deviation

from isotropy has become less significant than up until June 15, 2008.

The correlation with nearby radio galaxies was claimed based on events up until August 31, 2007. The claim was based on analysis done on the same set of events showing correlation with AGN. These events also showed a possible correlation with nearby radio galaxies with a correlation defined as a separation of 3.5^0. Of the 28 events above 57 EeV found until August 31, 2007, six correlate. Given a 0.1 chance for a single event to fall within 3.5^0 of a nearby radio galaxy, the expected number of correlations for the 28 events is 2.8 for an isotropic sky. The chance for an isotropic sky to get 6 correlations out of 28 is 3.1×10^{-7}. However, this correlation signal does not represent the true deviation from isotropy as it is probably the result of a scan in energy and angular separation. If it is, then it must be confirmed with an independent data set; such as, the events collected between August 31, 2007 and June 15, 2008 (Period C). Among the top ten events above 57 EeV seen during this period, none are found to correlate within 3.5^0 of a nearby radio galaxy. An average of one event would be expected from an isotropic sky. This seems to refute the claim made in [29].

Among the collection of nearby AGN and radio galaxies, Cen A is common to both. It is the closest of the nearby active galactic nuclei at 3.4 Mpc. Considering events up until May 26, 2006 above 57 EeV, five out of 14 correlations are found within the region 17^0 around Cen A. The chance probability of a single success is 0.04 giving a possible deviation 1.5×10^{-4} from isotropy. Using the 14 events above 57 EeV between May 26, 2006 and August 31, 2007 (Period B), three correlations are found at a probability of 0.017. Between August 31, 2007 and June 15, 2008 (Period C), two out of ten events correlate within 17^0 for a probability of 0.058.

Considering all events up until June 15, 2008, there are ten out of 38 correlations within 17^0. Given a chance of 0.04 for a single correlation to occur under the assumption of isotropy, this occurs

with a chance probability of 1.8×10^{-6} from Expression 8. The autocorrelation signal also shows that among these high-energy events above 57 EeV, an abundance of pairs (defined as separations of 10^0-20^0) occurs with a chance probability of only about 10^{-4}.

If all events since the initial observation of the signal for the region around Cen A on May 26, 2007 are considered as an independent data set, it can be concluded that to get five out of 24 events to correlate (with a 0.04 chance probability of a single correlation) within 17^0 of the region around Cen A is 2.3×10^{-3} from Expression 8. Although the results conclude that the region around Cen A deviates from isotropy with a confidence of 2.3×10^{-3}, this result does not indicate Cen A to be the source unambiguously. However, Cen A is the closest radio galaxy and the most likely source of UHECR anisotropy. If Cen A is shown to be the source, then the deflections undergone by its UHECR ($<17^0$) appear to indicate that their composition is CNO.

10.2 Summary

The region 17^0 around Cen A has an excess of UHECR with energies larger than 57EeV with a confidence of 2.3×10^{-3}. Presently, more data should be collected to determine if Cen A is the source unambiguously. A prescription should be set to monitor the area 17^0 around Cen A for an excess of events above 57 EeV. However, the analysis suggests that Cen A is the most likely source of UHECR anisotropy. This supports a bottom-up mechanism for UHECR production in agreement with the photon flux limits set by the Auger collaboration. In addition, the close distance of Cen A is in agreement with the GZK effect. The composition of the UHECR from the region of Cen A is likely CNO.

Bibliography

1: The Pierre Auger Collaboration, Correlation of the highest-energy cosmic rays with the positions of nearby active galactic nuclei, Astroparticle Physics 29 (2008), 188

2: N. Nagar and J. Matulich, Ultra-High Energy Cosmic Rays Detected by the Pierre Auger Observatory: First Direct Evidence, and its Implications, that a Subset Originate in Nearby Radiogalaxies, arXiv:0806.3220v1 [astro-ph]

3: M. S. Longair, High Energy Astrophysics, Cambridge University Press, 1981

4: MIT, Research notes of Bruno Rossi, http://libraries.mit.edu/archives/exhibits/rossi/index.html

5: Pierre Auger, P. Ehrenfest, R. Maze, J. Daudin, and Robley A. Fréon, Extensive Cosmic-Ray Showers ,Rev. Mod. Phys. 11, 288 - 291 (1939)[Issue 3-4 – July 1939]

6: John Linsley, Laboratory for Nuclear Science, Massachusetts Institute of Technology, Cambridge, Massachusetts , Evidence for a Primary Cosmic-Ray Particle with Energy 10^{20} eV, Phys. Rev. Lett. 10, 146 - 148 (1963)[Issue 4 – February 1963]

7: J. Elbert and P. Sommers, In Search of a Source for the 320 Eev Fly's Eye Cosmic Ray, Astrophys.J. 441 (1995) 151-161

8: J. Cronin, Cosmic rays: the most energetic particles in the universe ,Rev. Mod. Phys. 71, S165 - S172 (1999)[Issue 2 – March 1999],

9: A. M. Hillas, THE ORIGIN OF ULTRA-HIGH-ENERGY COSMIC RAYS, Ann. Reo. Astron. Astrophys. 1984.22: 425-44

10: M. Nagano and A. A. Watson, Observations and Implications of the Ultrahigh-Energy Cosmic Rays, Reviews of Modern Physics 72, 689 (2000)

11: J. Abraham et. al., Upper limit on the cosmic-ray photon flux above 10^19 eV using the surface detector of the Pierre Auger Observatory, Astroparticle Physics 29 (2008) 243-256

12: K. Dolag et all, Mapping deflections of extragalactic Ultra-High Energy Cosmic Rays in magnetohydrodynamic simulations of the Local Universe, JETP Lett. 79 (2004) 583-587 also arXiv:astro-ph/0310902v2

13: L. Anchordoqui and M. Dova, Ultrahigh Energy Cosmic Nuclei, Internal GAP Note GAP-2003-092, 2003

14: P. Blasi, D. Marco, The Small Scale Anisotropies, the Spectrum and the Sources of Ultra High Energy Cosmic Rays, Astropart.Phys. 20 (2004) 559-577

15: K. Greisen, End of the Cosmic Ray Spectrum?, Phys. Rev. Lett. 16, 748-750 (1966)

16: University of Delaware, Bartol Research Institute, http://neutronm.bartol.udel.edu/catch/cr2.html

17: University of Tokyo, Akeno Observatory, http://www-akeno.icrr.u-tokyo.ac.jp/Observatory/agasa0-e.html

18: University of Tokyo, Akeno Observatory, http://www-akeno.icrr.u-tokyo.ac.jp/AGASA/results.html#spectrum

19: N. Hayashida, Updated AGASA Event List above 4 x 10^{19} eV, Astron.J. 120 (2000) 2190, Also at arXiv:astro-ph/0008102

20: S. Yoshida, in Proceedings of the 29th ICRC, volume 10, page 297, 2005.

21: Joong Lee, The Cosmic Ray Spectrum as Measured by the Surface Detector of the Pierre Auger Observatory and its Theoretical Implications, PhD thesis, UCLA 2007

22: David Scott Barnhill, Composition Analysis of Ultrahigh Energy Cosmic Rays Using the Pierre Auger Observatory Surface Detector, PhD thesis, UCLA, 2005

23: Tohru Ohnuki, Small Scale Angular Clustering of the Highest Energy Cosmic Rays in the Surface Detector Data of the Pierre Auger Cosmic Ray Observatory, PhD thesis, UCLA, 2005

24: P. Allison et al. for the Auger Collaboration, Calibration of the Surface Array of the Pierre Auger Observatory, in Proceedings of the 29th ICRC, 2005.

25: Joong Lee, The Cosmic Ray Spectrum as Measured by the Surface Detector of the Pierre Auger Observatory and its Theoretical Implications, 2007

26: T.Yamamoto et. al., The UHECR spectrum measured at the Pierre Auger Observatory and its Astrophysical Implications ,arXiv:0707.2638v1 [astro-ph] 18 Jul 2007

27: P. Sommers, Cosmic Ray Anisotropy Analysis with a Full-Sky Observatory, Astropart.Phys. 14 (2001) 271-286

28: The Pierre Auger Collaboration, Correlation of the highest energy cosmic rays with the positions of nearby active galactic nuclei, arxiv:0712.2843v2 [astro-ph] 23 Jun 2008

29: B. M. Peterson, An Introduction to Active Galactic Nuclei, Cambridge University Press 1997

30: J. Abraham et. al., Correlation of the highest-energy cosmic rays with the positions of nearby active galactic nuclei, Astroparticle Physics 29 (2008) 188-204

31: Max Planck Institute, http://www.mpe.mpg.de/~hcs/Cen-A/cen-a-pictures.html,

32: Ian Robson, Active Galactic Nuclei, Wiley 1996

33: F. P. Israel, Centaurus A - NGC 5128, Astronomy and Astrophysics Review, Volume 8, Number 4 / August, 1998